Title
Mechanisms that specify promoter nucleosome location and identity

Author
Hartley, Paul

Publication Date
2009

Peer reviewed|Thesis/dissertation

Mechanisms that specify promoter nucleosome location and identity

by

Paul D. Hartley

DISSERTATION

Submitted in partial satisfaction of the requirements for the degree of

DOCTOR OF PHILOSOPHY

in

Biochemistry and Molecular Biology

in the

[redacted]

Acknowledgements

As I reflect on my graduate career, I must acknowledge those who have helped foster my intellectual and personal growth. I chose to do my graduate work in Hiten Madhani's lab in part because of his strong ability in teaching how to approach and solve scientific problems. He has been a source of many ideas for experiments and how to integrate an element of risk taking with experiments. He has also been supportive in allowing room for me to work on my own, which was instrumental for me to gain confidence in designing experiments and learning how to conduct data analysis with large data sets. Given the wealth of information to be found in large data sets and the emerging technology producing these data sets, having the necessary computational skills to do data analysis will be important for my career. I wouldn't have developed those skills without Hiten's willingness to give me the time to work on them. I look forward to seeing what new discoveries Hiten and his lab continue to make.

The Madhani lab worked on several different areas while I was in the lab: chromatin biology, *Cryptococcus neoformans* pathogenesis, MAPK signaling specificity and the role of variance/noise in the yeast mating pathway. All the members of the lab over the five-and-a-half years I was there have made helpful suggestions or comments about my work, and I've in turn learned all kinds of things from their work. Chromatin subgroup felt different after Bill Hwang, Marc Meneghini, Ryan Raisner, Rachel Tompa and Shiv Venkatasubrahmanyam all moved on with their careers. They were the original group of people working on

chromatin when I joined the lab, and they all helped get me started with the techniques used to study chromatin biology.

Joe DeRisi and Geeta Narlikar took the time to be a part of my thesis committee and provided valuable advice on my work. Joe, along with Carol Gross, Barbara Panning and Wallace Marshall helped me develop my qualifying exam proposal, which served as the starting point for the work I published in 2009.

I was provided with real-time captioning during my classes and meetings, and without this technology it would have been impossible for me to keep up with the flow of conversation. Eric Koenig and especially Mary Walsh in the Office of Student Life did a great job developing the resources for using this technology at UCSF for the first time. I had three primary captioners, Lee McCarthy, Audrey Spinka and Richard Walker, all of whom did an excellent job transcribing my classes and meetings, especially in the context of having to master scientific terminology.

I was fortunate to meet Margot Rowley in the lab and have her support over the past year as I completed my work. Cheers to our future together, hon! Last, but not least, my parents have provided invaluable support all my life, and I know I would have not gotten as far as completing a graduate degree without their tenacity.

Statement from Research Advisor: Author Contributions

This dissertation is comparable to a standard thesis. The contributions of Paul D. Hartley (PDH) to this dissertation are summarized as follows:

Chapter 1: PDH wrote this chapter.

Chapter 2: This chapter is reprinted with permission from the October 21, 2005 issue of *Cell* (vol. 123, pages 233-248). PDH conducted the experiments to obtain the results shown in Figure 6, Figure 7 and Figure 14. Ryan M. Raisner (RMR), Marc D. Meneghini and Marie Z. Bao performed the experiments to obtain the results shown in Figure 1. Chih Long Liu (CLL) conducted the experiments summarized in Figure 2, Figure 3 and Figure 11. RMR conducted the experiments to obtain results shown in Figure 4, Figure 5, Figure 8, Figure 9, Figure 10, Figure 12 and Figure 13. Hiten D. Madhani (HDM) directed the research, while Oliver J. Rando (OJR) provided guidance and materials for the experiments represented in Figure 2, Figure 3 and 11. Stuart L. Schreiber provided financial support for CLL. RMR, PDH, OJR and HDM wrote the paper.

Chapter 3: This chapter is reprinted with permission from the May 1, 2009 issue of *Cell* (vol. 137, pages 445-458). PDH conducted all experiments and data analysis under the guidance of HDM. PDH and HDM wrote the paper.

Mechanisms that specify promoter nucleosome location and identity

Paul D. Hartley

Abstract

The promoters of genes have a stereotypical chromatin architecture characterized by a nucleosome-free region (NFR), which contain DNA motifs that are involved in gene transcription. Additionally, at least one of the nucleosomes flanking a NFR tends to contain the histone H2A variant H2A.Z. The mechanisms behind NFR formation and H2A.Z deposition have not been well characterized. This dissertation encompasses approaches towards an understanding of these mechanisms. A specific sequence of DNA isolated from a yeast promoter was shown to be sufficient to program NFR formation and H2A.Z deposition. The remodeling activity of this sequence of DNA required the activities of the transcription factor Reb1 and chromatin remodeling complex RSC. The involvement of Reb1, RSC, and another transcription factor, Abf1, in nucleosome positioning at other gene promoters was assayed, and RSC was determined to play a significant role in the proper positioning of nucleosomes at promoters. Lastly, because H2A.Z deposition is not required for general NFR formation, the hypothesis that H2A.Z deposition requires prior NFR formation was tested.

Table of Contents

List of Tables

List of Figures

Chapter 1: Introduction

The information a cell uses to construct its components is stored as DNA in discrete blocks known as genes. As outlined by the classical Central Dogma, genes are transcribed by RNA polymerase machinery into RNA, and messenger RNA is translated by ribosomes into proteins. These proteins in turn serve as structural components or possess enzymatic activities in a cell. Before a gene can be transcribed, however, a cell must identify where to begin transcription. This task is in part accomplished by a class of DNA-binding proteins generally known as transcription factors, which recognize sequence or structural motifs of DNA. Regions of a genome that contain these motifs in association with a gene are known as promoters. When transcription factors recognize and bind promoters, they help recruit components of the RNA polymerase machinery to the promoter to prime genes for transcription.

The identification of promoters is not trivial in eukaryotic cells, which package their DNA into basic units called nucleosomes. One nucleosome consists of about 147 base pairs of DNA wrapped around a histone octamer, which has two copies each of the histones H2A, H2B, H3 and H4. As a strand of DNA is wrapped around an octamer, the face of the strand alternates from being against and not against the octamer because of the twisting structural conformation of the double helix (*1*). Such a physical property means that DNA motifs facing the histone octamer are less accessible for recognition by DNA binding proteins.

The ability for nucleosomes to occlude DNA binding motifs has been demonstrated through studies of the inducible *S. cerevisiae* gene *PHO5*, which is repressed when sufficient inorganic phosphate is present. The inactive *PHO5* promoter has a chromatin structure that is characterized by four well-positioned nucleosomes and a small region of nucleosome-free DNA (*2*). Activation of the *PHO5* gene under low phosphate conditions requires the Pho4 transcription factor. There is a Pho4 binding motif in the *PHO5* nucleosome free region (NFR) and within one of the nucleosomes. Under low phosphate conditions, Pho4 will bind to its site in the NFR, where its activator domain serves to program a significant remodeling of the *PHO5* promoter chromatin structure (*3*). This remodeling event allows Pho4 to bind to second, nucleosome-based site and recruit the components necessary to initiate transcription of *PHO5*.

Manipulations in the *PHO5* promoter system have demonstrated how nucleosomes can obstruct gene transcription. As one example, mutation of the Pho4 binding site in the *PHO5* NFR prevents induction of *PHO5* under low phosphate conditions because the second Pho4 binding site is in a nucleosome and is inaccessible (*4*). Overexpression of Pho4 is sufficient to restore induction of *PHO5* because the increased levels of Pho4 are able to overcome the nucleosome barrier imposed on the intact Pho4 binding site at the *PHO5* promoter (*4*). Indeed, the use of nucleosomes to regulate the accessibility of transcription factor binding sites may be important for regulating gene expression based on different cellular states (*5*). A second example of nucleosome inhibition at the *PHO5* promoter involves the TATA binding site for TFIID/TBP. This TATA

box must be precisely positioned relative to its associated nucleosome; a translational shift of only 2 or 3 base pairs is enough to force *PHO5* induction to require histone acetylation (*6*). A genome-wide study in *S. cerevisiae* on the effects of histone H4 depletion on gene expression suggested that there are no significant changes in expression for the majority of genes (*7*). Such an observation means that most genes in yeast already have a chromatin configuration amenable to gene transcription.

The technology and techniques used to map nucleosome positions were intrinsically limited to studies of individual gene promoters such as the one associated with *PHO5*. Advances in technology in recent years finally allowed the mapping of nucleosomes at a genome-wide scale using either microarray or sequencing technology. The first such study mapped nucleosome positions at a 20bp resolution in a fraction of the *S. cerevisiae* genome and revealed that a large proportion of genes have a nucleosome free region (NFR) in their promoters (*8*). Furthermore, nucleosomes downstream of the NFR at first tend to be well positioned and phased, but the further away a nucleosome is from a NFR, the less it maintains this ordering. A subsequent study mapped nucleosome positions in the entire yeast genome at a 4bp resolution and revealed that about 75% of genes have a NFR (*9*). These observations were also confirmed by whole-genome sequencing of nucleosome positions (*10*), (*11*). Importantly, the presence of NFRs at the majority of gene promoters has been observed for higher organisms, including Drosophila (*12*) and humans (*13*).

The general observation that gene promoters have NFRs suggests that there must be a functional importance tied to these NFRs. Given that nucleosomes are refractory to gene transcription, a reasonable hypothesis is that NFRs serve as sites where transcription machinery can assemble without nucleosomal interference. Several studies support this hypothesis. The sites of transcription initiation are within nucleosome free regions, but closer to the downstream edge rather than the middle of the NFRs (*9*). Known transcription factor binding motifs also tend to be enriched within NFRs (*9*). Peak enrichments for binding of Mediator subunits and general transcription factors such as TBP and several TFII subunits are within the NFR (*14*).

The mechanism of NFR formation can be approached by asking how nucleosomes are positioned relative to DNA. This positioning can occur through intrinsic structural properties of a sequence of DNA, or via trans-acting factors such as chromatin remodelers. A sequence of nucleotides has a direct effect on the pliability of DNA about a histone octamer. For example, homopolymeric runs of dA:dT nucleotides tend to exclude nucleosomes and are enriched in promoter regions (*15*) and in one case are important for inducible gene expression (*16*). Another nucleotide sequence pattern involves dinucleotide periodicity in which a strand of DNA with a 10bp periodicity of certain dinucleotides will be positioned along a histone octamer such that these dinucleotides are at thermodynamically favorable locations (*17*). These thermodynamic properties of dinucleotide periodicity were used to develop models that allowed computational prediction of nucleosome positioning (*18*), (*19*). It is more likely that such periodicity may be

involved in fine tuning of nucleosome positions rather than global nucleosome positioning (*9*), and this fine tuning would also involve trans-acting factors (*20*). These trans-acting factors likely are chromatin remodeling complexes, which are required for nucleosome reorganization at inducible gene promoters and more generally to prevent spurious antisense transcription (*21*).

Finally, regardless of how a nucleosome free region forms in gene promoters, there have been striking observations that the histone H2A variant H2A.Z is deposited at the one or both nucleosomes that immediately flank a NFR (*22*), (*23*), (*24*). H2A.Z deposition also correlates with nuclease-sensitive regions at chromosomal breakpoints in human cells (*24*). In *S. cerevisiae*, H2A.Z plays an important role in preventing the spread of silent heterochromatin into nearby euchromatic genes (*25*). Additionally, H2A.Z appears to have a variety of roles, including transcription induction kinetics (*26*), positioning of genes near nuclear pore complexes (*27*), suppression of antisense transcripts at convergent genes (*28*) and chromosome stability (*29*).

I began my graduate work in 2004, before the publication of data suggesting that gene promoters generally contain nucleosome free regions. At the time, members of my laboratory had obtained data that suggested H2A.Z deposition correlates with the 5' ends of genes. In particular, the *SNT1* gene was found to have a well-defined H2A.Z deposition profile at its promoter. We began to ask what specifically directs H2A.Z to be deposited at the *SNT1* promoter. My initial project, which is outlined in Chapter 2, was to test the hypothesis that there existed specific DNA sequence or structural motifs that recruit H2A.Z. I

discovered that a short sequence named Reb1:dT_7 contributed to H2A.Z deposition at *SNT1*, and I inserted it into a transcriptionally inactive gene to determine whether the sequence was sufficient to induce H2A.Z deposition there. Amazingly, this sequence indeed was sufficient to deposit H2A.Z as a well-defined peak over the insertion site. At about the same time, Oliver Rando's group had published their paper describing the general phenomenon of nucleosome free regions at yeast promoters. We collaborated with him to determine the H2A.Z deposition pattern at the genes he had studied, and we discovered a striking pattern in which H2A.Z was found at most of the assayed gene promoters in the nucleosomes immediately flanking a NFR. With this knowledge, I decided to do a more detailed study of the chromatin structure induced by the Reb1:dT_7 insertion, and I found that this insertion also programmed the formation of a nucleosome-free region whose flanking nucleosomes contained H2A.Z.

The remainder of my graduate career focused on the mechanisms behind the formation of the NFR programmed by Reb1:dT_7 and how these mechanisms apply to *bona fide* promoters in general. This work is described in Chapter 3. Briefly, I was able to determine that both the Reb1 transcription factor and the RSC chromatin remodeling ATPase, Sth1, were required for formation of the NFR programmed by Reb1:dT_7. I subsequently found that Sth1 was required for the proper positioning of nucleosomes at a large fraction of assayed promoters, while Reb1 and another transcription factor, Abf1, were required at a smaller subset. I also showed that H2A.Z deposition is not required for NFR formation in

general, and I tested the hypothesis that H2A.Z deposition required the prior formation of a NFR.

Chapter 2: Histone variant H2A.Z marks the 5' ends of both active and inactive genes in euchromatin

Ryan M. Raisner (*), Paul D. Hartley (*), Marc D. Meneghini, Marie Z. Bao, Chih Long Liu, Stuart L. Schreiber, Oliver J. Rando and Hiten D. Madhani

(*) denotes that these authors contributed equally to this work

Reprinted with permission from

Cell (2005) vol. 123, pages 233-248

Summary

In *S. cerevisiae*, histone variant H2A.Z is deposited in euchromatin at the flanks of silent heterochromatin to prevent its ectopic spread. We show that H2A.Z nucleosomes are found at promoter regions of nearly all genes in euchromatin. They generally occur as two positioned nucleosomes that flank a nucleosome-free region (NFR) that contains the transcription start site. Astonishingly, enrichment at 5' ends is observed not only at actively transcribed genes, but also at inactive loci. Mutagenesis of a typical promoter revealed a 22 bp segment of DNA sufficient to program formation of a NFR flanked by two H2A.Z nucleosomes. This segment contains a binding site of the Myb-related protein Reb1 and an adjacent dT:dA tract. Efficient deposition of H2A.Z is further promoted by a specific pattern of histone H3 and H4 tail acetylation and the bromodomain protein Bdf1, a component of the Swr1 remodeling complex that

deposits H2A.Z.

Introduction

The association of eukaryotic DNA with histone octamers to form nucleosomes has profound implications for all aspects of DNA metabolism. Epigenetic control mediated through chromatin is now recognized as a major form of genetic regulation that functions during both normal development and pathogenic processes such as tumorigenesis. Therefore, a critical challenge faced by dividing eukaryotic cells is the faithful maintenance of both active and inactive epigenetic states of specific genomic regions. Three known biochemical mechanisms exist to control the states of chromatin: histone posttranslational modifications (on both the unstructured N-terminal tails and core regions), ATP-dependent chromatin remodeling by Swi2/Snf2 family members, and histone variant substitution. The current goal of the field is to link these mechanisms to epigenetic regulation. Substantial progress has been made in understanding how silent heterochromatin is generated and maintained. Compared to heterochromatin, less is understood about how euchromatin is generated, maintained and inherited. Indeed, euchromatin has widely been viewed as a default state. More recently, however, several chromatin modifications have been identified that promote the euchromatic state by antagonizing silencing. These include the replacement of histone H2A by H2A.Z (*25*) and three histone modifications: acetylation on lysine 16 of the H4 tail (*30*), (*31*) and methylation of lysines 4 and 79 of H3 (*32*), (*33*), (*34*). In this paper, we focus on the deposition

pattern of H2A.Z in euchromatin and its implications.

In previous work, we demonstrated that in *S. cerevisiae,* the evolutionarily conserved histone variant H2A.Z functions in euchromatin to antagonize the spread of Sir-dependent silencing. Furthermore, we showed that at the right border of the *HMRa* silent mating type cassette, H2A.Z functions in parallel with a well-characterized boundary element (*25*). Thus, H2A.Z is a component of euchromatin that functions to antagonize the opposite chromatin state. One key question, therefore, is whether H2A.Z is randomly distributed through euchromatin and if not, how its deposition to specific sites is determined. We and others have also identified a 13 subunit ATP-dependent chromatin remodeling complex, the Swr1 complex, that is required for the deposition of H2A.Z in vivo (*35*), (*36*), (*37*). Where the Swr1 complex acts and how its specificity is determined is not known. A subunit of this complex is Bdf1, a protein containing two tandem bromodomains known to bind acetylated histone tails (*38*), (*39*). This suggests recognition of histone acetylation as one potential mechanism for the targeting of H2A.Z deposition to euchromatin.

Early chromatin immunoprecipitation (ChIP) experiments performed by Smith and coworkers suggested a relative enrichment of an epitope-tagged version of H2A.Z at the promoter regions of the highly inducible *GAL1-10* and *PHO5* genes in yeast (*40*). Moreover, these experiments demonstrated enrichment under non-inducing conditions for the linked genes and this enrichment decreased upon gene induction. However, it is difficult to make general conclusions from these studies for three reasons. First, since only four

intergenic regions were examined, their correlation with higher H2A.Z levels could have been coincidental. Second, since no intergenic regions lacking a promoter were examined, the correlation with H2A.Z levels could have reflected preferential H2A.Z deposition in intergenic regions rather than in promoters per se. Third, since nucleosome density was not examined in the gene induction experiments, whether H2A.Z was selectively removed upon gene activation relative to H3, for example, was not clear. Thus, the following issues remain unresolved: 1) where is H2A.Z deposited in general? 2) what is the relationship between H2A.Z deposition to transcription? and 3) what are the signals that induce its deposition?

Results

H2A.Z is preferentially enriched at 5' regions in general

Previous studies have described a prominent role for H2A.Z at heterochromatin-proximal regions to antagonize the spread of silencing; however, we were curious to examine whether H2A.Z might play a broader role in the genome. Such additional roles could be elucidated through knowledge of the deposition profile of H2A.Z across chromosomes. We chose to examine the H2A.Z deposition profile in *S. cerevisiae* Chromosome III because it contains the *HMRa* and *HMLα* silent mating type cassettes and is well-characterized with respect to the location of replication origins, cohesion sites and transcription initiation sites. This analysis was conducted with a strain carrying an allele of H2A.Z with an amino-terminal influenza hemeagglutinin epitope tag (*HA_3-HTZ1*)

that was integrated at the endogenous locus as the sole genomic copy. This allele is functional in that it can complement the synthetic lethality of *htz1*Δ with *bre1*Δ (*41*). ChIP and quantitative real-time PCR (QPCR) were used to determine H2A.Z enrichment at 300 bp segments whose 5' ends were spaced at 1000 bp intervals across Chromosome III. We observed a highly non-uniform and chromosome-wide distribution of H2A.Z (Figure 1A). Further analysis of our data indicated that the level of H2A.Z deposition at a given ChIP probe region was positively correlated with its proximity to the nearest 5' end of a gene (Figure 1B). However, we observed no apparent correlation with proximity to 3' ends of genes that are not near 5' ends, the transcription rate of the nearest gene, cohesion sites, or origins of replication (unpublished observations and see below).

We next increased the resolution of our Chromosome III analysis to a single intergenic region flanked by two non-converging ORFs. The intergenic region upstream of *SNT1* was chosen because it is significantly smaller relative to the *SNT1* coding region. A 4.2 kb continuous region starting from 2 kb upstream of the *SNT1* initiation codon to 2.2 kb downstream was assayed for H2A.Z enrichment by ChIP and QPCR using primer sets that tiled the region. This assay revealed a striking intergenic enrichment for H2A.Z with a sharp decline in the coding region of *SNT1* and in the upstream gene *BPH1* (Figure 1C).

We then identified a larger region of Chromosome III (the *LEU2-YCL012W* interval) containing a mixture of gene orientations: genes whose 5'

ends share an intergenic region (5'-5'); genes whose 5' ends are adjacent to a 3' end (5' only); and genes whose 3' ends converge (3-3'). We assayed the H2A.Z deposition profile within this 11 kb region by ChIP and QPCR. This tiling analysis revealed that for every H2A.Z peak of enrichment, there was a corresponding 5' end (Figure 1D). In most cases, the peak enrichment of H2A.Z was close to, or directly upstream of the initiation codon. The only shared 5' region in this dataset (the *DCC1-BUD3* intergenic region) had two distinct peaks of H2A.Z enrichment, one corresponding to the 5' end of each gene. The observed H2A.Z peaks in these promoter regions were not due to increased cross-linkability or nucleosome density of these regions because additional ChIP analysis of histone H3 across the same region revealed slightly lower, not higher, ChIP signals in intergenic regions (Figure 8). Finally, the two regions with converging ORFs (3'-3') had no observable peak of H2A.Z, supporting the notion that H2A.Z is indeed selectively enriched at 5' regions of genes.

High resolution chromosome-wide mapping of endogenous H2A.Z nucleosomes

Our initial analyses of H2A.Z deposition relied on a ChIP protocol that involved shearing DNA to an average size of 500 bp, which meant that QPCR analyses of immunoprecipitated material resolved multiple nucleosomes, thereby obscuring finer details of H2A.Z localization. In addition, the tiling methods we used to assay H2A.Z deposition at an appropriate resolution are not feasible for

rapidly examining much larger regions such as whole chromosomes. To overcome these two limitations, we used a ChIP and microarray hybridization protocol to analyze the distribution of endogenous, untagged H2A.Z at the resolution of single nucleosomes; the data were normalized for nucleosome density (see Experimental Procedures). The microarrays tiled the majority of Chromosome III and 223 additional regulatory regions at a resolution of 20 bp. These experiments yielded a nucleosome-resolution map of H2A.Z enrichment patterns across nearly half a megabase of the *S. cerevisiae* genome.

Analysis of the data recapitulated our initial conclusions about the specific deposition of H2A.Z at 5' ends of genes (Figure 1) and extended these conclusions to a larger portion of the yeast genome. Figure 2A shows the microarray data for the regions analyzed by QPCR in Figure 1C and Figure 1D. Consistent with the QPCR data, the region upstream of *SNT1* contains H2A.Z, and this H2A.Z signal has now been resolved into a striking distribution pattern in which two consecutive nucleosomes contain H2A.Z. Two H2A.Z nucleosomes are also found upstream of the *BPH1* gene, one upstream of the *FEN1* gene and two in the *RRP43-RBK1* intergenic region that is flanked by the 5' ends of the respective genes. In contrast, no H2A.Z peak was observed in the *FEN1-RRP43* intergenic region that is flanked by the 3' ends of those two genes. Also shown in Figure 2A is a portion of the *NFS1-YCL012C* region analyzed in Figure 2B; *LEU2* is missing because this gene is deleted in the strain profiled using the microarray method. The QPCR analysis of this region was precisely recapitulated by the microarray data: H2A.Z was found specifically in intergenic

regions that contain at least one 5' end of a gene. Indeed, analysis of the entirety of Chromosome III revealed H2A.Z upstream of most euchromatic genes and not at intergenic regions flanked by two converging 3' ends. Genes on Chromosome III that lacked detectable H2A.Z in their promoter regions correspond to genes in the *HML*α silent cassette, genes near the telomeres of Chromosome III, ORFs annotated as "dubious" and seven apparently bona fide euchromatic genes (*HIS4, POL4, ADY2, AGP1, RPS14A, PMP1,* and *YCR006C*). While it is not obvious why these genes lack H2A.Z in their promoter regions, we note that *YCR006C* contains a tRNA gene in its upstream regions. tRNA genes have been shown to contain boundary activity (*42*) and have been shown to inhibit expression of adjacent PolII-transcribed genes (*43*). Since genes lacking H2A.Z in their promoters represent a small minority, we conclude that H2A.Z generally marks the 5' ends of genes in euchromatin.

Recent work by Yuan and coworkers (2005) demonstrated that nucleosomes are generally uniformly distributed across yeast promoters and ORFs, but nearly all yeast genes contain a ~150 bp nucleosome free region (NFR) centered ~200 bp upstream of the initiation codon. cDNA hybridization studies demonstrated that these regions contain the initiation site for transcription of their associated genes (*8*). The genes represented in the H2A.Z microarray data were aligned by the center of their NFRs to generate a cluster hierarchy shown in Figure 2B. Remarkably, for about 2/3 of the genes analyzed, the NFR is flanked by two nucleosomes that contain H2A.Z. The remainder of these genes appears either to have H2A.Z present only at one nucleosome, or lack

H2A.Z entirely for potential reasons explained above. Thus, not only does H2A.Z mark the 5' ends of genes, but two positioned H2A.Z nucleosomes typically flank the transcription initiation site. These data demonstrate that H2A.Z nucleosomes are placed in a highly stereotyped and organized manner at the 5' ends of genes.

Active transcription is not required for H2A.Z enrichment

The striking localization of H2A.Z at most gene promoters suggested that there could be a relationship between H2A.Z and gene transcription. To address this issue, we selected from the H2A.Z ChIP microarray data those genes that contain two H2A.Z nucleosomes flanking a NFR and compared the levels of H2A.Z enrichment at each of the two nucleosomes to two distinct measurements of transcriptional activity for the corresponding gene (Figure 3). We used genome-scale data from either an analysis of initiation rates (*44*) Figure 3A and Figure 3C) or RNA polymerase II occupancy (*45*) Figure 3B and Figure 3D). Comparison of H2A.Z enrichment at genes to either dataset showed no correlation between H2A.Z enrichment and transcriptional activity. In other words, the transcription rate of a gene does not predict the levels of H2A.Z at a given promoter.

To further assess whether H2A.Z requires active transcription for its selective enrichment at gene promoter regions, we examined several promoter regions under conditions known to produce their tight repression. We first chose to examine the sporulation/meiosis-specific genes *DIT1, DIT2, HOP1*, and *SPO22* in a haploid strain grown in rich media. These genes are transcriptionally

inactive in haploid cells and in non-meiotic diploid cells (*46*). Additionally, these four occur in two pairs in which their 5' ends flank an intergenic promoter region. Strikingly, we observed peaks of H2A.Z enrichment at both of the shared promoter regions (Figure 4A and B). These patterns were not explained by underlying nucleosome density since H3 is relatively evenly distributed across these intervals (Figure 9). To attempt to observe de novo deposition of H2A.Z at these loci, we constructed a galactose-inducible HA epitope-tagged allele of *HTZ1* with which we could selectively induce or repress the transcription of H2A.Z. As expected, under the repressive glucose condition, virtually no H2A.Z is detectable by ChIP (Figure 10). However, after growth for several generations in galactose, peaks of H2A.Z enrichment were observed at the divergent promoters of both meiotic gene pairs (Figure 10). Thus, H2A.Z can be deposited at inactive genes.

Another region we examined is the highly regulated mating-type specific gene *AGA2*. In yeast, a-specific genes (asgs) such as *AGA2* have been well studied and are known to be active in *MATa* strains, but extremely tightly repressed by the α2-Mcm1 complex in *MATα* and *MATa*/α strains (*47*). We utilized isogenic strains harboring the chromosomal HA_3-*HTZ1* allele and differing only in the allele present at the mating type locus (*MAT*a or *MAT*α. Using ChIP and QPCR, we observed a peak of H2A.Z signal at *AGA2* in *MATa* and its continued presence in *MAT*α strains (Figure 4C). Although well above those seen in the ORF of the *BUD3* gene (Figure 4C), H2A.Z levels were approximately two-fold lower at the repressed *AGA2* locus compared to the

active locus even though promoter histone H3 signals were similar in a versus α cells (Figure 4C and Figure 9). Previous work showed that asg promoters display relative hypoacetylation on the histone H4 tails in *MAT*α strains relative to *MAT*a strains (*48*)**.** We performed ChIP using antibodies raised against a tetra-acetylated peptide derived from the N-terminal tail of histone H4 (Ac_4H4), and confirmed this result—an approximately two-fold reduction of acetylation was observed in the *MAT*α strains (Figure 4D). Interestingly, both the positioning and relative level of acetylation in a versus α cells closely parallels those of HA_3-*HTZ1* at *AGA2*, suggesting potential interplay between acetylation and H2A.Z deposition. Finally, we identified two genes involved in mating in the microarray data that have been shown not to be expressed under vegetative conditions: *FIG2* and *PRM1*. Previous work has shown that expression of these genes only occurs in response to mating pheromone (*49*), (*50*). Analysis of H2A.Z enrichment at these loci revealed peaks in their promoter regions (Figure 11).

Effect of gene induction on H2A.Z levels: activation of *FIG1* by mating pheromone

Our analysis revealed no correlation between H2A.Z levels normalized for nucleosome density and transcription rates or RNA polymerase II occupancies, suggesting no general relationship between transcription and H2A.Z levels. As described in the Introduction, previous studies of H2A.Z levels at *GAL1* and *PHO5* promoters revealed that it decreased upon gene induction, although whether this represented exchange of H2A.Z for H2A or general

nucleosome depletion was not determined. In contrast, we observed that while the inactive *AGA2* promoter contains H2A.Z, its levels are higher when the gene is active.

To extend these results, we examined H2A.Z and H3 levels at a gene that is highly inducible by mating pheromone, *FIG1* (*49*). As shown in Figure 12, *FIG1* expression is dependent on mating pheromone—treatment of cells with mating pheromone strongly induced mRNA accumulation over a one hr. time course as determined by quantitative RT-PCR. ChIP analysis revealed that H2A.Z is depleted during gene induction. However, H3 was also depleted from the *FIG1* promoter during the time course such at the 5, 15 , and 30 min. time points, the ratio of H2A.Z to H3 was constant (Figure 12). At the 60 min. time point, an apparent depletion of H2A.Z relative to H3 was observed; however, it seems likely that the promoter H3 signal at this time point was elevated as an artifact of signal from flanking nucleosomes that were not separated by sonication from the promoter nucleosomes prior to ChIP (Figure 12). The H2A.Z signal would not be subject to this problem since H2A.Z nucleosomes are distributed in a punctate pattern whereas H3-containing nucleosomes are distributed homogenously. Thus, with the possible exception of this late time point, activation of *FIG1* results in nucleosome loss rather than the specific replacement of H2A.Z with H2A.

Histone tail acetylation is required for efficient recruitment of H2A.Z

We performed a reporter-based genome-wide screen of the *S. cerevisiae*

knockout collection to identify genes that antagonize the spread of silencing from the *HMR*a silent mating type cassette (R.M.R. and H.D.M., unpublished observations). This screen identified Eaf1, a nonessential component of the essential NuA4 HAT complex and the bromodomain-containing proteins, Bdf1 and Bdf2. Bdf1 is a component of the Swr1 complex responsible for H2A.Z deposition, and both Bdf1 and Bdf2 bind to acetylated histone tails (*38*), (*39*). To test whether histone acetylation is important for H2A.Z deposition, we generated strains bearing the HA_3-*HTZ1* allele containing deletions of the genes encoding the H4-specific histone acetyltransferase (HAT) Eaf1 or the H3- and H4-specific HAT Elp3. In addition, we created a strain lacking both HATs. ChIP analysis revealed a dependence upon histone tail acetylation for robust H2A.Z enrichment (Figure 5A). At a majority of loci examined, deletion of *EAF1* resulted in a reproducible defect in H2A.Z levels. The defects varied from approximately 1.5- to 3-fold in magnitude. Likewise, deletion of *ELP3* also led to a defect at most loci, albeit more quantitatively modest than those of the *eaf1* mutant. The severity of the defects in the *eaf1 elp3* double mutant is not significantly greater than either of the single deletions (Figure 5A), suggesting Eaf1 and Elp3 may act in the same pathway to mediate H2A.Z deposition.

To further test the role of histone acetylation in H2A.Z deposition, we utilized a series of histone H3 and H4 mutants in which specific target lysine residues have been mutated to arginine which prevents acetylation. We observed a consistent quantitative defect in H2A.Z enrichment values at most of the 10 loci examined (Figure 5B, Figure 5C). In general, the strongest defects

were observed in cells harboring the H3-K9R mutant or the H4-K5R,K12R mutant. For the H4-K5R,K12R mutant, we performed ChIP using antibodies against H3 as well and found no differences in nucleosome density at the loci examined in Figure 5C, indicating that the defect in H2A.Z deposition was not caused by general nucleosome loss (Figure 13). Surprisingly, a deletion mutant in the H4 tail displayed a less severe defect than the H4-K5R,K12R mutant (Figure 5C). The H4-K8R,K16R mutant displayed no defect, indicating that not all mutants in acetylatable tail lysines produce a defect in H2A.Z deposition (Figure 5C).

Bdf1 and Bdf2 act redundantly to promote H2A.Z deposition

Having established a role for histone tail acetylation for complete H2A.Z deposition, we hypothesized that acetylation could be acting to recruit targeting of the Swr1 complex via binding of its subunit Bdf1 to acetylated tails. This is an attractive model because in addition to being important for anti-silencing, Bdf1 is known to bind preferentially to acetylated forms of histone H4, and is enriched in intergenic regions throughout the genome (*51*). However, ChIP analysis using polyclonal Htz1 antibody raised against the C-terminal tail region showed that a *bdf1* strain has little or no defect in H2A.Z enrichment at euchromatic loci (Figure 5E). We reasoned that this could be due to compensatory activity by the redundant gene *BDF2*, which when deleted yielded no detectable defect in H2A.Z enrichment (data not shown). Unfortunately, *bdf1*Δ *bdf2*Δ strains are inviable, precluding a test of this hypothesis using null alleles. Therefore, we

elected to generate a “knockdown” allele of *BDF2* by replacing its 3’ UTR region with a MX6 marker cassette. This maneuver has been found to consistently cause destabilization of the cognate mRNA (J. Weissman, pers. comm.). We refer to this allele as *bdf2-utr*Δ *,* and as is the case for the *bdf2*Δ , it also has no defect for H2A.Z enrichment (data not shown). As seen by tetrad dissection, the *bdf1 bdf2-utr*Δ double mutants grow more slowly than either single mutant, indicating a defect produced by *bdf2-utr*Δ (Figure 5D). Examining these strains by ChIP, we found that although *bdf1* cells showed little or no defects in H2A.Z deposition, the *bdf1 bdf2-utr* displayed a reproducible defect in H2A.Z deposition at a majority of loci examined (Figure 5E), while no defect was observed in the ORF of the control locus *PRP8*. These experiments clearly demonstrate a dependence on Bdf1 and its redundant homolog Bdf2 for full H2A.Z deposition at the 5’ regions of genes. However, since acetylation of promoter nucleosomes generally correlates with transcription (*52*), the requirement for Bdf1/2 and histone tail acetylation for efficient deposition of H2A.Z does not explain how it can be deposited at inactive genes in euchromatin.

Mutagenesis of the *SNT1* promoter reveals sequences necessary for H2A.Z deposition in vivo.

One hypothesis for how H2A.Z is deposited at inactive as well as active genes is that there exist specific DNA elements in promoters that program its deposition. Although there is no precedent for a DNA element that specifically induces variant histone deposition, we decided to pursue this model by

systematically mutagenizing a typical promoter that contains two positioned H2A.Z nucleosomes (Figure 14). For this analysis, we chose to analyze the *SNT1* promoter region described in Figure 1 because it was well separated from nearby promoters by the relatively large *BPH1* and *SNT1* ORFs.

To localize sequences required for H2A.Z deposition, we divided the *BPH1-SNT1* intergenic region into 75 bp segments and then precisely replaced each segment in the chromosome with a 75 bp fragment of the bacterial cloning vector pBluescript (Figure 14). Mutants in either of two adjacent intervals (termed 5 and 6 in Fig. S7) resulted in a modest two-fold reduction in H2A.Z enrichment (Fig. S7). However, a mutant that replaced both intervals resulted in a dramatic defect in H2A.Z enrichment (Figure 14). Interestingly, these two intervals roughly correspond to the nucleosome-free region between the two H2A.Z nucleosomes that lie upstream of the *SNT1* gene. RT-QPCR analysis of *SNT1* expression revealed only a two-fold drop in *SNT1* mRNA levels (unpublished observations). These data suggested the presence of partially redundant signals for H2A.Z deposition in intervals 5 and 6.

To further define these signals, we constructed 14 additional substitution mutants in the NFR of the *SNT1* promoter (Figure 6A). For these mutants, we replaced varying segments within intervals 5 and 6 with identical-sized segments from the ORF of *BUD3*, which lacks H2A.Z depositon (Figure 1). We examined H2A.Z deposition using primers that span the two flanking positioned H2A.Z nucleosomes. Of the 14 mutants tested only two, *mu1* and *mu3*, abolished H2A.Z enrichment (Figure 6A). The sequences replaced in *mu3* represent a

subset of those in *mu1*, defining the minimal segment that must be mutated to produce a complete loss of H2A.Z deposition in the *SNT1* promoter. Substitution of smaller segments resulted in increased H2A.Z enrichment. For example, *mu4* has the identical 5' endpoint as *mu3* but substitutes 10 fewer bp on the 3' end and displays robust H2A.Z enrichment (Figure 6A). These 10 bp are therefore critical for H2A.Z deposition in the context of *mu3*. Likewise, *mu10* substitutes 20 bp fewer than *mu3* on the 5' end and shows increased H2A.Z enrichment (Figure 6A), indicating that there are sequences that promote H2A.Z deposition in the 20 bp that distinguish *mu3* from *mu10*. We note that for mutants that display an intermediate level of H2A.Z deposition, our analysis does not distinguish between a decrease in H2A.Z deposition versus a shift in the position of the H2A.Z nucleosomes. Nonetheless, our identification of mutants that eliminate H2A.Z deposition in this region suggest that the segments identified play a role in deposition per se. Taken together, these data suggest the presence of two redundant signals for H2A.Z deposition, one that includes the 10 bp that distinguishes *mu3* from *mu4* and another that includes the 20 bp that distinguishes *mu3* from *mu10*.

A 22 bp segment from the *SNT1* promoter is sufficient to induce the formation of a NFR flanked by two H2A.Z nucleosomes

Our analysis of sequences necessary for H2A.Z deposition at the promoter of *SNT1* identified two discrete regions. We next tested whether these regions also sufficient to promote H2A.Z deposition at a novel site. To date, we

have not succeeded in identifying a fragment containing the 20 bp 5' region that is sufficient to promote H2A.Z deposition. Therefore, we focus below on a signal that contains the 3' 10 bp segment hypothesized above to contain a H2A.Z deposition signal.

A magnified view of this 10 bp sequence and flanking sequences is shown in Figure 6B. Two notable features of this sequence are a binding site for the general regulatory factor Reb1 and an adjacent tract of seven dT:dA base-pairs. Both sequence elements are disrupted in *mu3* compared to *mu4*. Moreover, previous studies had shown that a similar arrangement of sequences in the yeast *PFY1* promoter was important for the formation of a NFR in that promoter (*53*). Therefore, we tested whether a DNA segment containing this region could generate an NFR flanked by H2A.Z nucleosomes when placed elsewhere in the genome.

We inserted the 22 bp segment containing the Reb1 site and $(dT:dA)_7$ tract at an arbitrarily chosen site in the middle of an inactive gene, *PRM1* (Figure 7A). *PRM1* was selected because it had been shown previously to only be expressed in cells exposed to mating pheromone, and we sought to avoid the potentially complicating effects of transcription on H2A.Z deposition (*50*). Examination of H2A.Z deposition using probes flanking the insertion site revealed robust H2A.Z enrichment in the strain containing the insertion (Figure 7B). Replacement of the three G residues in the Reb1 consensus site abolished the effect of the insertion as did a deletion of the $(dT:dA)_7$ tract.

To determine whether an NFR was induced by the insertion, we

performed nucleosome scanning analysis (*54*) to determine the positions of nucleosomes containing H3 and H2A.Z in the parental strain and the strain containing the insertion. As described in the Experimental Procedures, crosslinked mononucleosomes were immunoprecipitated with antibodies to either H3 or H2A.Z and then analyzed by QPCR analysis using primer pairs that amplified 100 bp segments every 20 bp across the *PRM1* ORF. As shown in Figure 7C, five nucleosomes containing histone H3 were found in the *PRM1* ORF in the parental strain. The arrow in Figure 6C indicates the site of insertion, which was in the center of the +4 nucleosome. The 22 bp insert had two effects on the nucleosome pattern (Figure 7D). First it caused a delocalization of nucleosome pattern in the first part of the *PRM1* ORF. Second it results in a formation of an NFR. This can be deduced by examining the peak-to-peak distance of nucleosomes flanking the insertion site, which is 320 bp in the strain containing the insertion versus 180 bp between the center points of the +3 and +4 nucleosomes in the parental strain. Assuming that 147 bp of DNA is wrapped by the yeast histone octamer, one calculates that the insertion caused an expansion of the linker region between these two nucleosomes from approximately 33 bp to 173 bp.

We next determined the positions of H2A.Z nucleosomes in the parental and insertion strains. As shown in Figure 7E, little H2A.Z enrichment was observed in ORF of the *PRM1* gene in the parental strain, as expected. Strikingly, insertion of the 22 bp segment from the *SNT1* gene resulted in the appearance of two positioned variant H2A.Z nucleosomes (Figure 7F).

Moreover, the peaks were separated by 320 bp, confirming the formation of an NFR in the insertion strain (Figure 7F). Finally, we examined histone H4 acetylation in the *PRM1* ORF in the strain containing the insertion and found no difference compared to wild type (unpublished observations), indicating that this DNA signal functions in distinct pathway from acetylation and Bdf1.

Discussion

Our results show that nucleosomes containing the conserved histone variant H2A.Z occur in euchromatin in a highly organized rather than a random pattern. In particular, the experiments decisively demonstrate that H2A.Z is selectively present at the vast majority of gene promoter regions. Most commonly, it occurs as two positioned nucleosomes that flank a NFR that includes the transcription initiation site. The most striking finding is that H2A.Z enrichment is uncorrelated with transcription rates and is observed at promoters of genes that are not detectably transcribed. The implications of this observation are potentially far-reaching, as it indicates that cells can identify the 5' ends of genes in the absence of ongoing transcription. We describe two mechanisms that begin to provide insight into how this remarkable pattern of histone variant deposition occurs. Analysis of the *SNT1* promoter resulted in the identification of a 22 bp bipartite DNA element sufficient to promote H2A.Z deposition when placed in a novel context. This signal contains two necessary elements that are generally conserved in yeast promoters: a binding site for the Myb-related general regulatory factor Reb1 and an $(dT:dA)_7$ tract. In addition,

we demonstrated that H2A.Z deposition is linked to histone acetylation and Bdf1, a double bromodomain protein that binds acetylated histone tails.

H2A.Z nucleosomes mark the 5' ends of both active and inactive genes in euchromatin

Our results provide the first single nucleosome-resolution global picture of the deposition pattern of a conserved histone variant. Alignment of the microarray data based on the identified nucleosome-free regions (NFR) of yeast promoters that includes the transcription initiation site (*8*) revealed that most euchromatic genes contain two positioned H2A.Z nucleosomes which flank the NFR. Our analysis to date cannot distinguish whether these each nucleosomes contain two copies of H2A.Z, or one copy of H2A.Z and one copy of H2A. However, it has been suggested based on structural analysis that heteromeric H2A.Z/H2A nucleosomes may be unable to form due to steric clash (*55*). Because one of the two H2A.Z nucleosomes is typically downstream of the initiation site of transcription and one is not, it is unlikely that passage of RNA polymerase alone plays a role in either depositing or removing H2A.Z nucleosomes in general. Indeed, a small group of genes contains only the downstream H2A.Z nucleosome (Figure 2B). It is not yet obvious why these genes differ in their deposition pattern. Consistent with our previous data that indicated the exclusion of H2A.Z nucleosomes from the *HMRa* silent mating type cassette, the microarray analysis (which was performed in a mating type a strain) reveals an exclusion of H2A.Z from the *HML*α silent cassette and from

subtelomeric regions.

Most strikingly, we find that the levels of deposition of H2A.Z in promoters are clearly not correlated with either the transcription rate or RNA polymerase II occupancy of the linked coding sequences (Figure 4). This is in contrast to modifications such as trimethylation of lysine 4 of histone H3 in yeast, which does correlate with transcription rate and typically occurs on the first nucleosomes downstream of the transcription initiation site (*56*), (*57*), (*58*)**.** Indeed, our analysis of genes that are not transcribed and/or tightly repressed demonstrated enrichment of H2A.Z in their promoters. These include two meiotic gene pairs examined in haploid cells in rich media, the a-specific gene *AGA2* assayed in α cells, and two genes only expressed in pheromone treated cells, *FIG2* and *PRM1,* that were assessed in the absence of pheromone. Although we cannot rule out the possibility that H2A.Z deposition occurs at these genes in response to rare transcription events that produce mRNAs that fail to detectably accumulate, a simpler interpretation of our data is that cells have a transcription independent mechanism to specify H2A.Z deposition at the 5' ends of genes.

Although H2A.Z can be deposited at inactive genes, our data suggests that transcription can modulate H2A.Z levels in at least two ways. First, at *AGA2*, we observed higher H2A.Z levels when the gene was active than when it was inactive. Second, at *FIG1*, we observed that activation resulted in concomitant depletion of H2A.Z and H3, consistent with the removal of variant octamers. Since the relative levels of H2A.Z and transcription are uncorrelated when considering large numbers of genes (Figure 3), it seems likely that transcription

modulates the relative amounts of H2A.Z variant nucleosomes differently at different genes. Further work will be needed to define the relationships between transcription and H2A.Z promoter marking. Nonetheless, our results demonstrate that for cells to identify the 5' ends of genes and deposit H2A.Z, genes need not be transcribed.

Histone tail acetylation and Bdf1 promote deposition of H2A.Z

Our genetic experiments led us to investigate the potential connection between histone tail acetylation and H2A.Z deposition. ChIP analyses demonstrated that for various defects in histone tail acetylation, whether produced by mutation of acetylated lysines or deletion of genes encoding histone acetyltransferases, there is a moderate decrease in H2A.Z at most sites assayed. The quantitative rather than qualitative defect in H2A.Z deposition in these mutant backgrounds may reflect either a partial dependence on histone tail acetylation for deposition or that histone acetylation was only partially eliminated in our experiments. Distinguishing between these two possibilities is not trivial since the H3 and H4 N-terminal tails are together essential for viability (*59*). Moreover, cells lacking the catalytic subunit of the NuA4 HAT and cells lacking both the Gcn5 and Sas3 HATs are inviable (*60*), (*61*). We also note that the in vivo deposition assays used here do not measure the rate of H2A.Z deposition. Therefore, the modest defects observed in acetylation mutants at steady-state may reflect a more profound defect in the rate of deposition, especially if one considers that as few as one exchange event at a nucleosome per cell cycle

might be sufficient to produce wild-type levels of H2A.Z.

We find that the bromodomain proteins Bdf1 and Bdf2 act redundantly to promote H2A.Z deposition. Bdf1 is a subunit of both the Swr1 complex that deposits H2A.Z in vivo and is also associated with TFIID. Because Bdf1 contains two bromodomains and selectively binds acetylated versions of histone H4, we suggest that Bdf1 recognition of acetylated histone tails promotes recruitment of the Swr1 complex and deposition of H2A.Z. In vitro studies of the purified Swr1 complex and acetylated nucleosomal substrates will be required to confirm this model. It is notable that the H4-K8R, K16R mutation did not affect H2A.Z deposition: recent work has shown that deacetylation of H4-K16 is actually necessary for the association of Bdf1 with chromatin in vivo (*51*). Consistent with these observations, recent studies of histone acetylation patterns at the mononucleosome level demonstrated that the two nucleosomes flanking the NFR have a unique acetylation pattern (*52*). In particular, these nucleosomes are both highly deacetylated on H4-K8 and 16, and this deacetylation domain occurs independently of transcription level, thereby precisely paralleling the H2A.Z localization pattern presented here. Moreover, the nucleosome downstream of the NFR is acetylated on H3-K9,14 and H4-K5,12. It is unlikely to be coincidental that lysine-to-arginine mutation of the residues that are deacetylated on the NFR-flanking nucleosomes does not affect H2A.Z deposition, while mutation of acetylated residues inhibits H2A.Z deposition (Table 1). Together with the data showing that Bdf1 binding to chromatin is inhibited by H4-K16 acetylation, these results are consistent with a direct role for Bdf1 in recognizing the acetylation

patterns of the NFR-flanking nucleosomes to promote H2A.Z deposition. However, since acetylation of nucleosome downstream of the NFR correlates with transcription rates (Liu et al., 2005), efficient deposition of H2A.Z at highly deacetylated inactive promoters must involve mechanisms that would not in principle depend on ongoing transcription.

Identification of a bipartite DNA signal sufficient to induce H2A.Z deposition

We have defined one such mechanism, namely the existence of DNA signals that program H2A.Z deposition. Our analysis of the *SNT1* promoter revealed two segments of DNA that appear to function redundantly since mutations in two segments with the NFR were necessary to eliminate H2A.Z deposition. We showed that the 3' signal, which contains a site for the Myb-related general regulatory factor Reb1 and an adjacent $(dT:dA)_7$ tract, was sufficient to induce the formation of an NFR and the replacement of H2A with H2A.Z in the two flanking nucleosomes when placed into the middle of the coding sequence of inactive *PRM1* gene. Both the Reb1 site and $(dT:dA)_7$ motif were found to be necessary for H2A.Z deposition.

Reb1 was originally identified as an abundant nuclear protein involved in rDNA transcriptional termination but was subsequently shown to associate with a large number of yeast promoter regions (*62*). Recent studies of the conservation of the Reb1 DNA binding motif have shown that it is the single most conserved motif found in yeast promoters and is even more conserved across species than

the TATA box (*63*). Several studies have shown that tethering of Reb1 or related Myb-family general regulatory factors (Rap1, Abf1, or Tbf1) to DNA can prevent the spread of silent chromatin but the mechanism remains unknown (*64*), (*65*). Given our results, it could be that this property of these factors involves the induction of a NFR and/or the deposition of H2A.Z nucleosomes. Consistent with this possibility, there is a near match to the Abf1 binding consensus in the region of the *SNT1* NFR that contains the 5' signal for H2A.Z deposition (unpublished observations).

The second motif that we found to be important for H2A.Z deposition is a tract of dT:dA base pairs which have been noted to be common in yeast promoters, particularly in NFRs (*8*). Studies of global nucleosome density have also shown that the abundance of motifs containing dT:dA tracts correlate with nucleosome depletion from promoters (*66*), (*67*). These studies concluded that promoters show transcription-independent reductions in nucleosome density compared coding sequences, but this conclusion has been questioned on technical grounds (*68*). Our study is relevant to this issue as it shows the functional importance of an element containing a dT:dA tract flanked by a site for Reb1 in the formation of NFR. Our data may also be relevant to the recent proposal that dT:dA tracts promote the formation of NFRs in vivo because of their intrinsic nucleosome excluding properties in vitro (*54*). Although further work is necessary to understand how it functions, it seems unlikely that a sequence as short as 22 bp could act to program the formation of an ~170 bp NFR purely because of its intrinsic properties.

Although both Reb1 sites and dA:dT tracts are common features of yeast promoters, we do not yet know whether this is the sole type of DNA element that programs H2A.Z deposition at promoters. As mentioned above, other Myb-related factors might also be expected to play a role. A previous study identified a Reb1 site and an adjacent dA:dT tract in the NFR in the promoter of the yeast *PFY1* gene (*53*). This work showed that mutation of the Reb1 site eliminated the NFR; the role of the adjacent dA:dT tract was not assessed. Thus, it may be that Reb1 is generally important for the formation of NFRs in promoters. This raises the question of whether Reb1 promotes H2A.Z deposition and NFR formation through independent or coupled mechanisms. Our preliminary studies show that deletion of *HTZ1* or *SWR1* does not prevent the formation of the NFR in the strain containing the 22 bp insertion into *PRM1* (unpublished observations). Thus, the 22 bp element either promotes NFR formation and H2A.Z independently (e.g. via recruitment of different factors) or the formation of the NFR itself induces H2A.Z deposition. Regardless of the specific mechanisms involved, our studies indicate that DNA- and histone-based mechanisms allow cells to mark the 5' ends of genes and preserve their euchromatic state.

Experimental Procedures

Yeast Strains

Strains used in these studies are described in Table 2.

Mapping DNA sequences necessary for H2A.Z deposition

Chromosomal mutations were created as described (*69*). Heterologous sequences used are described in Table 3. Different sequences were used in Figure 14 and Figure 6 to ensure that the results were not dependent on the particular sequence used to replace *SNT1* sequences.

Galactose induction of HA-Htz1 Expression

Cultures were grown at 30°C. Strains bearing an HA_3 epitope-tagged allele of *HTZ1* driven by the *GAL1* promoter at the endogenous *HTZ1* locus were grown to saturation in YPAD, then diluted to an A_{600} of 0.1, and outgrown in YEP containing 2% glucose to an A_{600} of 0.6. 50 mL of the cultures were cross-linked and harvested. The remaining cells were washed twice in water and added to YEP containing 2% galactose and 2% raffinose to an approximate A_{600} of 0.001 and grown for 2 days. These cultures were then back diluted to fresh YEP containing 2% galactose and 2% raffinose to an A_{600} OD of 0.1 and grown to an A_{600} of 0.6, cross-linked and harvested. 3 absorbance units were harvested from each and analyzed by immunoblotting with antibodies against H2A.Z.

Induction of *FIG1* by mating pheromone

A wild-type *MAT***a** strain was grown in YPAD at 30°C overnight, diluted to an A_{600} of 0.1 and grown to an A_{600} of 0.6. 30 OD units were crosslinked and harvested for ChIP, and 3 OD units were harvested for total RNA isolation and RT-QPCR analysis of transcript levels using gene-specific primers for *FIG1* and *ACT1*. The remaining culture was split 4 ways and α−factor was added to a

concentration of 10 μM to each and grown to the appropriate time point (5 min., 15 min., 30 min. or 1 hr.), whereupon 30 and 3 OD of cells respectively were harvested as described above for ChIP and RT-QPCR analysis.

Mononucleosome preparation for microarray and nucleosome scanning experiments.

Mononucleosomes were preparared as described (*52*).

Chromatin Immunoprecipitation.

ChIP procedures were as in Meneghini et al. (2003) except for microarray and nucleosome scanning experiments, which were performed as described by Liu et al. (2005) and Sekinger et al (2005), respectively.

High density microarray tiling analysis of H2A.Z deposition profile.

The yeast strain used was BY4741. Hybridization and analysis was performed as described (*52*).

Table 1. Comparison of histone tail acetylation patterns at NFR-flanking nucleosomes and residues required for H2A.Z deposition

Modification	Present at NFR-flanking nucleosomes? (*52*)	Required for H2A.Z deposition?
Ac-H3-K9	Yes	Yes
Ac-H3-K14	Yes	Yes
Ac-H4-K5	Yes	Yes[a]
Ac-H4-K8	No	No
Ac-H4-K12	Yes	Yes[a]
Ac-H4-K16	No	No

[a]Based on H4-K5,12 double muant

Table 2. Strains used in the Chapter 2 study

Strain ID	Genotype
YM2113	*ura3-52, trp1-1 GAL2+*
YM1844	*his3Δ,leu2Δ,ura3Δ,lys2Δ,htz1Δ::HA3-HTZ1*
YM2114	*htz1Δ::HA3-HTZ1,lys2Δ,hht1hhf1::LEU2,hht1hhf1::LEU2,hht2hhf2::HIS3,HHT2HHF2-URA3-CEN,ade2Δ,trp1Δ,ura3Δ,leu2Δ,his3Δ,pWZ414-F12-TRP1-CEN*
YM2115	*htz1Δ::HA3-HTZ1,lys2Δ,hht1hhf1::LEU2,hht1hhf1::LEU2,hht2hhf2::HIS3,HHT2HHF2-URA3-CEN,ade2Δ,trp1Δ,ura3Δ,leu2Δ,his3Δ,pWZ414-F14-TRP1-CEN*
YM2116	*htz1Δ::HA3-HTZ1,lys2Δ,hht1hhf1::LEU2,hht1hhf1::LEU2,hht2hhf2::HIS3,HHT2HHF2-URA3-CEN,ade2Δ,trp1Δ,ura3Δ,leu2Δ,his3Δ,pWZ414-F15-TRP1-CEN*
YM2117	*htz1Δ::HA3-HTZ1,lys2Δ,hht1hhf1::LEU2,hht1hhf1::LEU2,hht2hhf2::HIS3,HHT2HHF2-URA3-CEN,ade2Δ,trp1Δ,ura3Δ,leu2Δ,his3Δ,pWZ414-F43-TRP1-CEN*

YM2118	*htz1Δ::HA3-HTZ1,lys2Δ,hht1hhf1::LEU2,hht1hhf1::LEU2,hht2hhf2::HIS3,HHT2HHF2-URA3-CEN,ade2Δ,trp1Δ,ura3Δ,leu2Δ,his3Δ,pWZ414-F49-TRP1-CEN*
YM2119	*htz1Δ::HA3-HTZ1,lys2Δ,hht1hhf1::LEU2,hht1hhf1::LEU2,hht2hhf2::HIS3,HHT2HHF2-URA3-CEN,ade2Δ,trp1Δ,ura3Δ,leu2Δ,his3Δ,pWZ414-F52-TRP1-CEN*
YM2120	*htz1Δ::HA3-HTZ1,lys2Δ,hht1hhf1::LEU2,hht1hhf1::LEU2,hht2hhf2::HIS3,HHT2HHF2-URA3-CEN,ade2Δ,trp1Δ,ura3Δ,leu2Δ,his3Δ,pWZ414-F53-TRP1-CEN*
YM2121	*ura3Δ,his3Δ,leu2Δ,eaf1Δ::KanMXΔ,met15Δ,LYS2+,htz1Δ::HA3-HTZ1*
YM2122	*ura3Δ,his3Δ,leu2Δ,elp3Δ::KanMXΔ,met15Δ,LYS2+,htz1Δ::HA3-HTZ1*
YM2123	*ura3Δ,his3Δ,leu2Δ,elp3Δ::KanMXΔ,eaf1Δ::KanMX,met15Δ,LYS2+,htz1Δ::HA3-HTZ1*
YM2124	*ura3Δ,his3Δ,leu2Δ,met15Δ,lys2Δ,htz1Δ::HA3-HTZ1*
YM2125	*ura3Δ,his3Δ,leu2Δ,met15Δ,lys2Δ,htz1Δ::HA3-HTZ1*
YM2126	*his3Δ/his3Δ,leu2Δ/leu2Δ,met15Δ/MET,lys2Δ/LYS2,ura3Δ/ura3Δ,bdf1Δ::HygMX/BDF1,BDF2/bdf2Δ-utr::NatMX*
YM2128	*his3Δ,leu2Δ,lys2Δ,ura3Δ*
YM2129	*his3Δ,leu2Δ,lys2Δ,ura3Δ*

YM2130	*his3Δ,leu2Δ,lys2Δ,ura3Δ*
YM2131	*his3Δ,leu2Δ,LYS2,ura3Δ,bdf1::HygMX*
YM2132	*his3Δ,leu2Δ,LYS2,ura3Δ,bdf1::HygMX*
YM2133	*his3Δ,leu2Δ,lys2Δ,ura3Δ,bdf1::HygMX*
YM2134	*his3Δ,leu2Δ,lys2Δ,ura3Δ,bdf2Δ-utr::NatMX*
YM2135	*his3Δ,leu2Δ,LYS2,ura3Δ,bdf2Δ-utr::NatMX*
YM2136	*his3Δ,leu2Δ,LYS2,ura3Δ,bdf2Δ-utr::NatMX*
YM2139	*his3Δ,leu2Δ,LYS2,ura3Δ,bdf2Δ-utr::NatMX,bdf1::HygMX*
YM2141	*his3Δ,leu2Δ,LYS2,ura3Δ,bdf2Δ-utr::NatMX,bdf1::HygMX*
YM2143	*his3Δ,leu2Δ,LYS2,ura3Δ,bdf2Δ-utr::NatMX,bdf1::HygMX*

Table 3. Primers used to tile the *PRM1* ORF to generate the data shown in Figure 7C-F

Locus	Forward Primer (5'-3')	Reverse Primer (5'-3')
0	GACATCTCCAAAATAATCAATAAAG	TGATTGACGACGTCATGTTACTGTC
20	TAAAGTGATCAAGGCCGCATCCAAA	TATGGTTAAGTTGACGCTTTTGATT
40	CCAAAGTAGAGAATTTTTTCACAGG	TATAAATTGTGAAGCGCAGATATGG
60	ACAGGTGATGACGATGACAGTAACA	CGTTGATTGAGGAAGGAATGTATAA
80	TAACATGACGTCGTCAATCAAAAGC	CGATAACTCTTCAAGCTTATCGTTG
100	AAAGCGTCAACTTAACCATATCTGC	GCAAAGTCCGGCGTCTTTGCCGATA
120	TCTGCGCTTCACAATTTATACATTC	TGGTTGTATTCTTAACCTGGGCAAA
140	CATTCCTTCCTCAATCAACGATAAG	GGGAACCGAGATCAGGTTCTTGGTT
160	ATAAGCTTGAAGAGTTATCGGC	TTCTTCCGAACTTCATTGAAGG

	AAA	GAA
	GCAAAGACGCCGGACTTTGCC	TGGCATTCACGGCCTTGATATT
180	CAGG	CTT
	CCAGGTTAAGAATACAACCAAG	GGTATCTCCGATTATATTGCTG
200	AAC	GCA
	AGAACCTGATCTCGGTTCCCTT	GGAGGTACGTACAAAACGGAG
220	CAA	GTAT
	TTCAATGAAGTTCGGAAGAATA	TACTGTTGTCAAGGGACACGG
240	TCA	GAGG
	TATCAAGGCCGTGAATGCCAG	ATTGGATGAGCAAATCCCAGTA
260	CAAT	CTG
	GCAATATAATCGGAGATACCTC	AAGGCCAAAATTTCTGATTGAT
280	CGT	TGG
	TCCGTTTTGTACGTACCTCCCG	CATGTCCCAAGATGGAATAAAA
300	TGT	GGC
	CGTGTCCCTTGACAACAGTACT	TACGGTGGCTATTTTCAGGACA
320	GGG	TGT
	CTGGGATTTGCTCATCCAATCA	ATCAATACGGTAATGCACACTA
340	ATC	CGG
	CAATCAGAAATTTTGGCCTTTTA	TCGCACCAACAGCGAAGCATAT
360	TT	CAA
380	TTATTCCATCTTGGGACATGTC	ATTCCATGCAACGGGCGCCATC

	CTG	GCA
	TCCTGAAAATAGCCACCGTAGT	CGCCTCCAGAGCTTGATTTCAT
400	GTG	TCC
	GTGTGCATTACCGTATTGATAT	GGTCTCTCATTCCGCAAAGGCG
420	GCT	CCT
	ATGCTTCGCTGTTGGTGCGATG	TTGCCTGCTCAGCATGTAATGG
440	GCG	TCT
	TGGCGCCCGTTGCATGGAATG	GAAAAGGACGTATACGAATCTT
460	AAAT	GCC
	GAAATCAAGCTCTGGAGGCGC	ATTCGTGCGTGTTTTCACTGGA
480	CTTT	AAA
	CCTTTGCGGAATGAGAGACCAT	ATCTCTAAATGGATCTTTCAATT
500	TAC	CG
	ATTACATGCTGAGCAGGCAAGA	TGGCCATTTTGTATAGGAGGAT
520	TTC	CTC
	GATTCGTATACGTCCTTTTCCA	AGCTTGCAATGACATCATATTG
540	GTG	GCC
	CAGTGAAAACACGCACGAATTG	TGTTTGAAAGCACTGCTGATAG
560	AAA	CTT
	TGAAAGATCCATTTAGAGATCC	CCTGCTATTCTTGTGTTCCATG
580	TCC	TTT
600	CCTCCTATACAAAATGGCCAAT	TAACAAGATTTGTCATCCAGCC

	ATG	TGC
	ATATGATGTCATTGCAAGCTAT	CTCTGGTGATTTTCCAAAGGTA
620	CAG	ACA
	ATCAGCAGTGCTTTCAAACATG	TTAGTCTTTGGGTCAATGTTCT
640	GAA	CTG
	TGGAACACAAGAATAGCAGGCT	CTACCCATTCTATTTTTTGTTTA
660	GGA	GT
	CTGGATGACAAATCTTGTTACC	TTCGGAGGTCATATAAGCCACT
680	TTT	ACC
	CCTTTGGAAAATCACCAGAGAA	CCAAGAACACACAGTGCTCTTT
700	CAT	CGG
	AACATTGACCCAAAGACTAAAC	AAATTCCCAAAAGTCCAATTCC
720	AAA	AAG
	ACAAAAAATAGAATGGGTAGTG	AAATTGGCATATGCACACTAAA
740	GCT	ATT
	TGGCTTATATGACCTCCGAAAG	TTTAACAGTGCTATCATGACAA
760	AGC	ATT
	AGAGCACTGTGTGTTCTTGGAA	ATGAATGGCTTATCTTGTGTTTT
780	TTG	AA
	AATTGGACTTTTGGGAATTTTA	GTCACCATCATTAGAAGTCAAT
800	GTG	GAA
820	TAGTGTGCATATGCCAATTTGT	TTCAGCAAATTTTGAACGCCGT

CAT CAC

GTCATGATAGCACTGTTAAAAC TATCGACGGCAGTGCTAGACTT

840 ACA CAG

ACACAAGATAAGCCATTCATTG AAGGCTCATTTGGTTCTCTATAT

860 ACT CG

TGACTTCTAATGATGGTGACGG TTATTAGTCTGAACGCTCCAAA

880 CGT GGC

GGCGTTCAAAATTTGCTGAAGT TCTCCGTAGTATTTATATATTTA

900 CTA TT

GTCTAGCACTGCCGTCGATATA TACTTCCTGATTGATATTGGTCT

920 GAG CC

TAGAGAACCAAATGAGCCTTTG GTCGTGTTTATCCACCCGAATA

940 GAG CTT

Figure 1. H2A.Z enrichment in euchromatin

A. Schematic of *HA_3-HTZ1* ChIP enrichment across Chromosome III. Bars represents IP/WCE value as determined by QPCR for a single 300 bp segment. Each 5' primer is separated by 1000 bp.

B. Log scale graph comparing H2A.Z enrichment values to distance to the nearest initiation codon. The correlation coefficient is 0.2662.

C. Diagram of the *BPH1-SNT1* interval assayed by ChIP and QPCR for *HA_3-HTZ1* deposition. Enrichment values are average IP/WCE ratios from triplicate samples with standard error of the mean (SEM) error bars. Vertical dashed lines are drawn through each gene's initiation codon. X-axis values are the chromosomal coordinates of the 5' primers of each pair used.

D. Same as C, except data for the *LEU2-YCL012c* interval are shown.

Figure 1

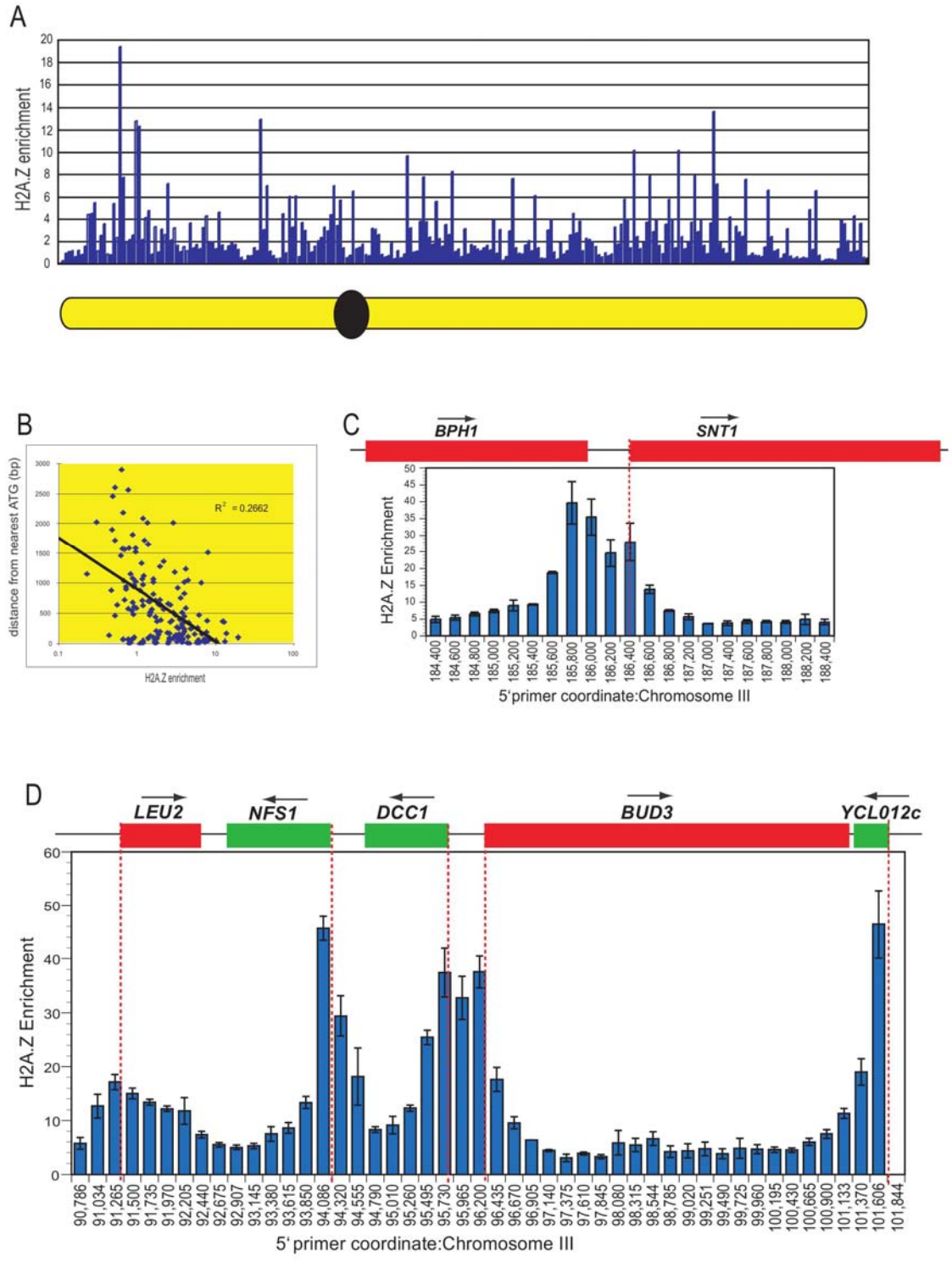
A
H2A.Z enrichment
B
distance from nearest ATG (bp)
R² = 0.2662
H2A.Z enrichment
C
BPH1
SNT1
H2A.Z Enrichment
5'primer coordinate:Chromosome III
D
LEU2
NFS1
DCC1
BUD3
YCL012c
H2A.Z Enrichment
5' primer coordinate:Chromosome III

Figure 2. High resolution mapping of H2A.Z nucleosomes

Shown is a color depiction of ratio of the ChIP signal for mononucleosomal DNA immunoprecipitated using anti-Htz1 antibodies divided by those for DNA extracted from mononucleosomes for regions covered by a high-resolution oligonucleotide tiling microarray.

A. H2A.Z enrichment in representative euchromatic regions analyzed in Figure 1C and Figure 1D. Shown are the data for five replicate microarray hybridizations. Yellow represents a positive relative enrichment for H2A.Z over the median enrichment versus blue for negative enrichment.

B. Clustered array dataset centered on nucleosome free regions (NFRs) of gene promoters. Shown are data from probes from up to 1 kb upstream and 1 kb downstream of the position of the NFR estimated from previous studies (*8*). Each row represents a single promoter region and columns correspond to data from microarray oligonucleotides at a given position with respect to the NFR.

Figure 2

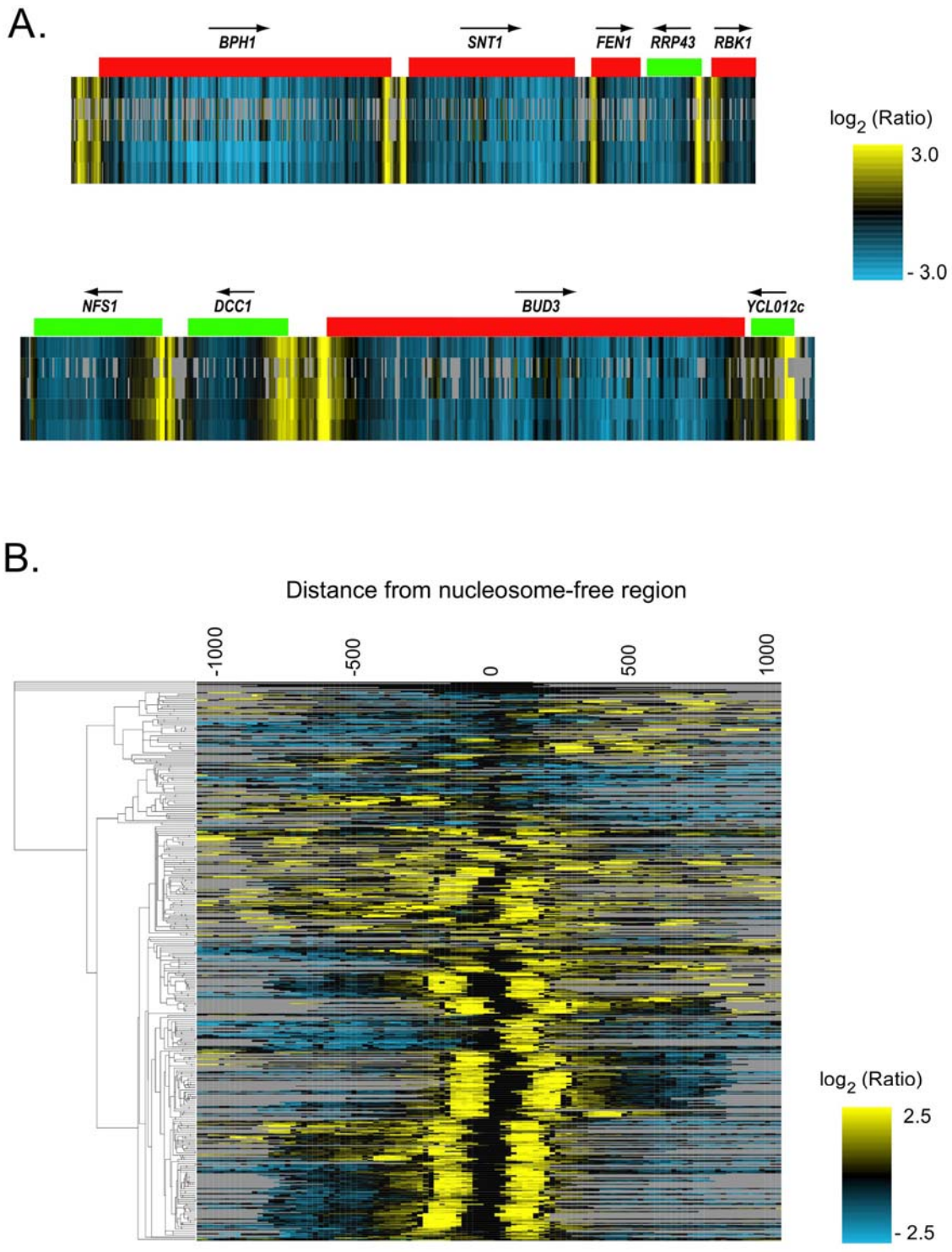
A.
BPH1
SNT1
FEN1
RRP43
RBK1
log2 (Ratio)
3.0
- 3.0
NFS1
DCC1
BUD3
YCL012c
B.
Distance from nucleosome-free region
-1000
-500
0
500
1000
log2 (Ratio)
2.5
- 2.5

Figure 3. Comparison of H2A.Z enrichment normalized for nucleosome density with transcription rate and RNA polymerase II occupancy

A. Transcription rates are plotted against H2A.Z enrichment values for nucleosomes downstream of the NFR.
B. RNA polymerase II occupancy values as determined by ChIP are plotted against H2A.Z enrichment values for nucleosomes downstream of the NFR.
C. Same as in A, except H2A.Z enrichment values represent nucleosomes upstream of the NFR.
D. Same as in B, except H2A.Z enrichment values represent nucleosomes upstream of the NFR.

Figure 3

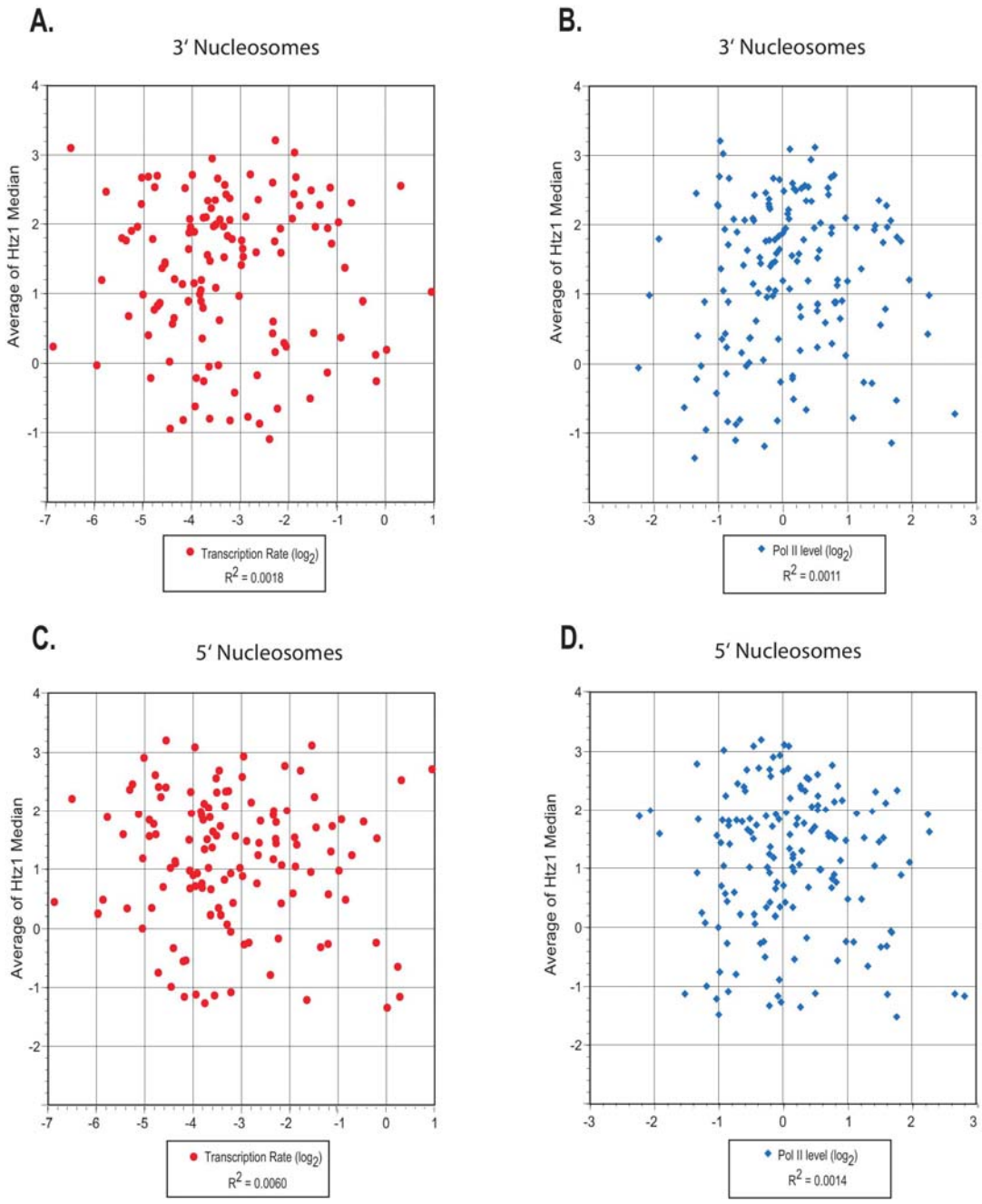
A.
3′ Nucleosomes
Average of Htz1 Median
Transcription Rate (log2)
R2 = 0.0018
B.
3′ Nucleosomes
Average of Htz1 Median
Pol II level (log2)
R2 = 0.0011
C.
5′ Nucleosomes
Average of Htz1 Median
Transcription Rate (log2)
R2 = 0.0060
D.
5′ Nucleosomes
Average of Htz1 Median
Pol II level (log2)
R2 = 0.0014

Figure 4. H2A.Z enrichment at meiosis-specific and a-specific genes

All enrichment values are triplicate averages of *HA_3-HTZ1* or Ac_4H4 ChIP DNA amounts normalized to the *BUD3* ORF region with SEM error bars. Sidebars show *BUD3* and *SGF29* (positive control) loci.

A. *HA_3-HTZ1* enrichment at the *DIT1/DIT2* promoter and ORF regions. QPCR fragments are for consecutive 200 bp segments; dashed lines are drawn through translation initiation sites to their approximate relative position.
B. Same as in A, except data are shown for the *HOP1/SPO22* region.
C. *HA_3-HTZ1* normalized enrichment at *AGA2* for *MAT***a** and *MAT*α strains. QPCR probes correspond to consecutive 100 bp segments with the position of the 5' primer relative to the initiation codon of *AGA2* denoted.
D. Same as in C, except enrichment values represent Ac_4H4.

Figure 4

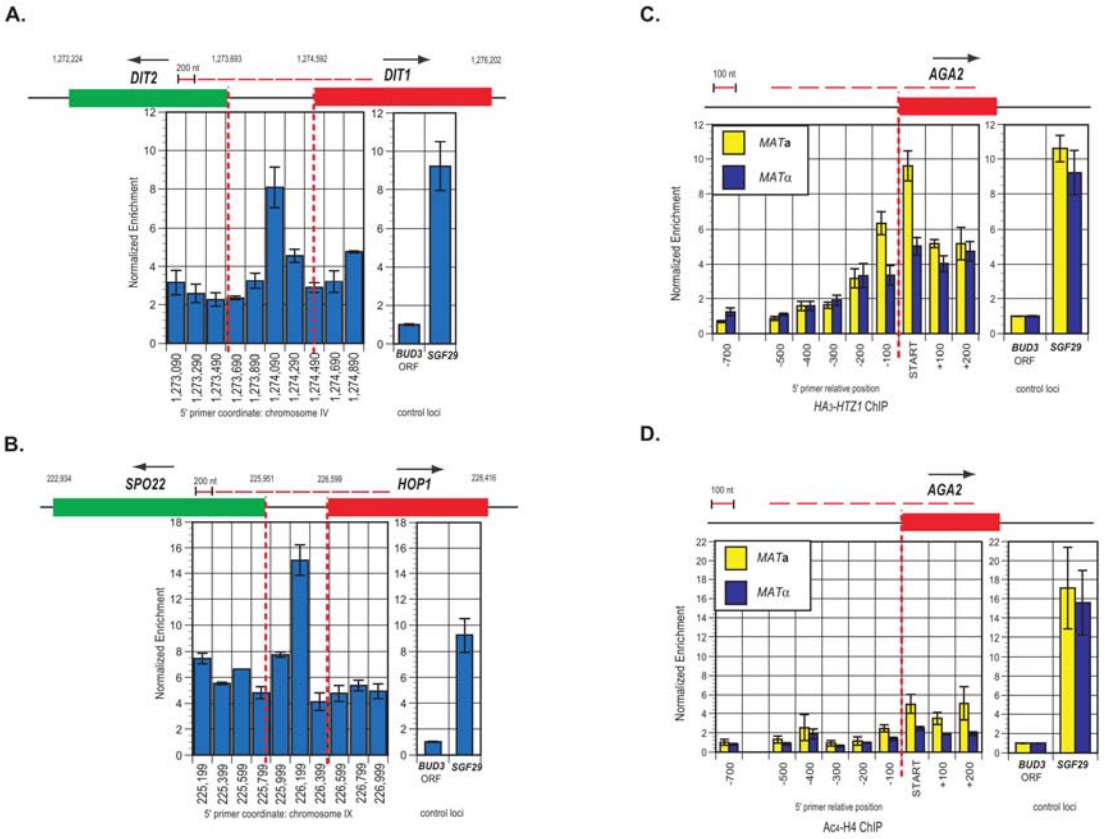
A.
DIT2
DIT1
Normalized Enrichment
BUD3
SGF29
ORF
5' primer coordinate: chromosome IV
control loci
B.
SPO22
HOP1
Normalized Enrichment
BUD3
SGF29
ORF
5' primer coordinate: chromosome IX
control loci
C.
AGA2
MATa
MATα
Normalized Enrichment
START
5' primer relative position
HA3-HTZ1 ChIP
control loci
D.
AGA2
MATa
MATα
Normalized Enrichment
START
5' primer relative position
Ac4-H4 ChIP
control loci

Figure 5. ChIP analysis of H2A.Z enrichment at selected euchromatic promoters in wild-type, histone acetylation-defective mutants and bdf1Δ mutants

For A-C, data shown are averages of triplicate enrichment ratios of indicated mutants relative to wild-type. Y-axis is on log scale and error bars are SEM.

A. HAT mutants relative to wild-type
B. Histone H4 mutants relative to wild-type
C. Histone H3 mutants relative to wild-type
D. Tetrad analysis of meiotic products of *BDF1*/*bdf1 BDF2*/*bdf2-utr* heterozygous diploids. Genotypes of first column of spores are shown. Their phenotypes are representative.
E. Quadruplicate normalized average H2A.Z enrichment values for mutant compared to wild-type with SEM error bars.

Figure 5

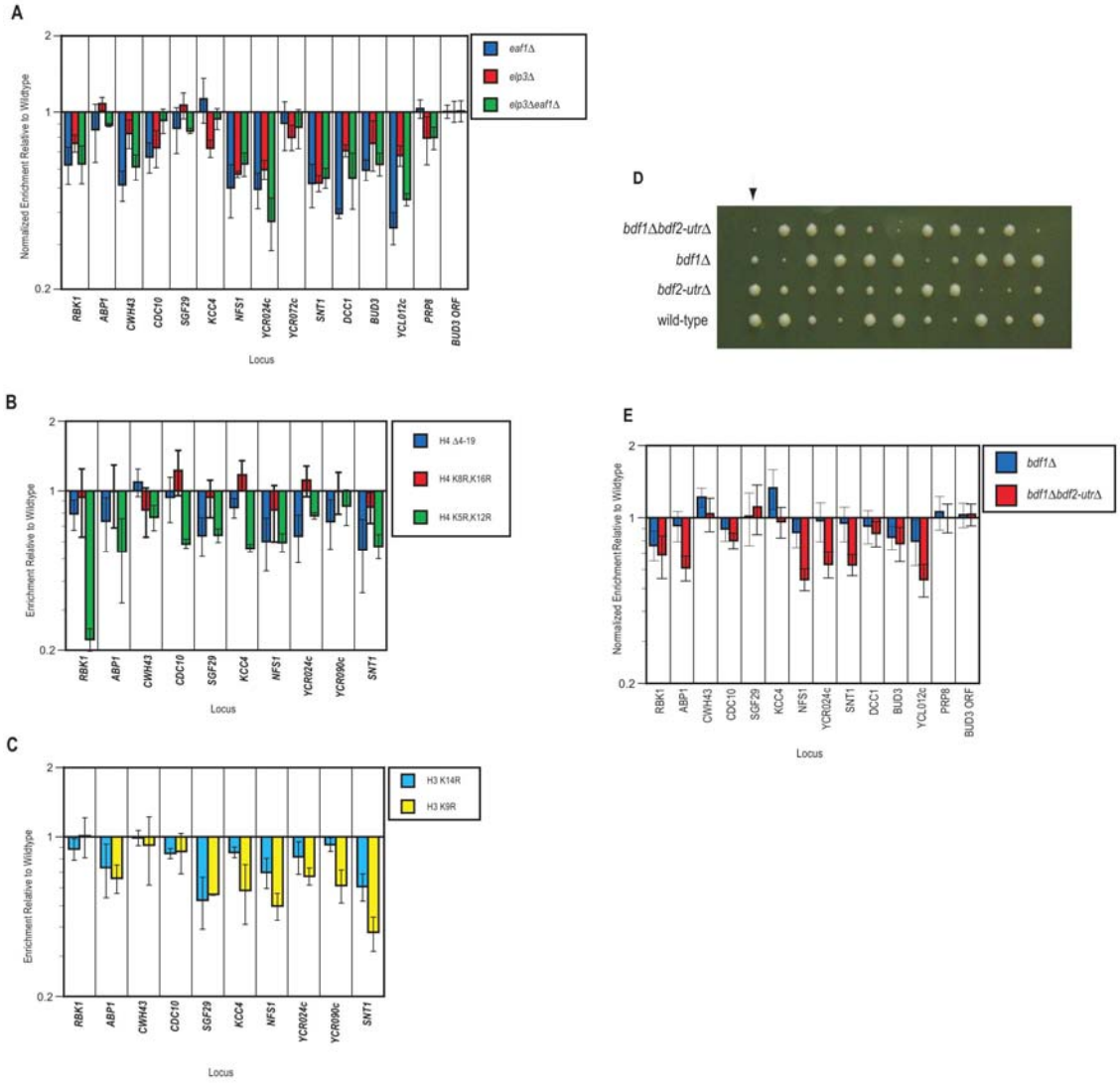
A
eaf1Δ
elp3Δ
elp3Δeaf1Δ
Normalized Enrichment Relative to Wildtype
Locus
RBK1
ABP1
CWH43
CDC10
SGF29
KCC4
NFS1
YCR024c
YCR072c
SNT1
DCC1
BUD3
YCL012c
PRP8
BUD3 ORF
B
H4 Δ4-19
H4 K8R,K16R
H4 K5R,K12R
Enrichment Relative to Wildtype
C
H3 K14R
H3 K9R
D
bdf1Δbdf2-utrΔ
bdf1Δ
bdf2-utrΔ
wild-type
E
bdf1Δ
bdf1Δbdf2-utrΔ

Figure 6. High-resolution substitution mutagenesis of the BPH1-SNT1 intergenic region defines sequence for H2A.Z deposition in vivo

A. Summary of substitution mutants. Shown is the *SNT1-BPH1* interval and microarray data from Figure 2 showing the position of the two H2A.Z nucleosomes that lie in the *SNT1* promoter region. The regions defined as intervals 5 and 6 in Figure 14 were subjected to further mutagenesis. Shown are the sequences that were replaced with heterologous sequences (Table 3). Mutants are designated *mu1-mu14*. To the right are shown the normalized H2A.Z enrichments as determined by standard ChIP and QPCR. Experiments were performed in triplicate. Mean values and their standard errors are displayed.

B. Detail of 3' signal identified by substitution mutagenesis of interval 5. Shown is wild-type sequence corresponding to the right end of interval 5 (underlined in A). Consensus DNA binding site for Reb1 is shown; residues shown in large font are invariant (*70*). Adjacent dT:dA tract is indicated in blue. Shown below are right endpoints of the *mu3* and *mu4* mutants from A and their H2A.Z deposition levels. Substituted sequences are indicated by dashes.

Figure 6

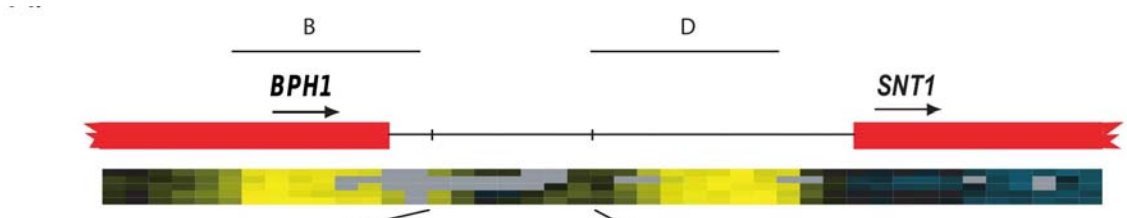

GTTTATATCTTTACTTTTGAAACTGATTTCTCATCCCATCTAGTATTGTAATTGCGTACGTATCCAATATCATTACCAACGCCGGGTATTTTTTTCTAGTA

GTTTATATCTTTACTTTTGAAACTGATTTCTCATCCCATCTAGTATTGTAATTGCGTACGTATCCAATATCATTACCAACGCCGGGTATTTTTT

GTTTATATCTTTACTTTTGAAACTGATTTCTCATCCCATCTAGTATTGTAATTGCGTACGTATCCAATATCATTACCAACGCC

TTTACTTTTGAAACTGATTTCTCATCCCATCTAGTATTGTAATTGCGTACGTATCCAATATCATTACCAACGCCGGGTATTTTTT

TTTACTTTTGAAACTGATTTCTCATCCCATCTAGTATTGTAATTGCGTACGTATCCAATATCATTACCAACGCC

TTTACTTTTGAAACTGATTTCTCATCCCATCTAGTATTGTAATTGCGTACGTATCCAATATCATT

TTTACTTTTGAAACTGATTTCTCATCCCATCTAGTATTGTAATTGCGTACGTATC

TTTACTTTTGAAACTGATTTCTCATCCCATCTAGTATTGTAATTG

AAACTGATTTCTCATCCCATCTAGTATTGTAATTGCGTACGTATCCAATATCATTACCAACGCCGGGTATTTTTT

AAACTGATTTCTCATCCCATCTAGTATTGTAATTG

CTCATCCCATCTAGTATTGTAATTGCGTACGTATCCAATATCATTACCAACGCCGGGTATTTTTT

CTCATCCCATCTAGTATTGTAATTG

CTAGTATTGTAATTG

CTAGTATTGT

AATTG

Strain	H2A.Z Deposition B	D
mu1	0.96 ±0.08	1.62 ± 0.15
mu2	4.76 ±0.83	5.72 ± 0.76
mu3	0.89 ±0.08	1.32 ±0.10
mu4	7.46 ±0.43	12.38 ±0.63
mu5	6.97 ±0.21	17.16 ± 1.12
mu6	5.50 ±0.47	11.63 ±1.25
mu7	5.27 ± 0.29	15.69 ±3.43
mu8	2.05 ± 0.05	3.92 ± 0.18
mu9	7.64 ±1.32	6.78 ± 0.64
mu10	3.98 ± 0.28	9.89 ±1.31
mu11	4.85 ± 0.05	11.65 ± 2.57
mu12	7.64 ± 0.43	11.17 ± 0.71
mu13	5.96 ± 0.36	9.65 ± 0.94
mu14	6.13 ± 0.51	12.50 ± 1.21
WT	13.25 ±1.05	9.75 ± 0.73
htz1Δ	1.06 ±0.14	1.49 ± 0.02

B.

Strain	Reb1 cGGGTAA	H2A.Z Deposition B	D
WT	CAACGCCGGGTATTTTTTTCTAGTA	13.25 ±1.05	9.75 ± 0.73
mu3	----------GGGTATTTTTTTCTAGTA	0.89 ±0.08	1.32 ±0.10
mu4	----------TCTAGTA	7.46 ±0.43	12.38 ±0.63

Figure 7. A 22 bp bipartite DNA sequence from the *SNT1* promoter sufficient to direct the deposition of two H2A.Z nucleosomes and the formation of a nucleosome-free region

A. Experimental Design. Shown is the sequence from the *SNT1* promoter and its arbitrarily chosen site of insertion in the *PRM1* ORF. PCR probes used in B are indicated.

B. Demonstration that 22 bp element from *SNT1* promoter is sufficient to promote H2A.Z deposition: standard ChIP analysis. Shown are the normalized H2A.Z enrichment values for the indicated probes for a wild-type strain and three isogenic strains containing either the 22 bp insertion shown in A, a GGG→TAA mutant in the Reb1 site, or a mutant that precisely deletes the T tract. Experiments were performed in triplicate. Mean values and standard errors are displayed.

C. Nucleosome scanning analysis of histone H3 positions in the *PRM1* ORF in wild-type cells. Shown is the analysis of mononucleosomes immunoprecipitated using an anti-H3 antibodies. Plotted is a four-window moving average for two replicate experiments (thin red and green lines) and their averages (thick black line). The moving average is plotted such that the first datapoint is relative to position 30, which is the center of the window. Indicated below are deduced positions of nucleosomes. Also marked is the site of the 22 bp insertion from the *SNT1* promoter, which was placed into the middle of the +4 nucleosome. Peak-to-peak distance between the two nucleosomes flanking the site of insertion is indicated.

D. Nucleosome scanning analysis of histone H3 positions in the *PRM1* ORF in cells containing the 22 bp insertion. Strain containing the insertion was analyzed as in C. Peak-to-peak distance between the two nucleosomes flanking the site of insertion is indicated.

E. Nucleosome scanning analysis of histone H2A.Z positions in the *PRM1* ORF in wild-type cells. Mononucleosomal material from the indicated strains was immunoprecipitated with anti-H2A.Z antibodies and analyzed as in C.

F. Nucleosome scanning analysis of histone H2A.Z positions in the *PRM1* ORF in cells containing the 22bp insertion. Mononucleosomal material from the indicated strains was immunoprecipitated with anti-H2A.Z antibodies and analyzed as in C. Peak-to-peak distance between the two nucleosomes flanking the site of insertion is indicated.

Figure 7

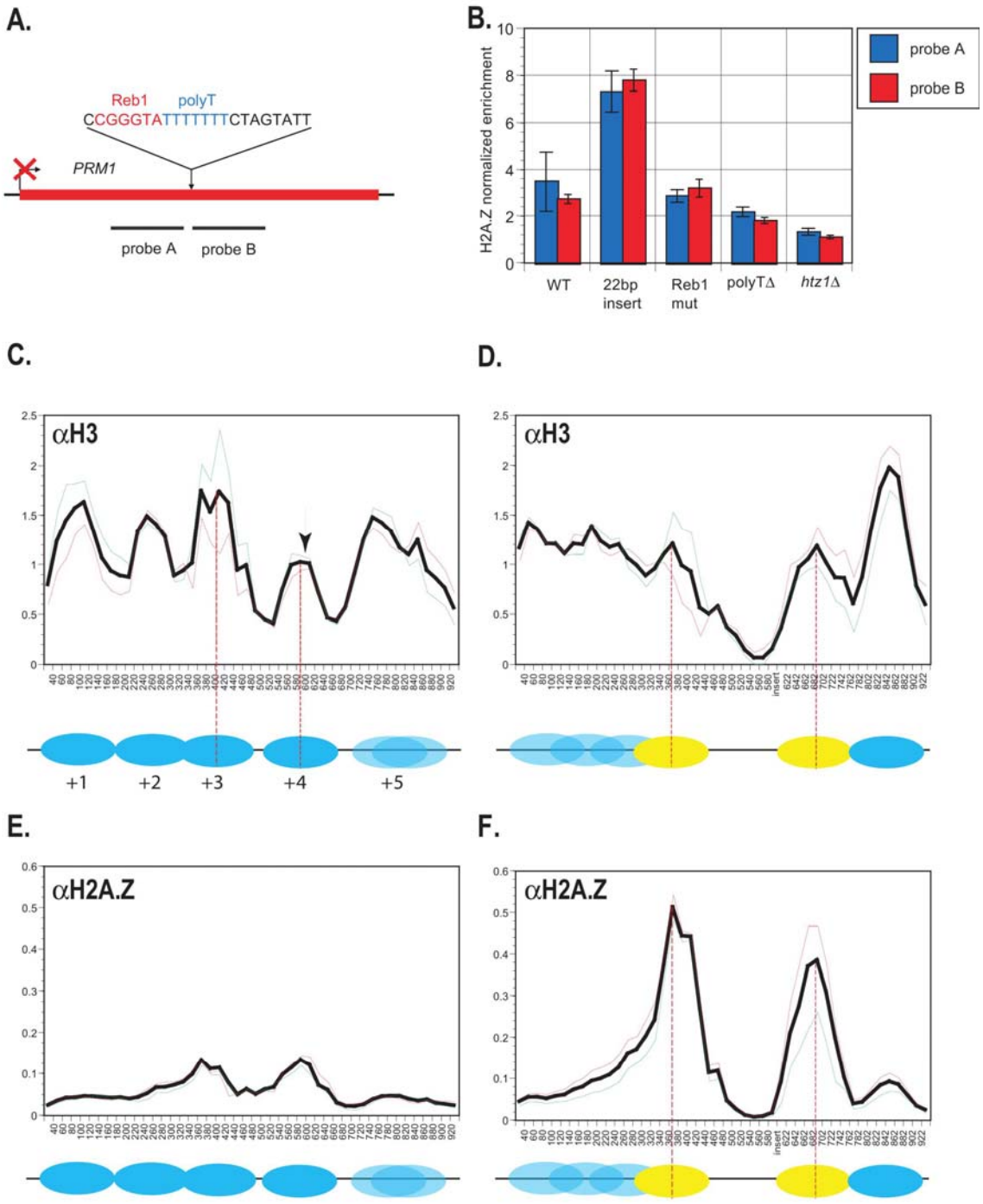
A.
Reb1
polyT
CCGGGTATTTTTTTCTAGTATT
PRM1
probe A
probe B
B.
H2A.Z normalized enrichment
probe A
probe B
WT
22bp insert
Reb1 mut
polyTΔ
htz1Δ
C.
αH3
+1
+2
+3
+4
+5
D.
αH3
E.
αH2A.Z
F.
αH2A.Z

Figure 8. Comparison of H2A.Z and H3 enrichment in the *LEU2-YCL012c* interval

Shown is a diagram of the *LEU2-YCL012c* interval with ChIP enrichment data for unmodified anti-H3 (blue) and anti-Htz1 (red). Enrichment values are average IP/WCE ratios from triplicate samples with standard error of the mean (SEM) error bars. Boxes represent genes encoded on the Watson strand (red), and the Crick strand (green) with arrows denoting the direction of transcription. Vertical dashed lines are drawn through each gene's initiation codon. X-axis values are the chromosomal coordinates of the 5' primers of each pair used.

Figure 8

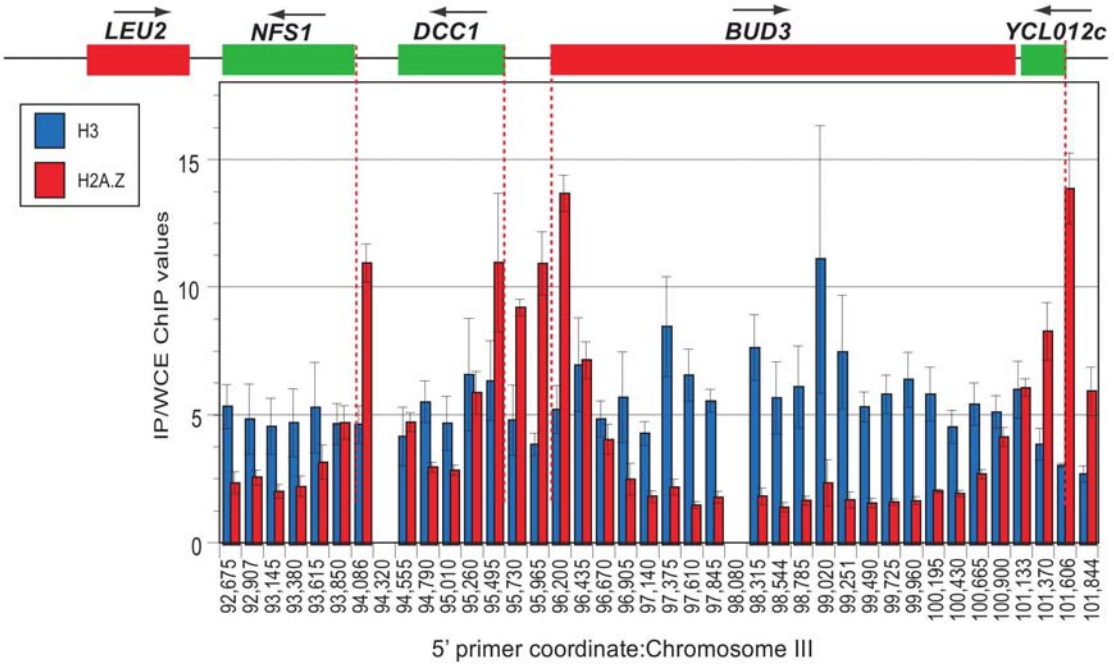
LEU2
NFS1
DCC1
BUD3
YCL012c
H3
H2A.Z
IP/WCE ChIP values
0
5
10
15
92,675
92,907
93,145
93,380
93,615
93,850
94,086
94,320
94,555
94,790
95,010
95,260
95,495
95,730
95,965
96,200
96,435
96,670
96,905
97,140
97,375
97,610
97,845
98,080
98,315
98,544
98,785
99,020
99,251
99,490
99,725
99,960
100,195
100,430
100,665
100,900
101,133
101,370
101,606
101,844
5' primer coordinate:Chromosome III

Figure 9. ChIP analysis of H3 enrichment at meiosis-specific and a-specific genes

All enrichment values are triplicate averages of unmodified anti-H3 ChIP DNA amounts normalized to the *BUD3* ORF region for the meiosis loci, or the *PRP8* ORF for *AGA2*, with SEM error bars.

A. H3 enrichment at the *DIT1/DIT2* promoter and ORF regions. QPCR fragments are for consecutive 200 bp segments; dashed lines are drawn through translation initiation sites to their approximate relative position.
B. H3 enrichment at the *HOP1/SPO22* promoter. Experimental setup is as in (A).
C. anti-H3 normalized enrichment at *AGA2* for *MAT***a** and *MAT*α strains. QPCR fragments are for consecutive 100 bp segments with the position of the 5' primer relative to the initiation codon of *AGA2* denoted.

Figure 9

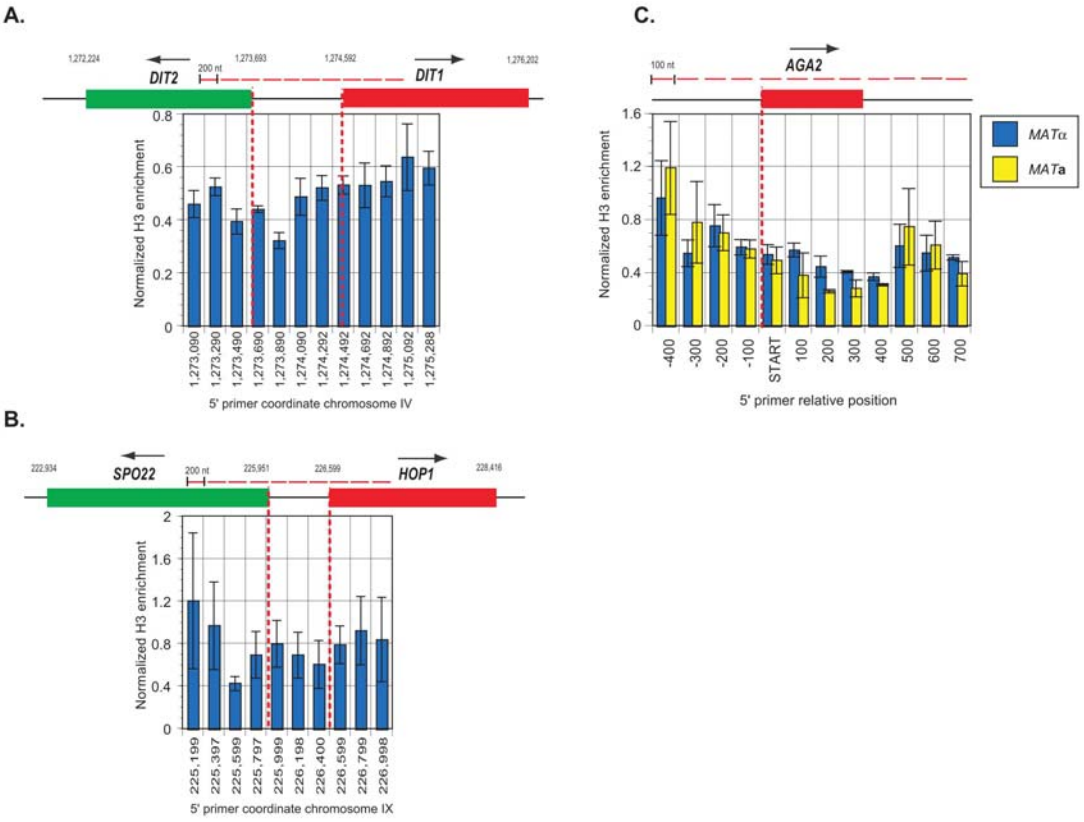
A.
1,272,224
DIT2
200 nt
1,273,693
1,274,592
DIT1
1,276,202
Normalized H3 enrichment
0
0.2
0.4
0.6
0.8
1,273,090
1,273,290
1,273,490
1,273,690
1,273,890
1,274,090
1,274,292
1,274,492
1,274,692
1,274,892
1,275,092
1,275,288
5' primer coordinate chromosome IV
B.
222,934
SPO22
200 nt
225,951
226,599
HOP1
228,416
Normalized H3 enrichment
0
0.4
0.8
1.2
1.6
2
225,199
225,397
225,599
225,797
225,999
226,198
226,400
226,599
226,799
226,998
5' primer coordinate chromosome IX
C.
100 nt
AGA2
Normalized H3 enrichment
0
0.4
0.8
1.2
1.6
MATα
MATa
-400
-300
-200
-100
START
100
200
300
400
500
600
700
5' primer relative position

Figure 10. ChIP analysis of galactose-inducible HA3-HTZ1 enrichment at meiosis-specific genes

All values are triplicate averages of HA_3-Htz1 ChIP DNA amounts (IP/WCE) with SEM error bars. Sidebars show IP/WCE ratios for *BUD3* ORF and *BUD3* promoter.

A. HA_3-Htz1 enrichment at the *DIT1/DIT2* promoter and ORF regions. QPCR fragments are for consecutive 200 bp segments; dashed lines are drawn through translation initiation sites to their approximate relative position.
B. HA_3-Htz1 enrichment at the *HOP1/SPO22* promoter and ORF regions. Experimental setup is as in A.
C. Immunoblot for HA_3-Htz1 protein levels for inducing (galactose) and repressing condition (glucose), showing tubulin loading control.

Figure 10

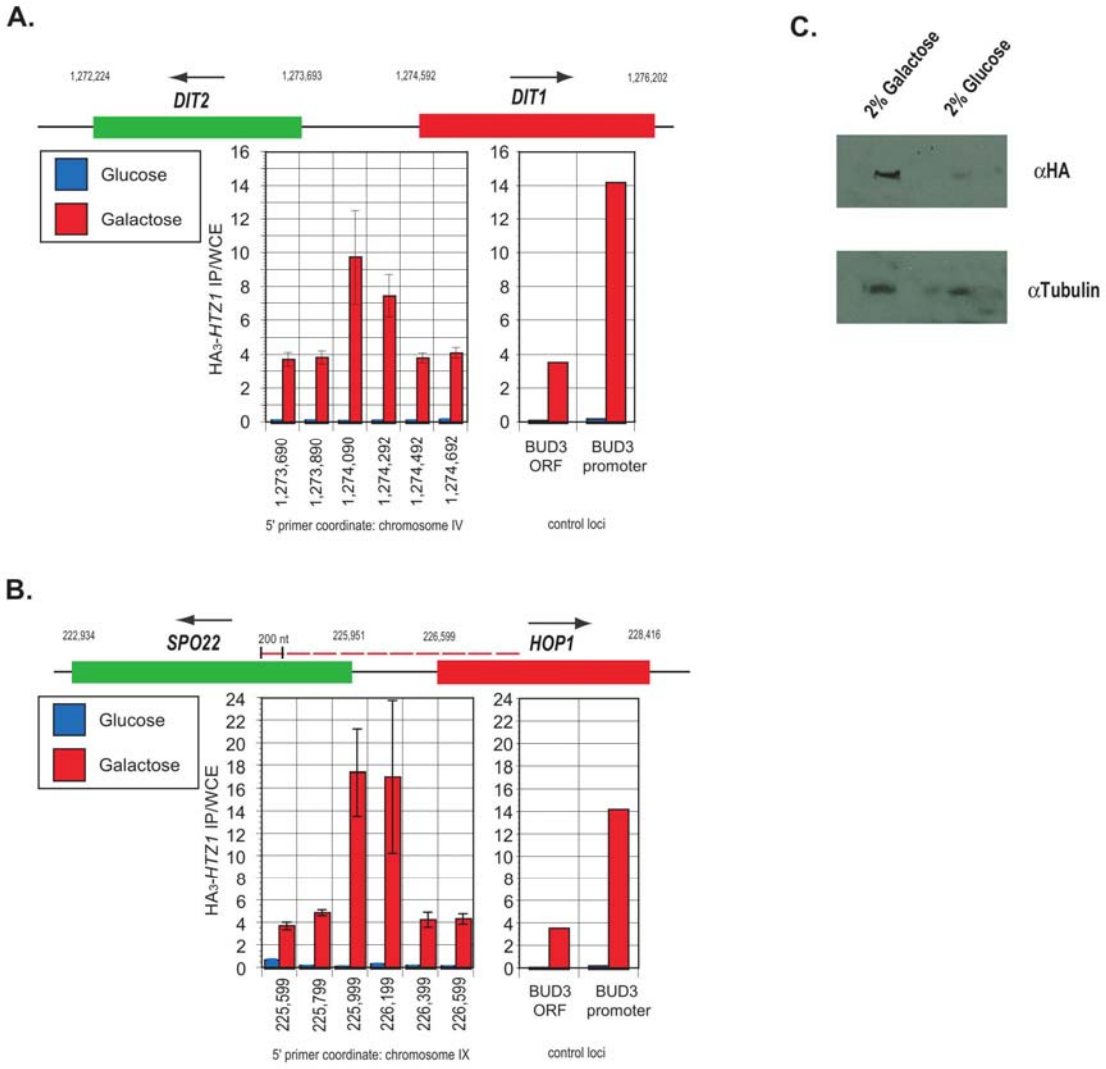
A.
1,272,224
DIT2
1,273,693
1,274,592
DIT1
1,276,202
Glucose
Galactose
HA3-HTZ1 IP/WCE
1,273,690
1,273,890
1,274,090
1,274,292
1,274,492
1,274,692
5' primer coordinate: chromosome IV
BUD3 ORF
BUD3 promoter
control loci
B.
222,934
SPO22
200 nt
225,951
226,599
HOP1
228,416
Glucose
Galactose
HA3-HTZ1 IP/WCE
225,599
225,799
225,999
226,199
226,399
226,599
5' primer coordinate: chromosome IX
BUD3 ORF
BUD3 promoter
control loci
C.
2% Galactose
2% Glucose
αHA
αTubulin

Figure 11. Microarray data for *FIG2* and *PRM1* regions

Shown are data for five ChIP-chip experiments using anti-H2A.Z antibody for the indicated gene loci.

Figure 11

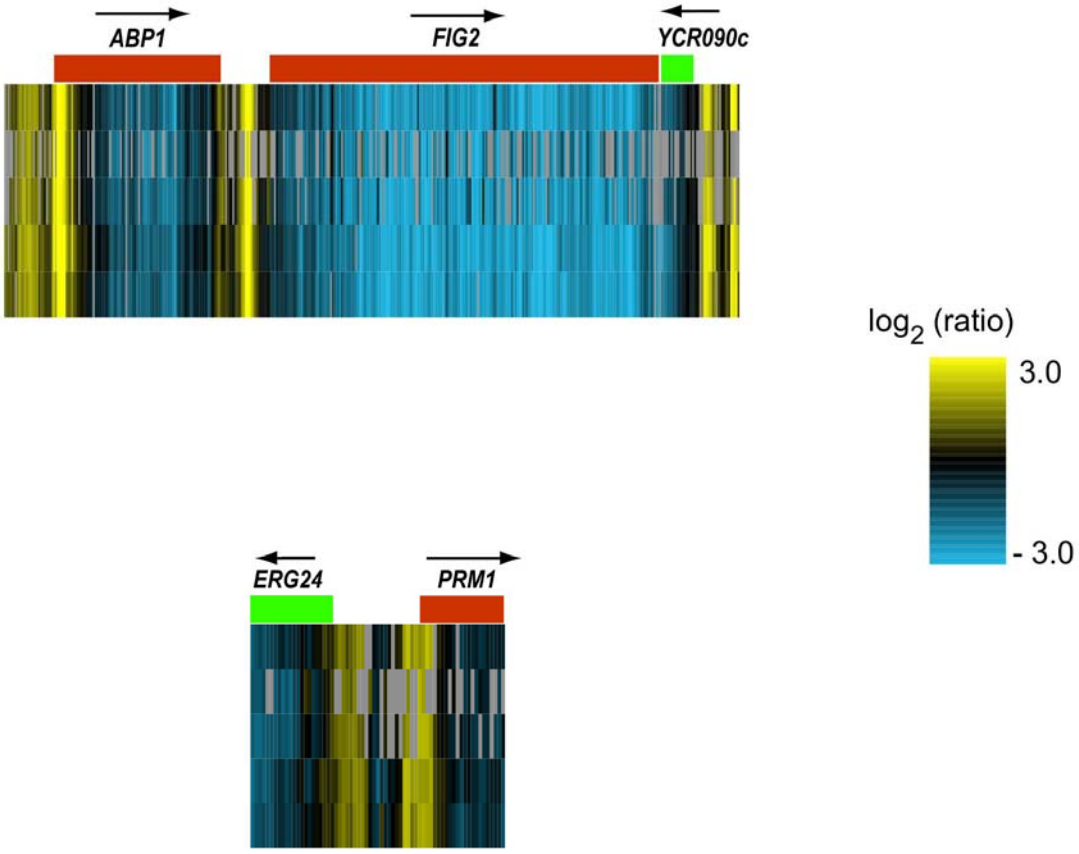

Figure 12. ChIP analysis of H2A.Z enrichment at *FIG1* in response to pheromone induction

All ChIP values are triplicate averages of H2A.Z or unmodified histone H3 ChIP DNA enrichments, normalized to *PRP8* with SEM error bars.

A. Htz1 ChIP enrichment values for a time-course of *FIG1* induction by α factor for 0' (dark blue), 5' (red), 15' (green), 30' (yellow), and 60' (light blue) across the *FIG1* promoter and ORF region
B. H3 ChIP enrichment values for the same time course described in (A).
C. Ratio of normalized Htz1 and H3 ChIP values across the *FIG1* promoter and ORF region. QPCR fragments are for consecutive 200 bp segments; *FIG1* and its upstream gene *ATP3* are shown with their approximate relative positions.
D. Quantitative RT-PCR values for *FIG1* expression normalized to *ACT1* during time-course.

Figure 12

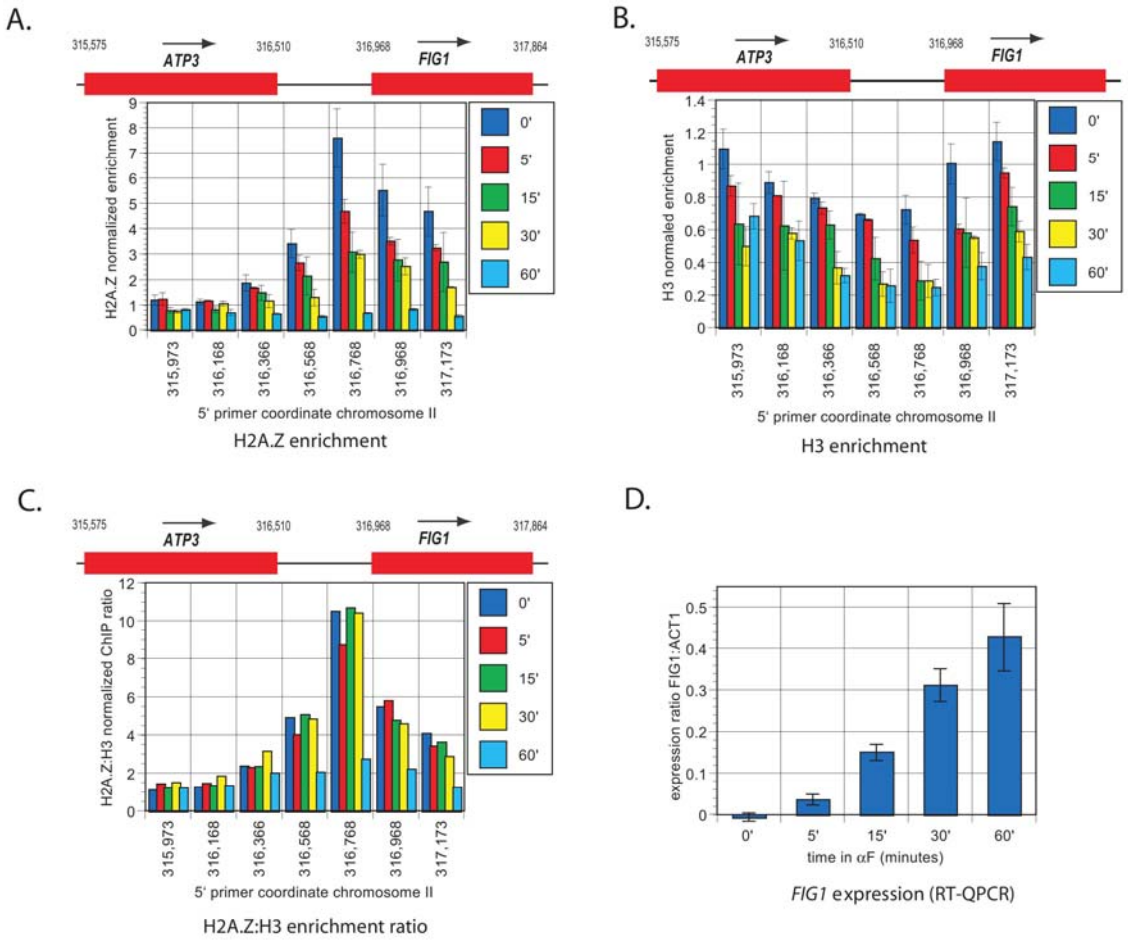
A.
315,575
ATP3
316,510
316,968
FIG1
317,864
H2A.Z normalized enrichment
0'
5'
15'
30'
60'
315,973
316,168
316,366
316,568
316,768
316,968
317,173
5' primer coordinate chromosome II
H2A.Z enrichment
B.
H3 normaled enrichment
H3 enrichment
C.
H2A.Z:H3 normalized ChIP ratio
H2A.Z:H3 enrichment ratio
D.
expression ratio FIG1:ACT1
time in αF (minutes)
FIG1 expression (RT-QPCR)

Figure 13. ChIP analysis of H3 enrichment at selected euchromatic promoters in wild-type and histone H4-K5R, K12R mutant

Triplicate average unmodified anti-H3 enrichment ratios for wild-type (blue bars) and histone H4-K5R, K12R mutant (red bars) strains, normalized to the *BUD3* ORF region, with SEM error bars.

Figure 13

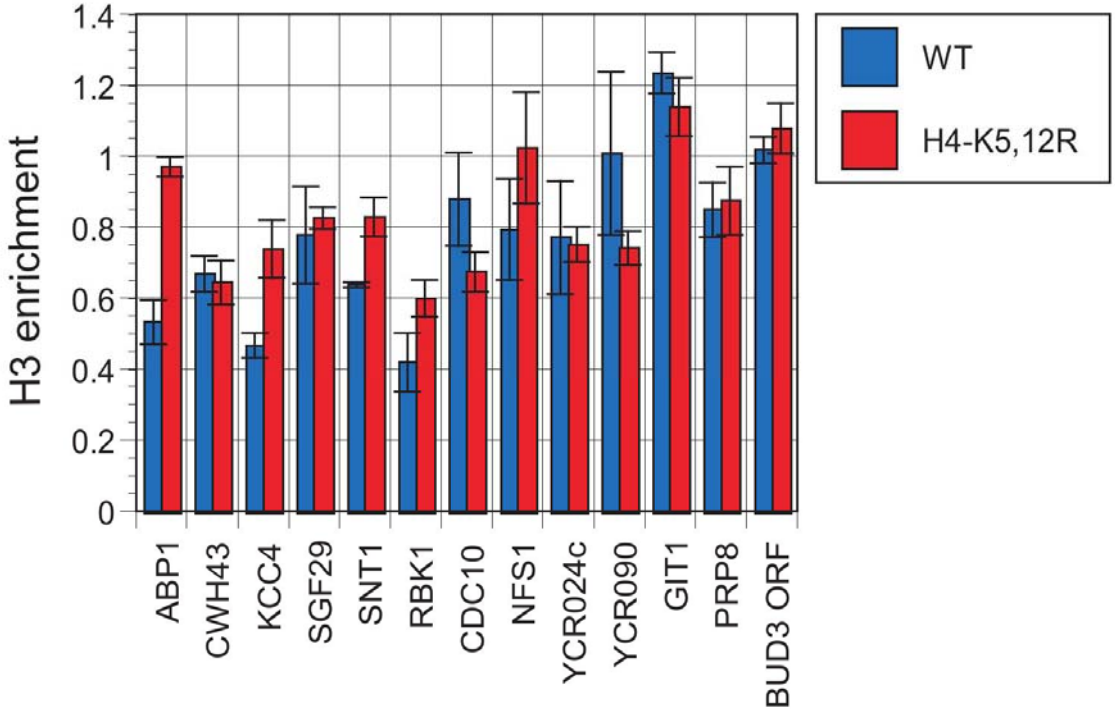
H3 enrichment
1.4
1.2
1
0.8
0.6
0.4
0.2
0
WT
H4-K5,12R
ABP1
CWH43
KCC4
SGF29
SNT1
RBK1
CDC10
NFS1
YCR024c
YCR090
GIT1
PRP8
BUD3 ORF

Figure 14. Low-resolution substitution mutagenesis of the *BPH1-SNT1* intergenic region

Shown is the *BPH1-SNT1* intergenic region and positions of seven 75 bp intervals that were subjected to substitution mutagenesis. Microarray data indicating the positions of the two H2A.Z nucleosomes and the intervening nucleosome-free region are shown. Mutants were constructed by replacing 75 bp segments with a fragment of pBluescript. Displayed below are the normalized H2A.Z deposition levels for each mutant determined using standard ChIP/QPCR and probes A-D. Experiments were performed in triplicate. Mean values and their SEM are displayed.

Figure 14

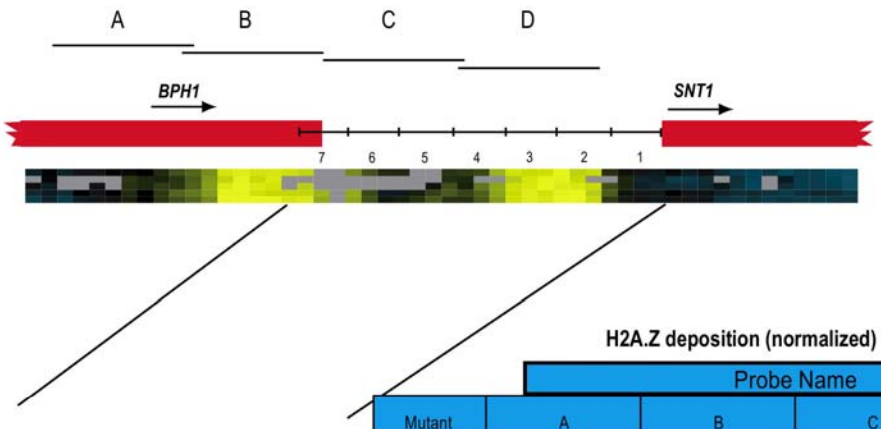

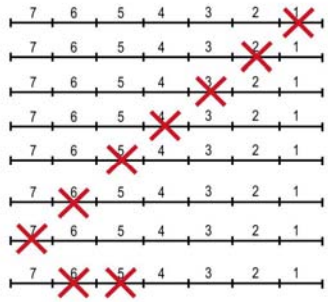

H2A.Z deposition (normalized) mean +/- SEM

	Probe Name			
Mutant	A	B	C	D
1	2.99 +/- 1.02	10.1 +/- 3.1	5.65 +/- 0.31	8.52 +/- 2.45
2	5.14 +/- 1.12	12.82 +/- 2.36	11.25 +/- 0.74	11.73 +/- 3
3	5.59 +/- 1.46	12.24 +/- 1.61	8.7 +/- 1.55	11.06 +/- 2.68
4	4.87 +/- 0.54	13.76 +/- 0.62	ND	4.45 +/- 0.64
5	2.5 +/- 0.43	5.44 +/- 0.89	6.3 +/- 0.65	5.01 +/- 0.28
6	2.14 +/- 0.33	4.64 +/- 0.23	6.19 +/- 1.42	6.72 +/- 0.7
7	3.7 +/- 0.38	10.04 +/- 0.71	8.96 +/- 0.79	7.84 +/- 0.47
5, 6	1.45 +/- 0.21	2.01 +/- 0.37	ND	1.29 +/- 0.22
wt	5.22 +/- 0.09	11.66 +/- 0.42	11.03 +/- 1.17	9.17 +/- 0.88

Chapter 3: Mechanisms that specify promoter nucleosome location and identity

Paul D. Hartley and Hiten D. Madhani

Reprinted with permission from

Cell (2009) vol. 137, pages 445-458

Summary

The chromatin architecture of eukaryotic gene promoters is generally characterized by a nucleosome-free region (NFR) flanked by at least one H2A.Z variant nucleosome. Computational predictions of nucleosome positions based on thermodynamic properties of DNA-histone interactions have met with limited success. Here we show that the action of the essential RSC remodeling complex in *S. cerevisiae* helps explain the discrepancy between theory and experiment. In RSC-depleted cells, NFRs shrink such that the average positions of flanking nucleosomes move toward predicted sites. Nucleosome positioning at distinct subsets of promoters additionally requires the essential Myb family proteins Abf1 and Reb1, whose binding sites are enriched in NFRs. In contrast, H2A.Z deposition is dispensable for nucleosome positioning. By regulating H2A.Z deposition using a steroid-inducible protein splicing strategy, we show that NFR establishment is necessary for H2A.Z deposition. These studies suggest an ordered pathway for the assembly of promoter chromatin architecture.

Introduction

Since the identification of a nucleosome-free region (NFR) in SV40 minichromosomes nearly 30 years ago (*71*), (*72*), the mechanisms underlying the positioning of nucleosomes have been an area of active study. Recent genome-scale surveys of nucleosome positions in a variety of eukaryotic organisms have revealed a stereotypical promoter chromatin architecture characterized by a nucleosome-free region (NFR) flanked by at least one nucleosome enriched for the histone H2A variant H2A.Z (*23*),(*9*),(*11*), (*12*),(*73*), (*22*), (*8*). As a class, NFR-adjacent nucleosomes are the most precisely positioned in the genome, with neighboring nucleosomes displaying less precision in their locations as their distance from NFRs increases. By acting as anchor points, the tight positioning of NFR-flanking nucleosomes may be a dominant mechanism by which nucleosomes are positioned genome-wide (*11*). In *S. cerevisiae*, NFR-flanking nucleosomes often occlude the transcription start site (TSS) such that the TSS is on average half a helical turn inside the +1 nucleosome and exhibits a rotational phasing which tends to place sites for transcription factors on the accessible surface of nucleosomal DNA (*23*). Significantly, recent detailed analysis of the *PHO* regulon in *S. cerevisiae* has shown that chromatin remodeling during phosphate starvation exposes a class of binding sites for the Pho4 activator that are initially masked by nucleosomes and that this plays a key role in shaping the input-output functions of promoters (*5*). Defects in the positioning of some promoter nucleosomes seen in *isw2* mutant cells correlates with the accumulation of cryptic antisense transcripts,

leading to the proposal that positioning of nucleosomes also prevents erroneous transcription initiation events (*21*).

While the fractional occupancy of H2A.Z in NFR-flanking nucleosomes in yeast is not correlated with transcription rates (*22*), loss of promoter nucleosomes including those containing H2A.Z occurs in response to transcriptional activation (*66*), (*13*), (*10*), (*74*). It has been reported that H2A.Z nucleosomes are less stable in vitro, and this property has been hypothesized to aid in their removal in vivo (*26*). In *Drosophila* and humans, NFRs flanked by nucleosomes enriched in H2A.Z are also a common feature of promoters (*24*), (*12*). In flies, the H2A.Z nucleosomes at promoters tend to occur downstream of the NFR, whereas in humans there appear to be H2A.Z nucleosomes both upstream and downstream of NFRs. Interestingly, both NFR formation and H2A.Z deposition seem to correlate with productive transcription in these organisms. These species-specific differences suggest additional complexity in metazoans. H2A.Z nucleosomes are also relatively enriched at flanking non-promoter NFRs that characterize enhancers and insulators in human T-cells (*24*). Taken together, nucleosome-free regions, whether or not associated with gene promoters, tend to be associated with H2A.Z. A conserved function of H2A.Z demonstrated in both S. cerevisiae and Arabidopsis thaliana is to act in euchromatin to antagonize gene silencing (*25*), (*75*).

Despite the high conservation across eukaryotic evolution of these basic aspects of promoter chromatin architecture identified by descriptive genomic

studies, the mechanisms by which NFRs flanked by H2A.Z nucleosomes form remain poorly understood. There exists evidence that octamer positioning genome-wide is mediated by a genomic nucleosome positioning code in which intrinsic DNA-octamer affinities, predicted computationally based on dinucleotide periodicity patterns and/or other sequence patterns, are a significant determinant of location, particularly at NFR-flanking nucleosomes (*76*), (*9*), (*18*). For example, one study (Segal et al., 2006) reported that 50% of nucleosome positions in *S. cerevisiae* chromosome III can be accurately predicted computationally. However, there are differences of opinion in the literature regarding how well computational methods predict actual positions determined experimentally compared to so-called random guess predictions (*77*), (*78*), (*20*). A recent study (Yuan and Liu, 2008) compared a number of methods and found that for *S. cerevisiae* datasets even improved methods required an error of ~70bp (nearly half a nucleosome) to obtain a prediction sensitivity of 80% and required a similar error to yield an specificity of 80%. These errors stand in contrast to the observed precision of nucleosome positioning in vivo relative to TSSs and transcription factor binding sites as described above.

The connection between NFR formation and H2A.Z deposition is likewise not well-defined. One report suggested that H2A.Z deposition plays a role in nucleosome positioning, while another proposed that H2A.Z deposition has no role (*79*),(*80*). H2A.Z nucleosomes have been reported to be poor in vitro substrates of chromatin remodeling enzymes compared to their H2A

counterparts (*80*). Thus, whether NFR formation is required for H2A.Z deposition or vice versa is unknown.

In the absence of a consensus view of how promoter chromatin architecture is specified with precision, we sought to clarify the underlying mechanisms. In previous work, we identified a segment of the *SNT1* promoter required for normal levels of H2A.Z deposition. Remarkably, insertion of a short segment of this region into the middle of a transcriptionally quiescent *PRM1* gene resulted in the formation of an NFR flanked by two nucleosomes containing H2A.Z (*22*). This sequence contained a putative binding site for the Myb family transcription factor Reb1 and an adjacent T tract. Below we describe further studies of this synthetic NFR as well as chromosome-wide studies of the roles of several essential factors in nucleosome positioning and H2A.Z deposition.

Results

Models for NFR formation and H2A.Z deposition.

We considered three models by which the DNA signal containing the Reb1 binding motif (henceforth called Reb1:dT_7) might program promoter chromatin structure (Figure 15A, Figure 15B). In Model I, the DNA signal first programs NFR formation, and then the NFR acts as a signal to induce H2A.Z deposition into the flanking nucleosomes. Model II proposes the reverse process of NFR formation such that a DNA signal first induces H2A.Z deposition, and H2A.Z then acts as a signal for NFR formation. Lastly, NFR formation and

H2A.Z deposition could occur in an independent, uncoupled fashion (Model III). To distinguish these models, we first sought to define *trans*-acting factors that mediate NFR formation.

Construction of conditional degron alleles of Reb1, Abf1 and the RSC ATPase, Sth1.

The mechanism by which Reb1:dT_7 induces formation of an NFR flanked by two nucleosomes carrying H2A.Z likely involves the recruitment of Reb1, although this was not tested directly in our previous study. We also hypothesized that Reb1 might recruit a chromatin remodeling enzyme to produce an NFR. A systematic study of protein interactions revealed that Reb1 physically associates with Rsc2, Rsc3 and Npl6, which are subunits of the essential chromatin remodeling complex RSC (*81*), (*82*), (*83*). Since the Reb1-related factor, Abf1, has also been implicated in the formation of a nuclease-sensitive site (*84*), we pursued its functional role.

As Reb1, Abf1, and the catalytic subunit of RSC (Sth1) are all essential proteins, we generated a series of conditional alleles Specifically, we used the temperature-sensitive degron system to engineer yeast strains in which we could control degradation of these proteins via the N-end rule pathway (*85*). This pathway operates through the recognition of destabilizing N-terminal amino acids by the nonessential E3 ubiquitin ligase Ubr1. A N-terminal arginine is the strongest signal for degradation by Ubr1, and traditional degron alleles encode proteins capped by an arginine followed by a temperature-sensitive murine

dihydrofolate reductase ($DHFR^{ts}$) peptide fused to the target protein. As translation initiates at an ATG codon, an ATG-initiated segment encoding a ubiquitin moiety is placed before the arginine codon. Once synthesized, this segment is cleaved in cells by ubiquitin C-terminal proteases to expose the N-terminal arginine. Such degron systems also place the modified allele of interest under the control of a regulatable promoter, which traditionally has been the copper-inducible promoter *pCUP1*.

We constructed *pCUP1::UBI4::DHFR^{ts}::c-myc::STH1* and *pCUP1::UBI4::DHFR^{ts}::c-myc::REB1* alleles in strains that had *UBR1* under the control of the *pGAL1* promoter. We were unable to achieve substantial degradation of these proteins or growth arrest under degron-inducing conditions, although such an allele for *STH1* has been reported (*86*). We achieved more complete degradation of Reb1 and Sth1 under degron-inducing conditions with a different construct (*pMET3::UBI4::DHFR^{ts}::3xHA*) that utilized the methionine-repressed *pMET3* promoter (Figure 15C). Yeast strains carrying Reb1-degron or Sth1-degron alleles were inviable under degron-inducing conditions (Figure 15D). While an Abf1 $DHFR^{ts}$ degron has been reported in the W303 strain background (*87*), we were unable to construct a viable *pMET3::UBI4::DHFR^{ts}::3xHA::ABF1* degron allele in our S288C background despite several attempts and strategies. We, however, successfully created a *pMET3::UBI4::abf1(M1R)* allele in a strain carrying a *pGAL1::UBR1* allele. As described above, the ubiquitin moiety of the translated protein is cleaved off soon after translation, leaving an Abf1 protein capped with a destabilizing N-terminal arginine. Under inducing conditions, this

Abf1-degron yielded growth arrest and displayed Abf1 depletion (Figure 15C, Figure 15D). We also constructed an Abf1 Reb1 "double degron" strain in order to simultaneously deplete both factors from cells (Figure 15C, Figure 15D). For the studies described below, we determined nucleosome positions by hybridizing mononucleosomal versus genomic DNA-derived probe with in-house printed custom tiling arrays that span *S.cerevisiae* chromosome III at 20bp resolution (*8*). The arrays also included oligonucleotides that tiled sequences corresponding to the *PRM1* gene to allow us to observe nucleosome positions programmed by Reb1:dT_7 (see Experimental Procedures for details). Unless otherwise specified, all experiments represent averages of four independent, biological replicates.

NFR formation mediated by a Reb1 binding site requires Reb1 and the chromatin remodeling complex RSC, but not H2A.Z

As expected from our previous study (*22*), nucleosome position analysis of the *PRM1* ORF with or without a Reb1:dT_7 insertion revealed that the insertion produces an NFR (Figure 16A). NFR formation was unaffected in strains carrying the Reb1-degron or Sth1-degron alleles under conditions in which the degron system was inactive (Figure 16B). We mapped nucleosome positions in strains carrying the Reb1-degron or the Sth1-degron five hours after activating the degron system, and these positions were compared to nucleosome positioning data from a control strain isogenic to the degron strains except that it lacked the Reb1 or Sth1 degron allele. The latter control strains were subjected to the identical culture growth protocol as the experimental strains. Depletion of

Reb1 resulted in loss of the NFR programmed by Reb1:dT_7 inserted into the *PRM1* ORF, consistent with a direct role for Reb1 (Figure 16B). Likewise, inactivation of the RSC complex through depletion of Sth1 resulted in complete loss of the NFR programmed by the Reb1:dT_7 sequence (Figure 16B), supporting the hypothesis that Reb1 functions by recruiting RSC.

Model II above proposes that NFR formation requires the prior deposition of H2A.Z into chromatin, which is mediated by the Swr1 chromatin remodeling complex. We tested whether H2A.Z or Swr1 is required for NFR formation induced by the Reb1:dT_7 signal. We constructed *htz1Δ* and *swr1Δ* strains and mapped the nucleosome positions in these strains. NFR formation meditated by insertion of Reb1:dT_7 at *PRM1* did not require H2A.Z or Swr1 (Figure 16C).

To test whether NFR formation at *PRM1* might be a consequence of transcription, we examined whether NFR formation induced by Reb1:dT_7 was associated with the production of transcripts. Transcript levels were examined using RT-PCR analysis of extracted total RNA. In a control strain in which the *PRM1* gene was induced with mating pheromone for 1hr, a specific signal was obtained (Figure 23). We examined strains containing the insert and the Sth1 degron under both degron-inducing and permissive conditions as well as a strain lacking the insert. In these three cases, multiple peaks rather than a single peak were obtained in the QPCR melting curves indicating that cross-reacting cDNAs, instead of products specific to the *PRM1* locus, were being detected. Moreover, no quantitative differences were observed (Figure 23). Taken together, these

data suggest that NFR formation was not associated with transcription that could be detected by these methods.

Reb1 is required for the formation of a subset of NFRs

We next examined the chromosome-wide requirement for Reb1 in NFR formation. We mapped and compared nucleosome positions in the Reb1-degron strain and an isogenic control strain that lacked the Reb1-degron under conditions described above. Figure 17A shows a gene-by-gene "difference map" of the positioning data in which genes were aligned to each other based on the position +1 nucleosome downstream of the NFR in control strains and then the mutant signal subtracted from the control signal (yellow indicates more nucleosomal DNA signal in the mutant than in wild-type cells). The data were organized by K-means clustering. Two clusters are evident, one in which positioning was affected (Cluster I affecting 12% of assayed promoters), and another where no effect was evident (Cluster II). Line traces of the average signals of the control and degron strains for these two clusters are shown in Figure 17B. Inspection of Cluster I indicates that the two NFR-flanking nucleosomes move inward towards the center of the NFR, and this movement propagates further such that other flanking nucleosomes also shift their positions (Figure 17B) Figure 17C shows that the changes in the size of the trough signal representing the NFR between degron and control strains were dependent on the induction of the degron.

A previous study of transcription factor association at promoters assigned likelihood scores for a given transcription factor binding to a given promoter (*88*). We compared these scores for Reb1 to the highest fold-change probe in the NFRs of promoters we assayed that were assigned scores. As shown in Figure 17D, there was a significant correlation ($p=7.81x10^{-7}$ based on a hypergeometric test using a likelihood score cutoff of $p< 0.05$). Consistent with this finding, promoters that contained at least one copy of the most conserved Reb1 binding site (TTACCCG, (*70*)) tended to experience changes in NFR structure (Figure 17E). Cluster I was enriched for the most conserved Reb1 consensus site; indeed, 14 out of the 18 promoters in Cluster I contained this motif ($p= 5.07x10^{-13}$, Figure 17F). Relaxing the consensus to reflect the poorer conservation of the first two residues of the consensus still yielded highly significant enrichments (Figure 17F).

Abf1 is required for the formation of a subset of NFRs

We next performed the same analysis on Abf1 degron strain. Difference map analysis and clustering (Figure 18A) show that 9.3% of promoters were affected, and these promoters were distinct from promoters affected by Reb1 depletion (see below). As with the Reb1 degron, the affected cluster displays a smaller NFR and movement of flanking nucleosomes towards the NFR (Figure 18B), and these changes were dependent on induction of the degron (Figure 18C). Likewise, affected NFRs were enriched for Abf1 binding (Figure 18D) and for an Abf1 consensus site (Figure 18E, F). The latter correlations are weaker

than for the Reb1 site, perhaps because of the higher degeneracy of the Abf1 consensus site (*89*).

RSC is required for proper positioning of NFR-flanking nuclesomes

We next examined the effects of Sth1 depletion on nucleosome positioning using strains carrying the Sth1-degron as described above. Strikingly, our analysis showed that Sth1 depletion affected a majority (55%) of promoters (see Cluster I in Figure 19A). The affected cluster displayed shrinking of the NFR and movement of flanking nucleosomes, whereas little change in nucleosome position was apparent for members of Cluster II (Figure 19B). As with the Reb1 and Abf1 degron strains, growth under degron-inducing conditions was required to observe these differences (Figure 19C). Figure 24 shows a superposition of a histogram of the locations of mapped TSSs (*90*) and the positioning data. Consistent with previous studies, TSSs tend to lie just inside the downstream nucleosome and the movement observed in Sth1-depeleted cells moves these sites further into the nucleosome core (Figure 24). This may explain why RSC depletion has been reported to cause cessation of transcription by RNA polymerase II (*86*).

When RSC, Abf1, or Reb1 were depleted, NFRs shrank but were not eliminated. We hypothesized that intrinsic positioning sequences might explain the positions of nucleosomes under these conditions. Therefore, we compared the positions we observed in Cluster I of Sth1-depleted cells with those predicted by Pugh and colleagues (*76*) based on AA/TT dinucleotide periodicity

enrichment. As shown in Figure 19E, the average nucleosome position of the +1 and -1 nuclesomes of Cluster I relax towards positions specified by the NPS signature. For the largely unaffected cluster (Cluster II), a discrepancy between the NPS-predicted and observed positions is still apparent for the +1 nucleosome, whereas the -1 nucleosome is poorly aligned in this despite the sharp NPS prediction peak (Figure 19E).

To test whether Sth1 depletion results in changes in gene expression, we performed expression profiling of the Sth1 degron strain against a control strain under degron-inducing conditions. As we expected global changes in gene expression, we incorporated external spiked-in RNA controls into our normalization procedure (see Experimental Procedures). We then asked whether there was an enrichment for genes whose expression was reduced in Sth1-depleted cells in Cluster I vs. Cluster II. As shown in Figure 19D, Cluster I is indeed highly enriched for genes whose expression requires Sth1, indicating that that the changes in positioning correlate with changes in expression. Given this result, we tested whether loss of transcription might be responsible for changes in positioning. We mapped nucleosome positions in a temperature-sensitive RNA polymerase II strain (*rpb1-1*) which ceases transcription within minutes upon shift into restrictive conditions (*91*). The *rpb1-1* mutant was grown at either 25°C or shifted for 1 hour to 37°C. The average nucleosome positions in these conditions were determined for Clusters I and II of the Sth1 degron difference map. There were were no detectable differences in nucleosome positions in either cluster (Figure 19F, Figure 25). Hence, the changes in NFR

structure observed upon Sth1 depletion appear to be due to the action of RSC rather than from cessation of transcription *per se*.

Abf1 and Reb1 are required for NFR formation at distinct sets of promoters

To identify promoters that are redundantly controlled by Abf1 and Reb1, we examined a double degron strain that carried the Abf1-degron and Reb1-degron alleles (Figure 15C, D). The resulting difference map was clustered together with difference maps for the Abf1 single degron strain, the Reb1 single degron strain, and the Sth1 degron strain (Figure 20A; Figure 20B shows that NFR changes in the double degron are dependent on degron induction). K-means clustering revealed that the promoter NFRs affected by loss of either Abf1 or Reb1 were reproducibly affected in the double degron strain, but there were no other promoter NFRs that were significantly affected in the double degron strain. It is also evident that most NFRs affected by loss of Reb1 also required Sth1 for proper positioning of nucleosomes (Figure 20A), consistent with the data obtained with the synthetic NFR described above (Figure 16B). The NFRs affected by loss of Abf1 appeared to have a somewhat lesser degree of dependence for Sth1 for nucleosome positioning (Figure 20A). Likewise, there clearly are many NFRs that require RSC, but not Abf1 or Reb1, for proper nucleosome positioning (Figure 20A), suggesting the existence of additional RSC recruitment mechanisms. Analysis of average nucleosome positions for each cluster indicates that the the changes observed (Figure 20A) are due to shifts in nucleosome positions (Figure 26).

As with the Sth1 degron strain, we examined the Abf1- Reb1- double-degron strain for changes in transcript levels using whole genome microarrays and spiked-in external controls. As shown in Figure 20C, we found a significant correlation between decreases in NFR size and decreases in transcript accumulation.

H2A.Z deposition is generally dispensable for nucleosome positioning

To complete our analysis of positioning, we used cells lacking H2A.Z (*htz1*∆) or lacking the ATPase subunit of its deposition complex (*swr1*∆) to determine whether H2A.Z exchange was required for nucleosome positioning chromosome-wide (Figure 27). Based on the results with the synthetic NFR (Figure 16C), we expected to see no differences in positioning. Indeed, as shown by line traces of the average positions of aligned promoter nucleosomes, H2A.Z deposition resulted in no detectable changes. Of course, we cannot rule out the possibility that there could be changes too subtle to observe using our 20bp resolution tiling arrays.

Development an inducible H2A.Z deposition system

Nonetheless, these data argue against Model II (Figure 15B), which proposed that H2A.Z deposition is essential for NFR formation. We then considered the two remaining models: (1) the deposition of H2A.Z at a promoter requires the presence of an NFR at that promoter (Model II), or (2) H2A.Z deposition occurs independently of NFR formation (Model III). In principle, these

models could be distinguished through development of a system in which NFR loss is induced under conditions where H2A.Z is not deposited into chromatin, but then H2A.Z is induced and its deposition examined. The Sth1 degron provides a tool to trigger abrogation of the synthetic NFR programmed by Reb1:dT_7 and a shrinkage of bona fide promoter NFRs. However, since global transcription is shut off in RSC-depleted cells, we sought a posttranslational method to control H2A.Z deposition.

We utilized an engineered *M. tuberculosis* RecA intein whose intrinsic protein splicing is controlled by the human estrogen receptor ligand binding domain (*92*). This construct was used previously to interrupt several coding sequences in yeast, and its splicing was shown to be activated in vivo using the estrogen agonist 4-hydroxytamoxifen (4-HT). The chemistry of splicing requires cysteine cleavage sites and leaves a single cysteine residue at the splice junction.

We initially targeted the Swr1 and Swc2 subunits of the Swr1 complex by inserting the intein construct before the codons for several native cysteine residues in the corresponding genes. These alleles abrogated H2A.Z deposition in *vivo*, but addition of 4-HT did not restore H2A.Z deposition (unpublished observations), suggesting that the placement of the intein was incompatible with protein stability and/or intein splicing. We next attempted engineering a spliceable *HTZ1* allele under the assumption that the smaller size of H2A.Z relative to the intein construct would make the protein context less likely to interfere in proper structural formation of the intein. H2A.Z, however, lacks

cysteine residues, so such a spliced allele would by necessity contain a cysteine point mutation. Four H2A.Z residues (Ala46, Thr68, Thr88 and Asp100) that did not confer a significant growth defect in high precision measurements when mutated (S. Braun, D. Breslow, J. Weissman, H. D. M., unpublished observations) were replaced with the intein construct. These alleles initially replaced wild-type *HTZ1* at its native chromosomal locus, but none displayed detectable spliced product in the presence of 4-HT (unpublished observations). We therefore placed these alleles under the control of a *pGAL1* promoter on a high-copy 2 micron plasmid vector. The allele in which Ala46 was replaced with the intein construct yielded a protein that was spliced in vivo when cultures were treated with 4-HT; Ala46 is a residue in the core histone fold domain (Figure 21A, 7B). As splicing produced somewhat higher levels of H2A.Z than in that found in wild-type cells (Figure 21B), we placed the construct on a low-copy *CEN-ARS* plasmid. Regulated splicing of the H2A.Z intein was also observed (Figure 28A), and this construct was used in further experiments. We refer to this *pGAL1::htz1(A46intein)* allele on a *CEN-ARS* plasmid as the H2A.Z intein construct.

We examined the deposition of H2A.Z whose synthesis was directed by this construct using chromatin immunoprecipitation (ChIP). Although splicing in the H2A.Z intein is regulated, a small amount of H2A.Z deposition was observed in the absence of 4-HT, presumably due to low levels of background splicing (Figure 28C); however, the H2A.Z enrichment signal steadily increases over time

in response to 4-HT treatment (Figure 28D), indicating stimulation of H2A.Z deposition by the activation of splicing.

Focused H2A.Z deposition in response to Reb1:dT$_7$ requires prior NFR formation by RSC

We introduced the H2A.Z intein into *htz1Δ* strains that carried *pGAL1::UBR1* and either the Sth1-degron or a wild-type Sth1. Simultaneous activation of the degron system and synthesis of unspliced H2A.Z were accomplished by transferring cells to 37°C media containing galactose. After 5 hours of growth, intein splicing was initiated by the addition of 4-HT, and cells were collected after 3 hours of further incubation at 37°C to allow for H2A.Z deposition. Chromatin immunoprecipitation for H2A.Z and histone H3 were carried out, and quantitative PCR was used to measure H2A.Z enrichment relative to H3 enrichment. The H2A.Z/H3 enrichment values were normalized to an amplicon in the middle of the large *BUD3* ORF where there is little detectable H2A.Z (*22*). Nucleosome positions were also mapped for the Sth1-degron H2A.Z intein strain prior to degradation of Sth1, after 5 hours of Sth1 depletion, and 3 hours after addition of 4-HT. We determined that unspliced H2A.Z was being produced and was spliceable, and we found that Sth1 degradation still occurred in the presence of the H2A.Z intein construct and during 4-HT treatment (Figure 28A, B).

We sought to examine the deposition profiles of H2A.Z at NFRs whose structure is unaffected upon Sth1 depletion and at NFRs that undergo significant

changes upon Sth1 depletion. The two NFRs located within an intergenic region containing the *DCC1* and *BUD3* promoters do not appear to require Sth1 for their organization (Figure 21C, top panel). The H2A.Z deposition profiles across the *DCC1-BUD3* intergenic region in both the Sth1-degron and control strains were similar (Figure 21C bottom) and indicated that H2A.Z deposition could still occur under these conditions. We next examined how loss of the NFR programmed by insertion of Reb1:dT_7 into *PRM1* affected the recruitment of H2A.Z. This NFR essentially collapses upon Sth1 depletion in the H2A.Z intein strain carrying the Sth1-degron (Figure 21D, top panel). In the strain that did not have the Sth1-degron and therefore maintained the NFR programmed by Reb1: dT_7 inserted into *PRM1*, H2A.Z deposition occurred in the middle of *PRM1*, with its peak deposition at the Reb1: dT_7 insertion site (Figure 21D, bottom left panel). In contrast, upon Sth1 depletion, there was no H2A.Z deposition focus about the Reb1: dT_7 insertion site (Figure 21D, bottom right panel). The apparently undirected, background H2A.Z deposition in the *PRM1* ORF is similar to that observed in cells lacking the Reb1:dT_7 insertion (*22*), and similar global patterns of untargeted H2A.Z deposition have been seen in genome-wide studies (*23*). Thus, the focused peak of H2A.Z deposition induced by the Reb1:dT_7 DNA signal appears to require the Sth1-dependent formation of an NFR directed by the signal.

RSC depletion did not produce complete collapse of NFRs on endogenous promoters, and, as described above, this may be due to intrinsic positioning signals. Nonetheless, we examined the H2A.Z deposition profile at the

promoters of *YCR016W* and *YCR023C*, both of which experience significant nucleosome encroachment into their NFRs upon Sth1 depletion (Figure 21E and F, top panels). We observed H2A.Z deposition at these promoters under conditions in which their NFRs were unaffected as well as under conditions where their NFRs were affected (Figure 21E and F, bottom panels). However, the H2A.Z deposition profile at affected NFRs differed in that there was a significant decrease in H2A.Z enrichment in the vicinity of the +1 nucleosome relative to the NFR (see amplicon "D" for Figure 21E and amplicon "C" for Figure 21F). Whether the otherwise fairly robust H2A.Z deposition seen at these two promoters under conditions of intein induction is explained by the presence of a residual NFR driven by NPSs or by NFR-independent mechanisms that stimulate H2A.Z deposition such as histone acetylation and its subsequent recognition by Bdf1 (*22*) is not clear. The latter model is difficult to test since cells lacking H2A.Z and Bdf1 are inviable (*22*).

Discussion

Based on the results of a number of genome-scale studies, it has become increasingly clear in organisms as diverse as yeast and humans that gene regulatory regions display stereotypical patterns of nucleosome positioning and identity. Although there are species-specific differences, promoters are generally characterized by an NFR flanked by at least one H2A.Z nucleosome. Despite the power of these descriptive genome-wide studies as well as work that indicates that these characteristics of promoters play key roles in gene regulation

(see Introduction for references), they leave open the question of how these structures are programmed.

Two lines of studies have come to distinct conclusions regarding NFR formation mechanisms. One group of studies has suggested that the direct effects of sequence on DNA-octamer affinity programs NFR formation (see Introduction for references). In contrast, our previous work defined a short signal from the *SNT1* gene containing a putative site for a DNA binding protein, Reb1, that is sufficient to program a NFR flanked by H2A.Z nucleosomes when placed into the middle of a positioned nucleosome in an inactive gene (*22*). Others have also implicated Reb1 and Abf1 in the formation of nucleosome gaps within the specific promoter regions (*53*), (*84*). The work described here helps reconcile these two lines of research and provides insight into the relationship between NFRs and H2A.Z deposition. Our principal conclusions are as follows:

(1) RSC displaces NFR-flanking nucleosomes away from their average NPS-predicted positions

A striking result presented here is that at a majority of promoters, the normal positioning of NFR-flanking nucleosomes requires the essential multisubunit chromatin modeling complex RSC. Such a central role for RSC in generating promoter chromatin architecture is consistent with several of its properties: 1) RSC, unlike most chromatin remodeling enzymes in yeast, is essential for viability (*81*), (*82*), 2) RSC slides nucleosomes in vitro (*93*), and 3) RSC is required globally for RNA polymerase II transcription (*86*). Our studies

are also consistent with a recent lower-resolution study that concluded that RSC affected histone density at a number of promoters (*86*). A recent study indicated changes in the positioning nucleosomes at ~12% of promoters in cells lacking the Isw2 chromatin remodeling complex (*21*). The primary function of Isw2 appears to be in transcriptional repression and in suppressing antisense transcription (*21*). Interestingly, in contrast to RSC, Isw2 appears to move nucleosomes in vivo toward the NFR, raising the possibility that it antagonizes the action of RSC at some promoters. The potential for dynamic involvement of multiple ATPases at promoters further underscores the active nature of mechanisms that position nucleosomes in vivo.

The finding in this study and in the previous study that the final resting positions of nucleosomes are strongly influenced by ATP-dependent chromatin remodeling mechanisms argues that that the intrinsic affinity of the octamer for underlying DNA sequences is not determinative for the final positioned state. However, our observation that depletion of Sth1 causes nucleosome positions to relax on average closer to those predicted by an NPS signature strongly suggests that sequence properties play a role in a stepwise mechanism for NFR formation. That is, NPS-mediated positioning exposes binding sites for factors such as Reb1 and Abf1, which in turn induce the action of RSC to move nucleosomes to their steady-state average positions in wild-type cells. Such a model is also consistent with in vitro and in vivo observations that suggest that the Isw2 remodeling enzyme moves nucleosomes into energetically unfavorable sites (*94*). We speculate that, compared to a purely “hard-wired” system, this

more dynamic, ATP-dependent mechanism may facilitate binding of DNA binding proteins to nucleosomal sites and transcription initiation. It is important to note that NPS predictions vary in their accuracy considerably at the level of individual genes, suggesting they likely do not predict with full accuracy the intrinsic thermodynamics of octamer-DNA interactions. A histogram of predictions (*76*) reveals that NPS-predicted positions for individual genes deviate significantly from experimental positions even in the Sth1 degron strain (Figure 29). Nonetheless, the close correspondence of the average profiles supports the two-step model proposed above.

(2) Sequence-specific DNA binding proteins are required for positioning of NFR-flanking nucleosomes at a significant fraction of promoters.

Using a signal for NFR formation/H2A.Z deposition we identified previously, we demonstrated a role for the Reb1 protein and RSC for NFR formation programmed by this isolated signal. Given the previously reported biochemical interactions between Reb1 and subunits of RSC, the simplest interpretation is that recruitment of RSC by Reb1 generates the NFR. Our examination of the generality of this mechanism across chromosome III suggests that a subset of promoters, enriched for Reb1 binding sites, use this mechanism in a nonredundant fashion. Abf1, another essential Myb family member, operates at a distinct subset of promoters. These observations are consistent with studies that show that Reb1 and Abf1 sites are highly enriched in NFRs compared to the binding sites for nearly all other studied DNA binding proteins (*9*). The remaining

promoters presumably target RSC and other remodeling mechanisms through other means. In this regard, it is interesting to note that four subunits of RSC contain potential DNA binding domains. Using standard ChIP protocols as well as ones using additional crosslinking agents, we have been unable to detect either wild-type Sth1 or an induced catalytically-dead version of Sth1 at the Reb1:dT_7 signal inserted into *PRM1,* suggesting transient binding of RSC to this site (unpublished data). Likewise, only a fraction of intergenic regions display RSC binding in published ChIP-chip experiments (*95*), despite the global requirement for RSC in pol II transcription (*86*). We suggest that at many sites of action the off-rate of the RSC complex in vivo may be too high to allow detection by ChIP.

(3) H2A.Z deposition is dispensable for NFR formation but NFR formation promotes H2A.Z deposition.

We find no evidence that nucleosome positioning in general requires H2A.Z deposition. While a previous report suggested that H2A.Z controls nucleosome positioning *in vivo*, this conclusion was largely based on a single 20bp shift observed in the position of a nucleosome in the *GAL1* promoter in *htz1*Δ cells (*79*). Another study examined nucleosome positioning in *htz1*Δ cells at four other loci (*SUC2*, *COQ3*, *POS5*, and *COQ1*), which are all highly enriched for H2A.Z and saw no differences in positioning (Li et al., 2005). Our results are generally in line with the latter study. However, we note that the technology used in our study, while cost-effective and allowing for multiple experimental

replicates, does not have the ability to detect shifts of less than 20bp. Thus, we cannot rule out the possibility that our studies would have missed a more subtle role for H2A.Z deposition in nucleosome positioning.

To explore the relationship between NFR formation and H2A.Z deposition we implemented a steroid-regulated protein splicing strategy to induce H2A.Z deposition under conditions in which NFR structure was abrogated by depletion of Sth1 Our data show that deposition of H2A.Z about the NFR programmed by insertion of Reb1:dT_7 into *PRM1* required the prior action of Sth1, which presumably acts to induce formation of the NFR. This defect in deposition was not due to a general defect in H2A.Z deposition in RSC-depleted cells as normal deposition occurred at the *BUD3-DCC1* intergenic region and significant albeit reduced H2A.Z deposition occurred at the promoters of two genes whose NFRs shrank in response to RSC depletion. Our results predict that in vitro studies of the exchange activity of the purified Swr1 deposition complex may show a dependence on adjacent nonnucleosomal DNA. Such a property would not be without precedence as the ACF complex has been shown to have nucleosome-sliding catalytic activity that is stimulated in vitro by flanking DNA (*96*). These observations may explain the general linkage observed in yeast, plants and metazoans between NFRs of various sizes and enhanced deposition of H2A.Z in flanking nucleosomes.

Experimental Procedures

Yeast strains

The strains used in this study are described in Table 4. Yeast transformants were generated by conventional lithium acetate and polyethylene glycerol procedures with selectable or counter-selectable transforming DNA. Insertions at the *PRM1* ORF were obtained by a two-step process in which a construct containing I-SceI and its restriction site was first inserted and subsequently replaced with a desired sequence (*69*).

Gene expression profiling

For each strain, total RNA from four independently grown cultures was prepared using a TRIZOL procedure and spiked with RNA from the Agilent Dual-color RNA Spike-in Kit. Aminoallyl-dUTP-labeled probe was generated by reverse transcription, and hybridizations were carried out using 4x44k Agilent microarrays that cover 6256 *S. cerevisiae* features, each of which are replicated 7 times on the array (Agilent design ID 015072). Dye swaps were incorporated such that for each experiment, there were 2 arrays of one dye configuration, and vice-versa. Data normalization was performed using a composite loess procedure that used 1:1 DCP probes for the spike-in loess curve (*97*). Expression ratios for each gene per array then were derived by calculating the mean of up to 7 technical replicates, while discarding any replicates that were not within 2 standard deviations.

Mapping nucleosome positions using tiling microarrays

Nucleosome positions were mapped by hybridizing probe representing mononucleosomal-sized DNA against genomic reference DNA. Mononucleosomal-sized probe was obtained from chromatin isolated from cultures that had been grown to an OD_{600} of 0.7-0.9 prior to 1% formaldehyde crosslinking for 15 minutes at the same growth temperature and followed by a 0.125 M glycine quench. Genomic reference probe was obtained from purified genomic DNA. Detailed explanations of the microarray platform and how the mononucleosomal-sized and genomic DNA reference probes were prepared can be found in the supplemental methods. Briefly, probe was prepared by micrococcal nuclease digestion of chromatin or genomic DNA, followed by T7 in vitro transcription linear amplification to synthesize aminoallyl-RNA probe that could be labeled for hybridization.

Analysis of nucleosome positions

Detailed explanations of data processing are presented below. Final values for each tiling microarray probe were background median subtracted and normalized using a LOESS algorithm. Areas of nucleosome enrichment could be visualized using line traces connecting physically contiguous probes. Most data analysis used difference maps of nucleosome positions created by subtracting the log2 values of nucleosome positions of a control dataset from the corresponding positions in an experimental dataset. Prior to this transformation, nucleosome positions were aligned at the first nucleosome downstream of the NFR.

Antibodies

H2A.Z-specific polyclonal antisera were generated against a peptide specific for the C-terminus of *S. cerevisiae* H2A.Z (custom-generated). The HA epitope tag in the degron alleles was detected using monoclonal antibody HA.11 (Covance). Abf1 was detected using polyclonal antibodies directed towards the Abf1 C-terminus (yC-20, Santa Cruz). Histone H3-specific polyclonal antibodies were directed towards the C-terminus of human histone H3 (ab1791, abcam).

Assaying the requirement of essential genes with degron technology

The essential genes *ABF1*, *REB1*, and *STH1* were studied by regulated degradation of their encoded protein via degron alleles. Each degron allele was under the control of the *pMET3* promoter, which is repressed by methionine. The *REB1* and *STH1* degron alleles had an arginine-capped N-terminal fusion of *DHFRts* and a triple-HA tag, while the *ABF1* degron allele was an *abf1(M1R)* allele. UBR1, the N-end rule pathway E3 ubiquitin ligase, was placed under the control of a *pGAL1* promoter.

To study phenotypes arising from loss of Abf1, Reb1 or Sth1, degron cultures were grown at 30°C to mid-log phase in synthetic complete media lacking methionine and cysteine with 2% raffinose and 0.1% dextrose as carbon sources. Activation of the degron was achieved by first adding galactose to a final concentration of 2% for 30 min, followed by centrifugation at room

temperature to collect the cells. These cells were next grown at 37°C in rich media prewarmed at 37°C and supplemented with 2% galactose (YPAG).

Preparation of mononucleosomal-sized DNA for tiling microarrays

Approximately 20 OD_{600} units of cells were spheroplasted with 0.25 mg Zymolyase 100-T (Seikagaku) in 2 ml Buffer Z (1M sorbitol, 50mM Tris-Cl pH 7.4, 10mM β-mercaptoethanol) at 30°C with shaking. The spheroplasting time ranged from 30 min to 75 min, depending on the strain and media conditions used for growth. The ideal spheroplasting time was one that yielded appropriately digested chromatin (~90% mononucleosomal-sized DNA) after 20 min of micrococcal nuclease (MNase) treatment. Spheroplasts were collected by centrifugation at 4°C and resuspended in 500µl MNase digestion buffer (0.075% NP-40, 50mM NaCl, 10mM Tris-Cl pH 7.4, 5mM $MgCl_2$, 1mM $CaCl_2$). Chromatin was digested with 3 units of MNase (Worthington) for 20 min at 37°C. Digestions were quenched with 50mM EDTA, and spheroplasts were lysed with 0.1% SDS and centrifuged to transfer the supernatant away from insoluble material. The supernatant containing solublized chromatin was incubated at 65°C overnight with 0.4 mg/ml proteinase K to deproteinize DNA and reverse methylene crosslinks. DNA was recovered by two extractions with phenol and one extraction with chloroform, followed by ethanol precipitation and resuspension in Tris-EDTA (TE) pH 8.0 supplemented with 10 µg/ml RNase A. After a 30 min treatment at 37°C, the DNA was ready for probe generation by linear amplification.

Preparation of reference genomic DNA for tiling microarrays

Genomic DNA was prepared by purification with a Qiagen 100 column after treating spheroplasts with RNase A and proteinase K. Purified DNA was digested with MNase at room temperature to obtain DNA that ranged in size from 100-300bp. This digested DNA was phenol-extracted twice, chloroform-extracted once, and then ethanol-precipitated and resuspended in TE pH 8.0. Genomic reference probe was then prepared by linear amplification in the same manner as mononucleosomal-sized probe.

Linear amplification of DNA to generate microarray RNA probe

Probes for use in microarray experiments were prepared by linear amplification (Liu et al., 2003) but instead of preparing aminoallyl-cDNA probe, aminoallyl-RNA probe was prepared. In brief, DNA obtained by MNase digestion was first treated with calf intestinal phosphatase (New England Biolabs (NEB)) and then thymidine-tailed using terminal dideoxytransferase (NEB). A T7 promoter was adapted to these T-tailed DNA via second strand synthesis with Klenow exo- polymerase (NEB). RNA was next generated using a MegaScript T7 RNA polymerase kit (Ambion) with a 2.3:1 ratio of aminoallyl-UTP to UTP.

Mapping nucleosome positions using tiling microarrays

Nucleosome positions were mapped using a 20bp resolution tiling microarray with the majority of the probes being identical to a previously

described microarray version (*8*). We designed the remaining probes, which included coverage of the *PRM1* ORF. This tiling microarray was printed using a custom arrayer and consisted of 32 print blocks with a total of 16,429 bona fide probes. Unless otherwise specified, nucleosomes were mapped in four independently grown cultures for each strain by hybridizing 5µg of mononucleosomal-sized probe and 5µg of reference genomic DNA probe. Hybridizations were conducted at 65°C for at least 12 hr prior to scanning. Dye swaps were incorporated into the experiments in a balanced manner such that with four mononucleosome:reference replicates, two were labeled as Cy3:Cy5 and the remaining two Cy5:Cy3.

Microarray data processing

Raw microarray data was processed and analyzed using custom-written software implemented with Python. Algorithms for statistical analysis were provided by the R statistics software package. A mononucleosome:reference ratio was calculated for each feature by first subtracting the feature median background intensity from the feature foreground intensity and then taking the log base 2 transformed ratio. The feature ratios in each print block were normalized for intensity-dependent bias using a LOESS regression algorithm with a smooth value of 0.4 (LOESS function provided by the R statistics package).

Preparing nucleosome position data for analysis.

Analysis of nucleosome enrichment data was done using custom-written software implemented with Python that integrated statistical algorithms from the R statistics package. Nucleosome enrichment values for each experiment were determined by taking the mean of the experiment replicates and applying a centered moving average with a window of 5 features (100 bp). This moving average was strictly implemented such that no missing values were permitted within the window, and each feature in the window must be offset by 20 bp (the array resolution) from its immediate neighbor.

Generation of difference maps.

While results from two experiments can be compared side-by-side, generation of a difference map that represents differences between experiments is useful to highlight how the datasets differ from one another. As nucleosome enrichment data are in log2 space, difference maps were generated by subtracting probe data for a control experiment from corresponding probe data for the second experiment. For example, to generate the difference map shown in Figure 17A, probe data from a control experiment that lacked the Reb1 degron were subtracted from corresponding probe data from an experiment that contained the Reb1 degron. The strains used for both experiments were grown under the same conditions.

Analysis of nucleosome position data as a one-dimensional line trace.

Nucleosome positioning data shown in the Figures were generated by the Matplotlib plotting engine module for Python using a coordinate system with probe data representing nucleosome positions overlaid on the positions of features in the genome.

Generation of two-dimensional stacks of nucleosome positioning data and alignment of data at the boundary between NFRs and their downstream nucleosomes.

Comparison of nucleosome positions among a set of ORFs is easily achievable by generating a two-dimensional stack in which each row represents data associated with one ORF and each column represents probe data that is relative to a defined reference point in each ORF. These two-dimensional stacks were generated using custom-written Python software for graphical visualization with Java TreeView.

For the specific purposes of this work, all two-dimensional stacks were generated for ORFs that were associated with probe data. As the resolution of the tiling microarray platform is 20bp, bins of 20bp were defined relative to the translational start site of each ORF, and available probe data 1000bp upstream and downstream of each ORF were assigned to the appropriate bin by the coordinate representing the last nucleotide of the probe. This process generated a two-dimensional stack of data arranged by ORF, but centered at the translational start site. This is not an ideal arrangement for analyzing nucleosome-free regions as the distance between translational start sites and

NFRs can vary among ORFs. Therefore we developed a method of analyzing nucleosome positions about NFRs in a two-dimensional stack of data in which data for each ORF was aligned at the nucleosome downstream of the NFR.

Analyzing experimental data in aligned two-dimensional stacks.

Alignments of extracted ORF data at the +1 nucleosome downstream of the NFR were calculated only for experimental data that served as controls. In this work, alignments were calculated using data from a strain isogenic to the degron strains, except that they lacked a degron allele, from a wild-type strain with the Reb1:dT_7 sequence inserted into the *PRM1* gene, and from a *rpb1-1* strain at its permissive temperature. Nucleosome positions for the degron control strain were aligned using data under both degron-inactive and degron-active growth conditions.

Once these alignment maps were generated, experimental data were overlaid onto these maps to determine how nucleosome positioning is affected. For example, nucleosome positioning data from a strain carrying the Sth1-degron grown under degron-inducing conditions were overlaid on the alignment map generated from the control strain grown under the same conditions. Difference maps that highlighted the changes in nucleosome positions between strains were overlaid on alignment maps by first subtracting control probe data from corresponding experimental probe data, and then overlaying the differences onto alignment maps generated from nucleosome positions in the control data.

Microarray data

Microarray data can be obtained from NCBI GEO at series accession GSE13446.

Chromatin immunoprecipitation and QPCR

Chromatin immunoprecipitation and subsequent analysis by QPCR was performed as previously described (*22*), (*25*).

Table 4. Strains used in the Chapter 3 study

YM#	Genotype	Source
1731	*MATa his3Δ1 leu2Δ0 ura3Δ0 lys2Δ0 met15Δ0*	Segregant of BY4741 x BY4742 (ref 1)
3202	*MAT***a** *ura3-52 rpb1-1*	Ref. 2
3531	*MAT***a** *his3Δ1 leu2Δ0 ura3Δ0 lys2Δ0 met15Δ0 prm1::pGAL1::I-SceI::KanMX::KlURA3*	this study
3532	*MAT***a** *his3Δ1 leu2Δ0 ura3Δ0 lys2Δ0 met15Δ0 prm1::CCGGGTATTTTTTT*	this study
3533	*MAT***a** *his3Δ1 leu2Δ0 ura3Δ0 lys2Δ0 met15Δ0 htz1Δ::KanMX prm1::CCGGGTATTTTTTT*	this study
3534	*MAT*a *his3Δ1 leu2Δ0 ura3Δ0 lys2Δ0 met15Δ0 swr1Δ::KanMX prm1::CCGGGTATTTTTTT*	this study
3535	*MAT***a** *his3Δ1 leu2Δ0 ura3Δ0 lys2Δ0 HIS3::pGAL1::UBR1 URA3::pMET3::DHFRts::3xHA::REB1 prm1::CCGGGTATTTTTTT*	this study
3536	*MAT***a** *his3Δ1 leu2Δ0 ura3Δ0 lys2Δ0 HIS3::pGAL1::UBR1 URA3::pMET3::DHFRts::3xHA::STH1*	this study

	prm1::CCGGGTATTTTTTT	
3537	*MAT***a** *his3Δ1 leu2Δ0 ura3Δ0 lys2Δ0* *HIS3::pGAL1::UBR1* *KanMX::pMET3::abf1(M1R)* *prm1::CCGGGTATTTTTTT*	this study
3538	*MAT***a** *his3Δ1 leu2Δ0 ura3Δ0 lys2Δ0* *HIS3::pGAL1::UBR1* *URA3::pMET3::DHFRts::3xHA::REB1* *KanMX::pMET3::abf1(M1R)* *prm1::CCGGGTATTTTTTT*	this study
3539	*MAT***a** *his3Δ1 leu2Δ0 ura3Δ0 lys2Δ0* *HIS3::pGAL1::UBR1* *prm1::CCGGGTATTTTTTT*	this study
3540	*MAT***a** *his3Δ1 leu2Δ0 ura3Δ0 lys2Δ0* *HIS3::pGAL1::UBR1* *prm1::CCGGGTATTTTTTT*	this study
3541	*MAT***a** *his3Δ1 leu2Δ0 ura3Δ0 lys2Δ0* *HIS3::pGAL1::UBR1* *URA3::pMET3::DHFRts::3xHA::STH1* *prm1::CCGGGTATTTTTTT <LEU2::CEN-* *ARS::pGAL1::htz1(A46intein)>*	this study
3542	*MAT***a** *his3Δ1 leu2Δ0 ura3Δ0 lys2Δ0*	this study

	HIS3::pGAL1::UBR1 *prm1::CCGGGTATTTTTTT <LEU2::CEN-* *ARS::pGAL1::htz1(A46intein)>*	

Ref 1: Brachmann, et al., Yeast 14:115

Ref 2: Nonet, et al. (1987). MCB 7:1602

Figure 15. Models and tools

A. Diagram of the Reb1:dT_7 signal used in this study. Circles indicate nucleosomes. Yellow circle indicates H2A.Z variant nucleosome.

B. Models for relationships between NFR formation and H2A.Z deposition.

C. Conditional degron alleles of *ABF1, REB1* and *STH1* display protein depeletion under degron-inducing conditions. Strains were shifted to YPA media containing 2% galactose for the indicated times and analyzed by immunoblotting with anti-HA or anti-Abf1 antibodies. Ponceau staining of blots demonstrated equal protein loading (Figure 22)

D. Growth of degron strains under noninducing and inducing conditions. Shown are serial dilutions of strains plated on the indicated media. Plates were photographed after 2 days of incubation.

Figure 15

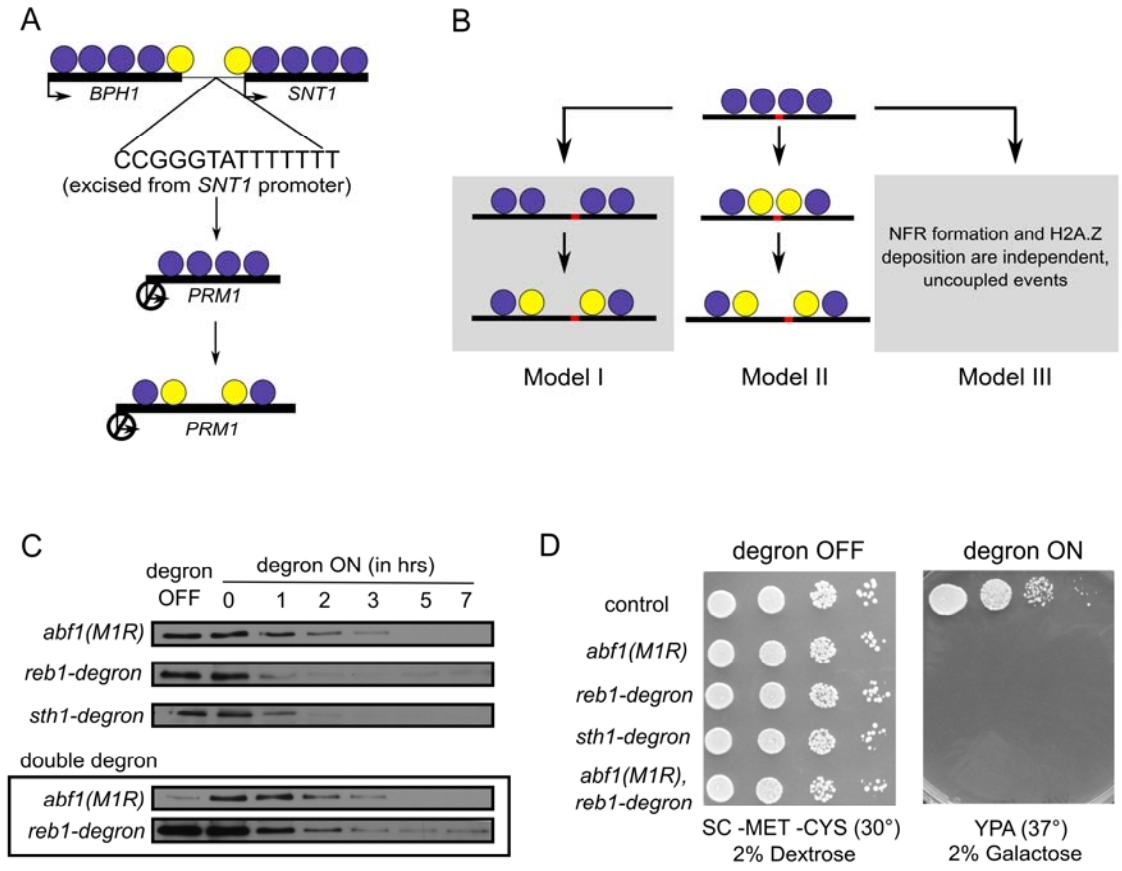
A
BPH1
SNT1
CCGGGTATTTTTTT
(excised from SNT1 promoter)
PRM1
PRM1
B
NFR formation and H2A.Z deposition are independent, uncoupled events
Model I
Model II
Model III
C
degron
degron ON (in hrs)
OFF 0 1 2 3 5 7
abf1(M1R)
reb1-degron
sth1-degron
double degron
abf1(M1R)
reb1-degron
D
degron OFF
degron ON
control
abf1(M1R)
reb1-degron
sth1-degron
abf1(M1R), reb1-degron
SC -MET -CYS (30°) 2% Dextrose
YPA (37°) 2% Galactose

Figure 16. Tiling array analysis of nucleosome positions in the *PRM1* ORF containing the Reb1:dT$_7$ insertion.

A. Analysis of the effect of Reb1:dT$_7$ sequence insertion on nucleosome positioning. Shown are line traces of a moving average of mononucleosome/genomic probe signals across the *PRM1* gene with and without the indicated sequence insertion. Triangles indicate the insertion site.

B. Analysis of effects of Reb1 and Sth1 depletion on NFR formation mediated by Reb1:dT$_7$. Indicated strains containing the Reb1:dT$_7$ insertion in the *PRM1* gene were analyzed as described in A.

C. Analysis of effects of *htz1*Δ and *swr1*Δ mutations on NFR formation mediated by Reb1:dT$_7$. Indicated strains containing the Reb1:dT$_7$ insertion in the *PRM1* gene were analyzed as described in A.

Figure 16

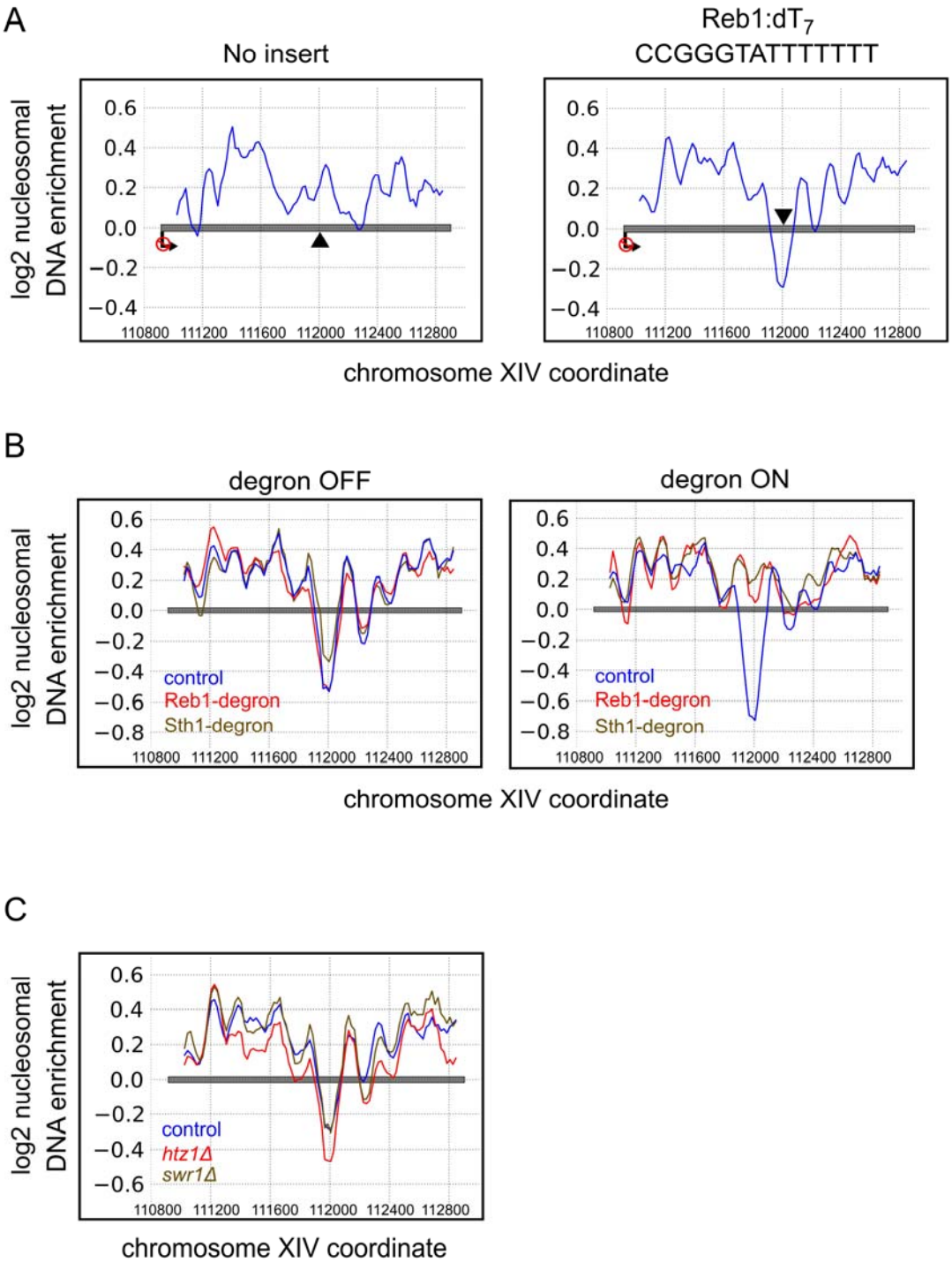
A
No insert
Reb1:dT7
CCGGGTATTTTTTT
log2 nucleosomal DNA enrichment
0.6
0.4
0.2
0.0
−0.2
−0.4
110800 111200 111600 112000 112400 112800
chromosome XIV coordinate
B
degron OFF
degron ON
control
Reb1-degron
Sth1-degron
−0.6
−0.8
C
htz1Δ
swr1Δ

Figure 17. Chromosome-wide tiling array analysis of nucleosome positions in cells depleted of Reb1

A. Difference map analysis of effects of Reb1 depletion on nucleosome positions. Map represents nucleosome positioning data from a control strain lacking the Reb1-degron subtracted from a strain with the Reb1-degron. See Experimental Procedures for further details. Nucleosome positioning data 1kb upstream and downstream of the ATG of 150 genes are shown and orientated such that the direction of transcription is to the right. Asterisks indicate center of the +1 nucleosome downstream of the NFR in the control strain. The x-axis represents the distance (in bp) from the center. Data are organized into two clusters using the k-means method.

B. Line traces of average nucleosome positions of the two clusters shown in A The indicated strains were grown under degron-inducing conditions.

C. Scatter plots of the lowest probe signal in NFRs. Points indicate the lowest probe signal in the NFR for a locus in control versus degron strains grown under the indicated conditions.

D. Correlation between Reb1 binding and changes in nucleosomal enrichment at NFRs at promoters. The significance values (log10 p-value) of Reb1 binding at promoters (Harbison, et al. 2004) are compared against the highest fold changes of nucleosome positioning signals at the associated NFR.

E. Correlation between Reb1 consensus sites in promoters and the highest fold change of nucleosome enrichment at the associated NFR under the indicated promoters.

F. Enrichment of Reb1 sites in clusters. Shown are the p-values (hypergeometric testing) of the significance of the indicated Reb1 motifs in the indicated clusters.

Figure 17

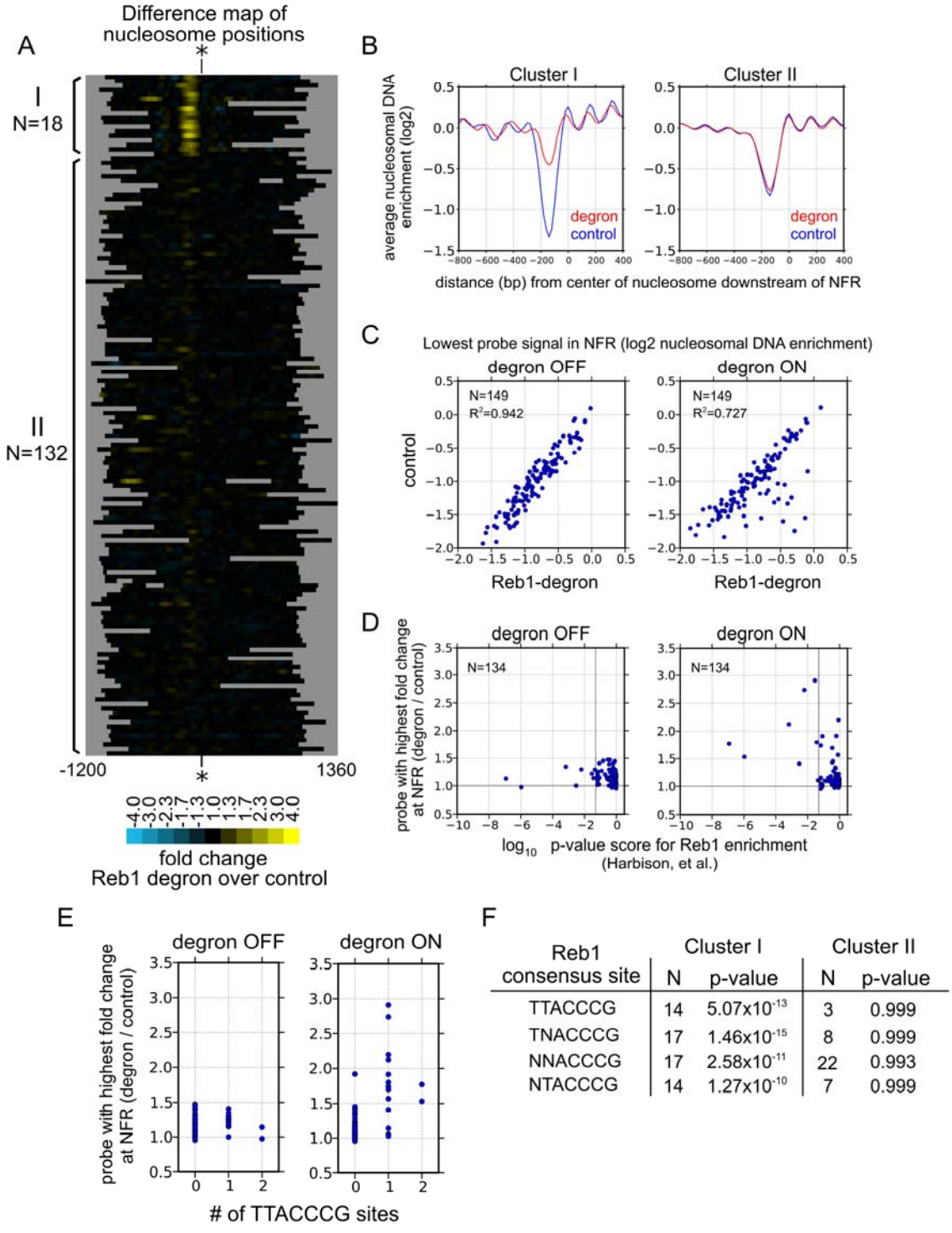

F

Reb1 consensus site	Cluster I N	Cluster I p-value	Cluster II N	Cluster II p-value
TTACCCG	14	5.07×10^{-13}	3	0.999
TNACCCG	17	1.46×10^{-15}	8	0.999
NNACCCG	17	2.58×10^{-11}	22	0.993
NTACCCG	14	1.27×10^{-10}	7	0.999

Figure 18. Chromosome-wide tiling array analysis of nucleosome positions in cells depleted of Abf1

A-F. These panels are analogous to those of Figure 17 except that a strain with the Abf1-degron was compared to the same control strain used for analysis of nucleosome positions upon Reb1 depletion.

Figure 18

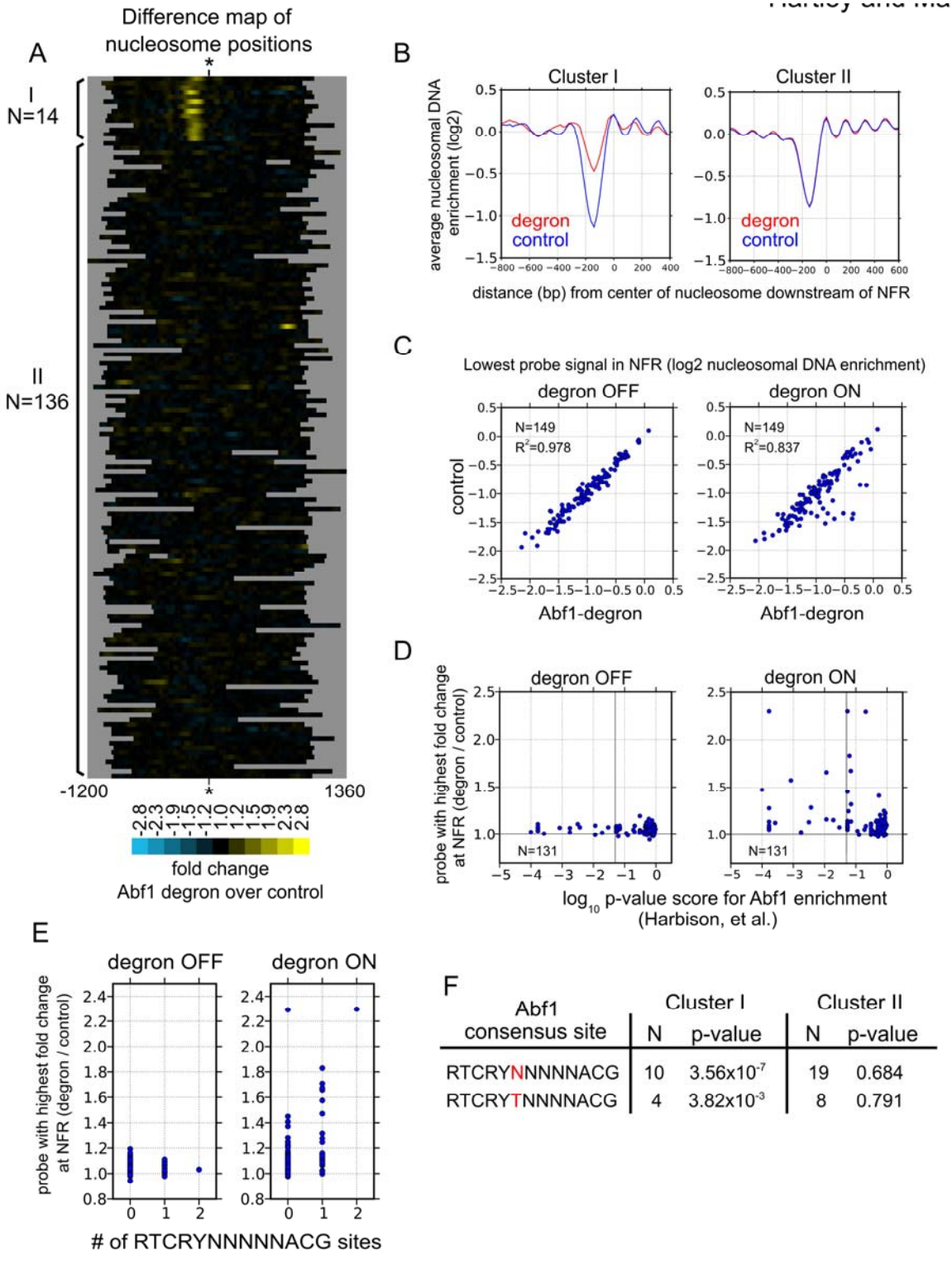

F

Abf1 consensus site	Cluster I N	Cluster I p-value	Cluster II N	Cluster II p-value
RTCRYNNNNNACG	10	3.56×10^{-7}	19	0.684
RTCRYTNNNNACG	4	3.82×10^{-3}	8	0.791

Figure 19. Chromosome-wide tiling array analysis of nucleosome positions in cells depleted of Sth1

A-C. These panels are analogous to those of Figure 17 except that a strain with the Sth1-degron was compared to the same control strain used for analysis of nucleosome positions upon Reb1 depletion.

D. Gene expression analysis. Shown is the correlation between mRNA and NFR changes in cells depleted of Sth1. Ploted are the values for genes on chromosome III. Shown on right is the p-values (hypergeometric testing) of the significance of the enrichments in the indicated gene groups using a 1.5-fold cutoff for decreases in mRNA levels. Expression data were not available for all genes in the clusters; hence, Cluster I N=79 , Cluster II N=64.

E. NPS signature averages. Lines traces of NPS predictions (Ioshikes et al., 2006) for genes in the indicated gene clusters are shown in green. These predictions were smoothed using a 51bp moving average window. Experimental nucleosome position averages (control is blue, Sth1-degron is red) are shown as in panel B.

F. Effect of transcription on nucleosome positioning. Shown are the average nucleosome positions for the indicated gene clusters in *rpb1-1* strains grown under permissive conditions or for 1 hr under nonpermissive conditions.

Figure 19

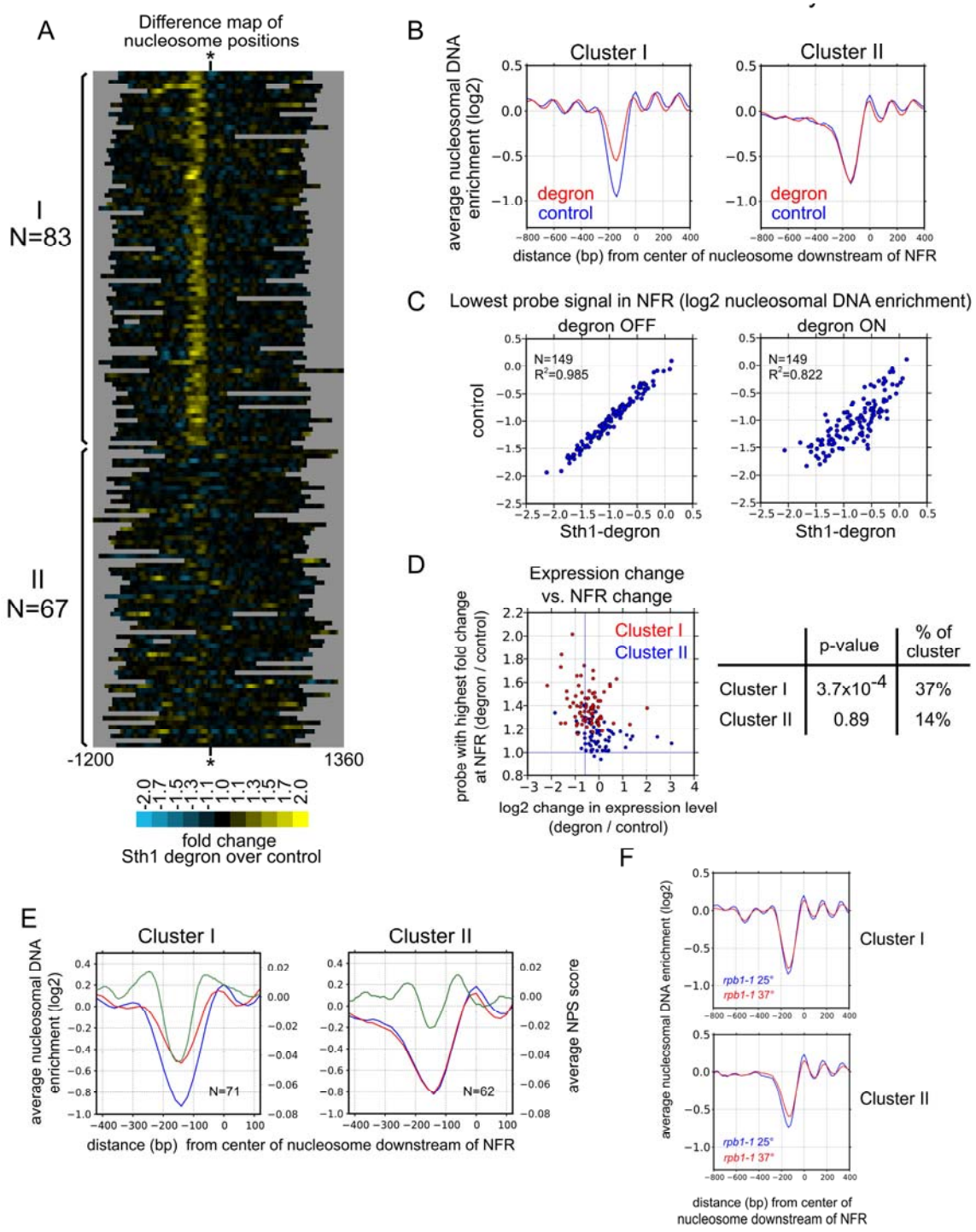
A
Difference map of nucleosome positions
I
N=83
II
N=67
-1200
1360
fold change
Sth1 degron over control
B
Cluster I
Cluster II
average nucleosomal DNA enrichment (log2)
degron
control
distance (bp) from center of nucleosome downstream of NFR
C
Lowest probe signal in NFR (log2 nucleosomal DNA enrichment)
degron OFF
degron ON
N=149
R²=0.985
R²=0.822
control
Sth1-degron
D
Expression change vs. NFR change
probe with highest fold change at NFR (degron / control)
log2 change in expression level (degron / control)
p-value
% of cluster
Cluster I
3.7x10-4
37%
Cluster II
0.89
14%
E
average NPS score
N=71
N=62
distance (bp) from center of nucleosome downstream of NFR
F
rpb1-1 25°
rpb1-1 37°
distance (bp) from center of nucleosome downstream of NFR

Figure 20. Comparison of the roles of Abf1, Reb1, and RSC in nucleosome positioning

A. Clustering analysis of difference maps. Shown are difference maps for the indicated strains including the Abf1-Reb1 “double degron” strain. K-means (K=15) clustering was applied. Line traces of cluster averages are shown in Figure 26.

B. Scatter plots of double degron. Analysis was performed as in Figure 17C.

C. Gene expression analysis. Shown is the correlation between mRNA and NFR changes in cells depleted of both Reb1 and Abf1. The p-value (hypergeometric testing) of the significance of the enrichments in the group of genes (N=20) consisting of those affected in NFR size by Abf1- or Reb1-depletion (Cluster I in Figure 17 and Cluster I in Figure 18; corresponding points are colored red in this figure) using a 1.5-fold cutoff for decreases in mRNA levels was 1.2×10^{-6}. The p value for the remaining, unaffected genes (N=123) was 0.99.

Figure 20

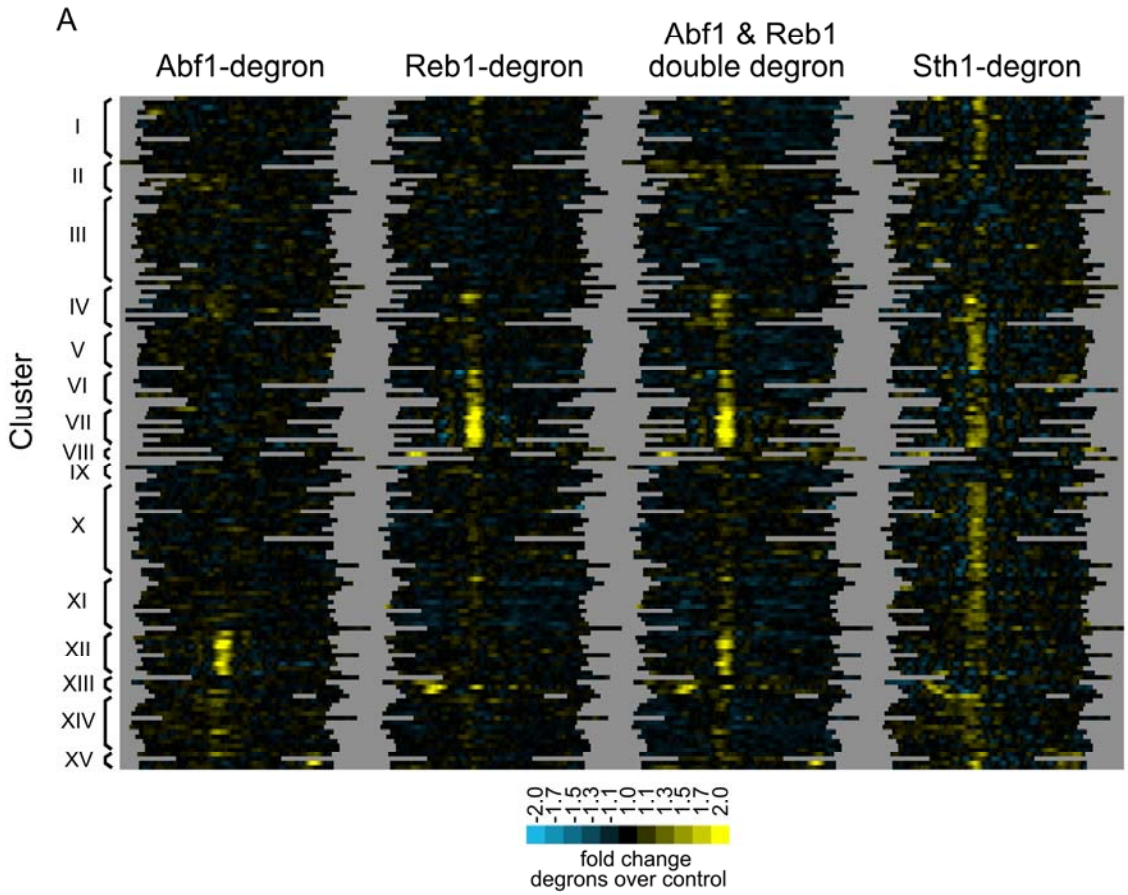
A
Abf1-degron
Reb1-degron
Abf1 & Reb1
double degron
Sth1-degron
Cluster
I
II
III
IV
V
VI
VII
VIII
IX
X
XI
XII
XIII
XIV
XV
-2.0
-1.7
-1.5
-1.3
-1.1
1.0
1.1
1.3
1.5
1.7
2.0
fold change
degrons over control

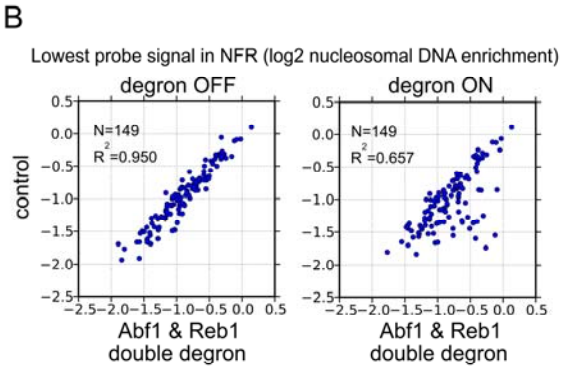
B
Lowest probe signal in NFR (log2 nucleosomal DNA enrichment)
degron OFF
degron ON
N=149
R2=0.950
N=149
R2=0.657
control
Abf1 & Reb1
double degron
Abf1 & Reb1
double degron

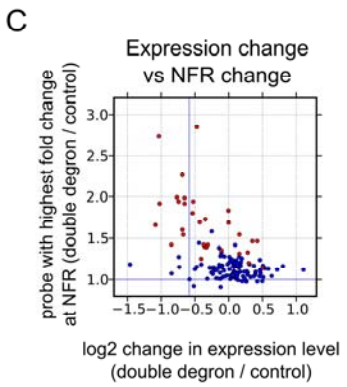
C
Expression change
vs NFR change
probe with highest fold change
at NFR (double degron / control)
log2 change in expression level
(double degron / control)

Figure 21. Analysis of H2A.Z deposition requirements using a steroid-regulated intein

A. Schematic of H2A.Z intein constructs. An engineered *M. tuberculosis* RecA intein controlled by the human estrogen receptor ligand binding domain was placed at a chosen site in *HTZ1* gene (encoding H2A.Z). The *HTZ1* promoter was replaced with the galactose-inducible *pGAL1* promoter. Protein splicing would occur in the presence of 4-hydroxytamoxifen (4-HT) and leave a cysteine residue ("scar") at the splicing junction.

B. Splicing of the H2A.Z intein construct occurs with an allele that replaces Ala46 with the intein construct. The 4-HT-regulated intein was inserted in place of four different residues in H2A.Z, and these constructs each were placed on a 2μ plasmid under the control of a *pGAL1* promoter and transformed into a *htz1Δ* strain. Strains were grown to mid-log phase in the presence of 2% galactose and, when indicated, 10 μM 4-HT. Shown is a Western using polyclonal antibody specific to the C-terminus of H2A.Z. A strain with a chromosomal-based, wild-type copy of *HTZ1* and a *htz1Δ* strain are included as controls.

C. Analysis of H2A.Z deposition requirements. A strain carrying the Sth1 degron was shifted to degron-inducing conditions which also induces synthesis of unspliced H2A.Z intein construct. After 5 hrs, 4-HT was added to 10μM to induce splicing. Cells were collected after 3 hrs of further incubation, and H2A.Z enrichment at select loci was determined

relative to histone H3 enrichment and normalized to a locus in the middle of the large *BUD3* ORF. H2A.Z/H3 enrichment profiles under Sth1-depleted conditions were compared against control profiles. Top panels indicate nucleosomal DNA enrichment in various conditions (blue: degron-OFF conditions, red: 5 hrs of degron-ON, green: 8 hrs of degron-ON, with the last 3 hrs in the presence of 4-HT). Bottom panels represent normalized H2A.Z/H3 enrichment values at the indicated amplicons. Data are shown for the promoters of *DCC1/BUD3.*

D. Same as in C, except data are shown for the *PR*M1 ORF containing the Reb1:dT_7 insertion.

E. Same as in C, except data are shown for the promoter of *YCR016W.*

F. Same as in C, except data are shown for the promoter of *YCRO23C.*

Figure 21

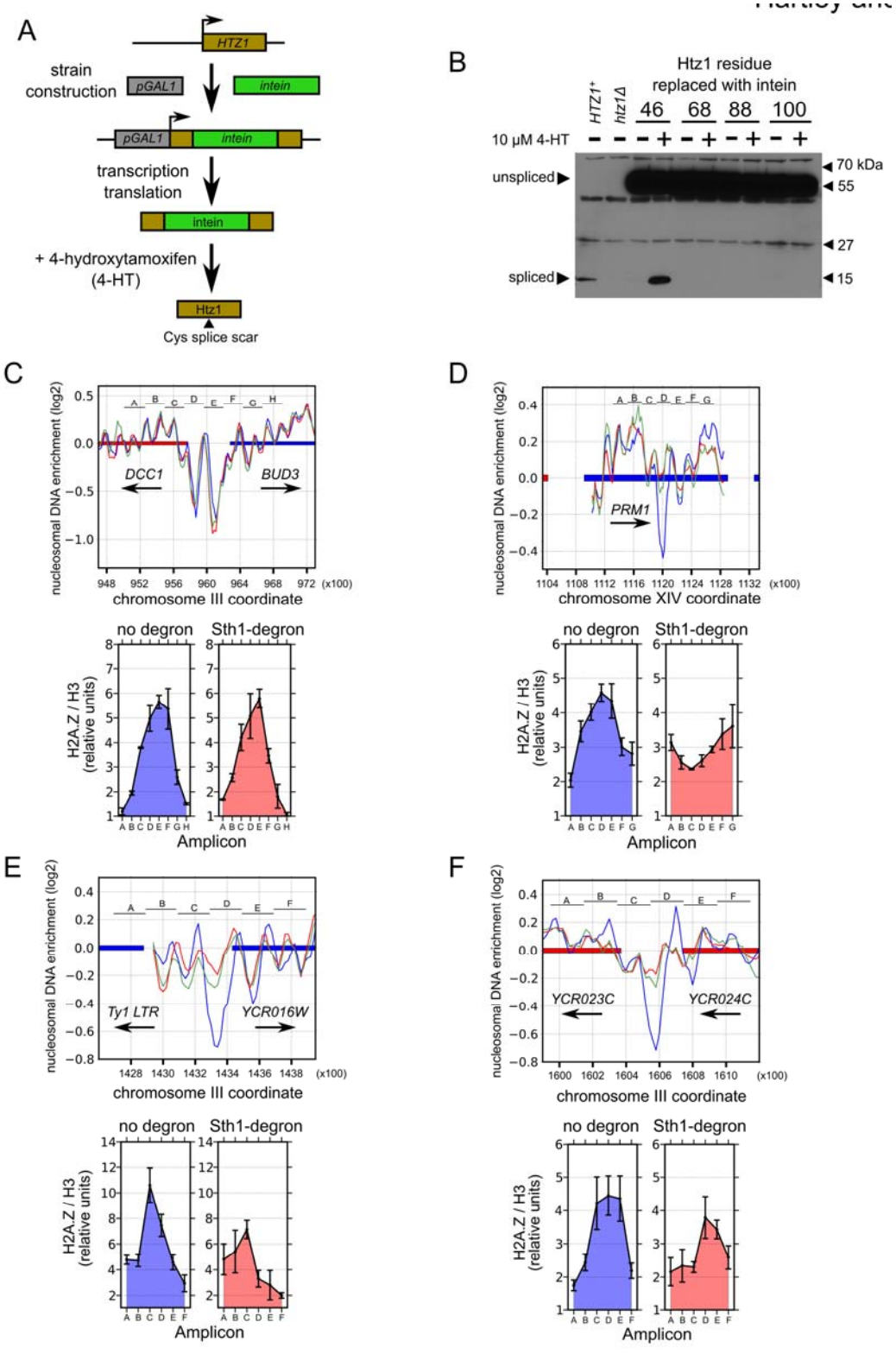
A
HTZ1
strain construction
pGAL1
intein
pGAL1
intein
transcription translation
intein
+ 4-hydroxytamoxifen (4-HT)
Htz1
Cys splice scar
B
Htz1 residue replaced with intein
HTZ1+
htz1Δ
46
68
88
100
10 μM 4-HT
unspliced
spliced
70 kDa
55
27
15
C
nucleosomal DNA enrichment (log2)
DCC1
BUD3
chromosome III coordinate
no degron
Sth1-degron
H2A.Z / H3 (relative units)
Amplicon
D
PRM1
chromosome XIV coordinate
E
Ty1 LTR
YCR016W
F
YCR023C
YCR024C

Figure 22. Ponceau stains of gels used to prepare blots for Western experiments shown in Figure 15C. Lanes are oriented as in Figure 15C.

A. Abf1 degron strain

B. Reb1-degron strain

C. Sth1-degron strain

D. Abf1 & Reb1 double degron strain.

Figure 22

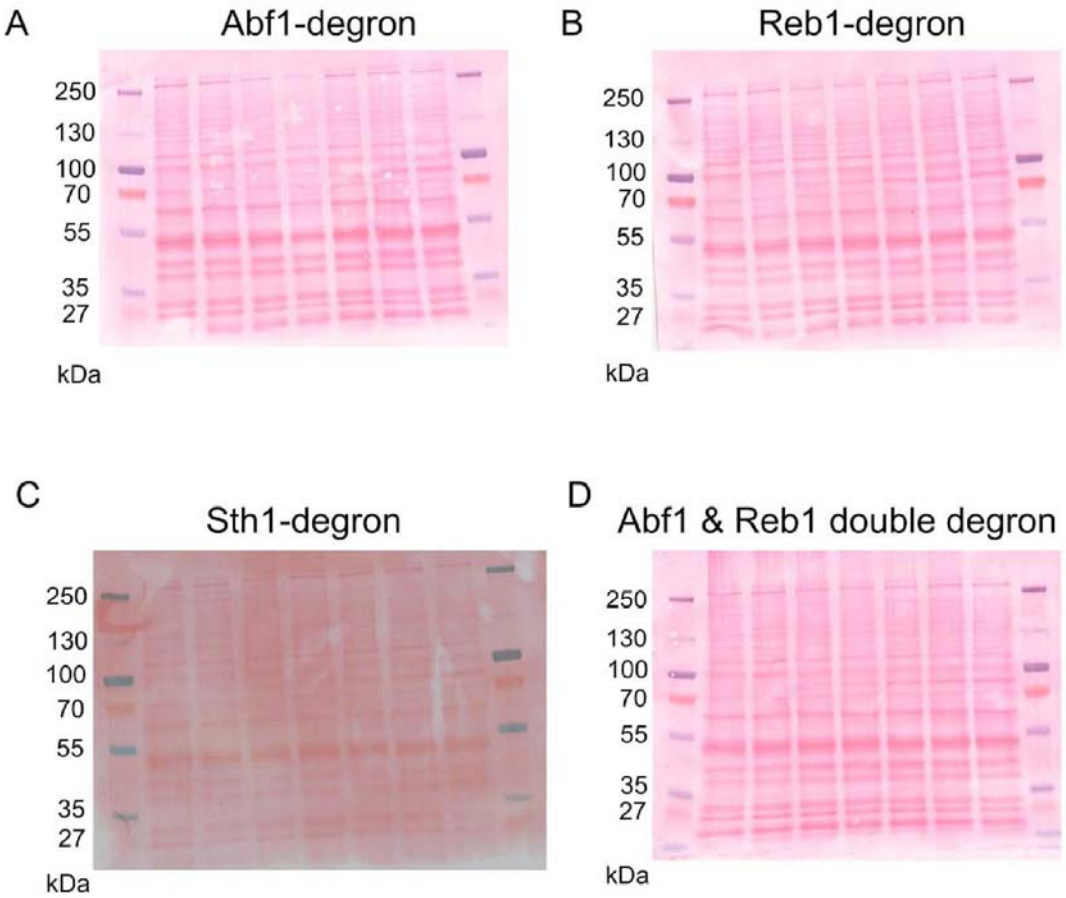
A
Abf1-degron
250
130
100
70
55
35
27
kDa
B
Reb1-degron
250
130
100
70
55
35
27
kDa
C
Sth1-degron
250
130
100
70
55
35
27
kDa
D
Abf1 & Reb1 double degron
250
130
100
70
55
35
27
kDa

Figure 23. Analysis of transcripts arising from PRM1 using RT-QPCR of a 200bp amplicon centered at 420bp downstream of the Reb1:dT7 insertion site in *PRM1*

Shown are actin-normalized transcript levels for the indicated strains. Asterisks indicate multiple peaks were present in the melting curves, suggesting that only cross-reacting transcripts were detected. The first two columns represent an average of four biological replicates, while the last two columns represent one biological replicate. αF refers to alpha-factor.

Figure 23

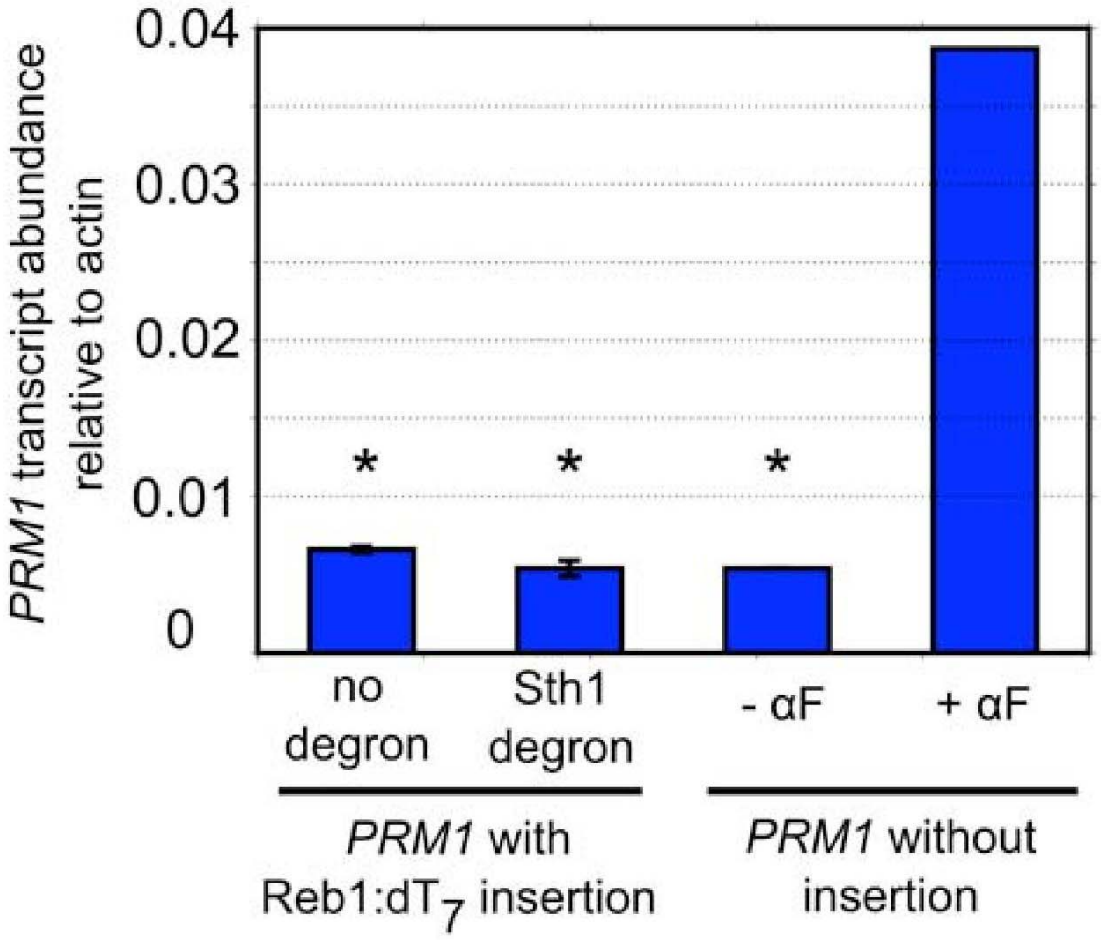
PRM1 transcript abundance relative to actin
0.04
0.03
0.02
0.01
0
*
*
*
no degron
Sth1 degron
- αF
+ αF
PRM1 with Reb1:dT7 insertion
PRM1 without insertion

Figure 24. Relationship of transcription start sites (TSSs) and nucleosome positions

Shown are the average nucleosome positions under degron-inducing conditions of a strain containing the Sth1 degron (red line) and a control strain lacking a degron allele (blue line). Clusters I and II refer to the clusters shown in Figure 19A. Transcription start sites are given by (*90*).

Figure 24

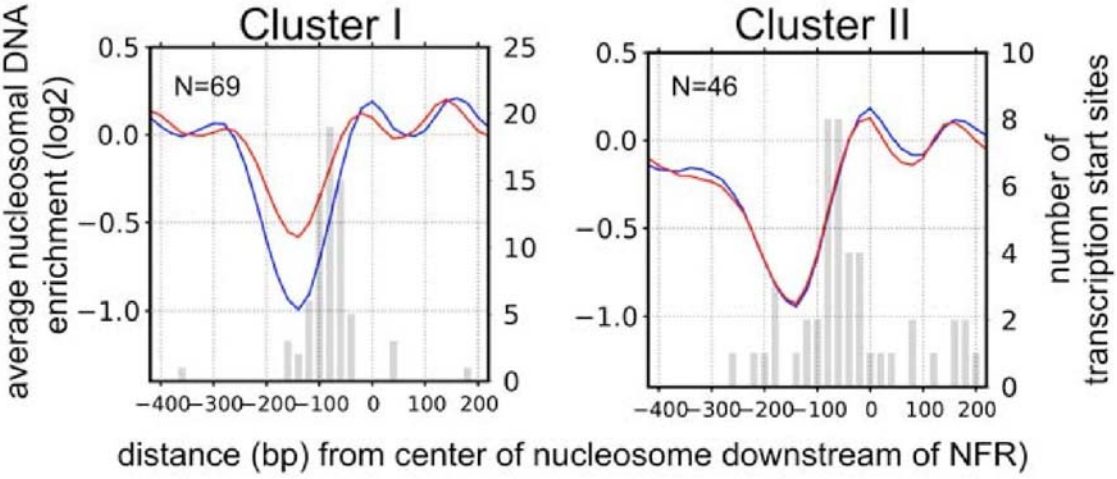
Cluster I
Cluster II
N=69
N=46
average nucleosomal DNA enrichment (log2)
number of transcription start sites
distance (bp) from center of nucleosome downstream of NFR)

Figure 25. Correlation plot of the lowest nucleosomal DNA signal in the NFRs promoters of a *rpb1-1* strain grown at the permissive temperature (25º) or 1 hour at the restrictive temperature (37º)

Figure 25

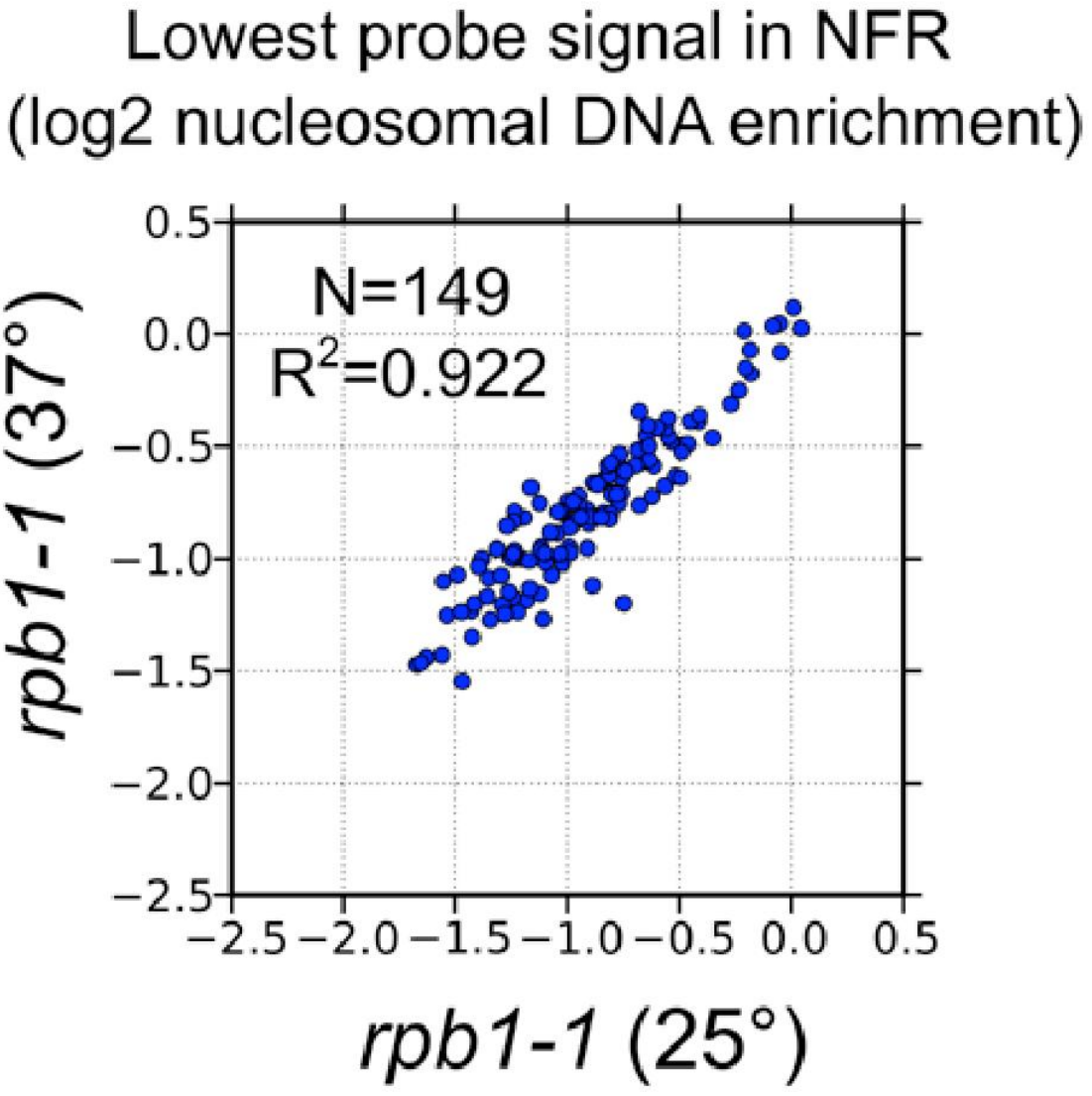
Lowest probe signal in NFR
(log2 nucleosomal DNA enrichment)
N=149
R2=0.922
rpb1-1 (37°)
rpb1-1 (25°)
0.5
0.0
−0.5
−1.0
−1.5
−2.0
−2.5
−2.5 −2.0 −1.5 −1.0 −0.5 0.0 0.5

Figure 26. Average nucleosomal DNA enrichments about the NFRs of genes found in the clusters shown in Figure 26

The nucleosome positioning data shown are derived from degron-inducing strain growth conditions. Strains are indicated in color as given by the last panel of the 4th row. Cluster names are given in Roman numerals and correlate with the cluster names shown in Figure 26.

Figure 26

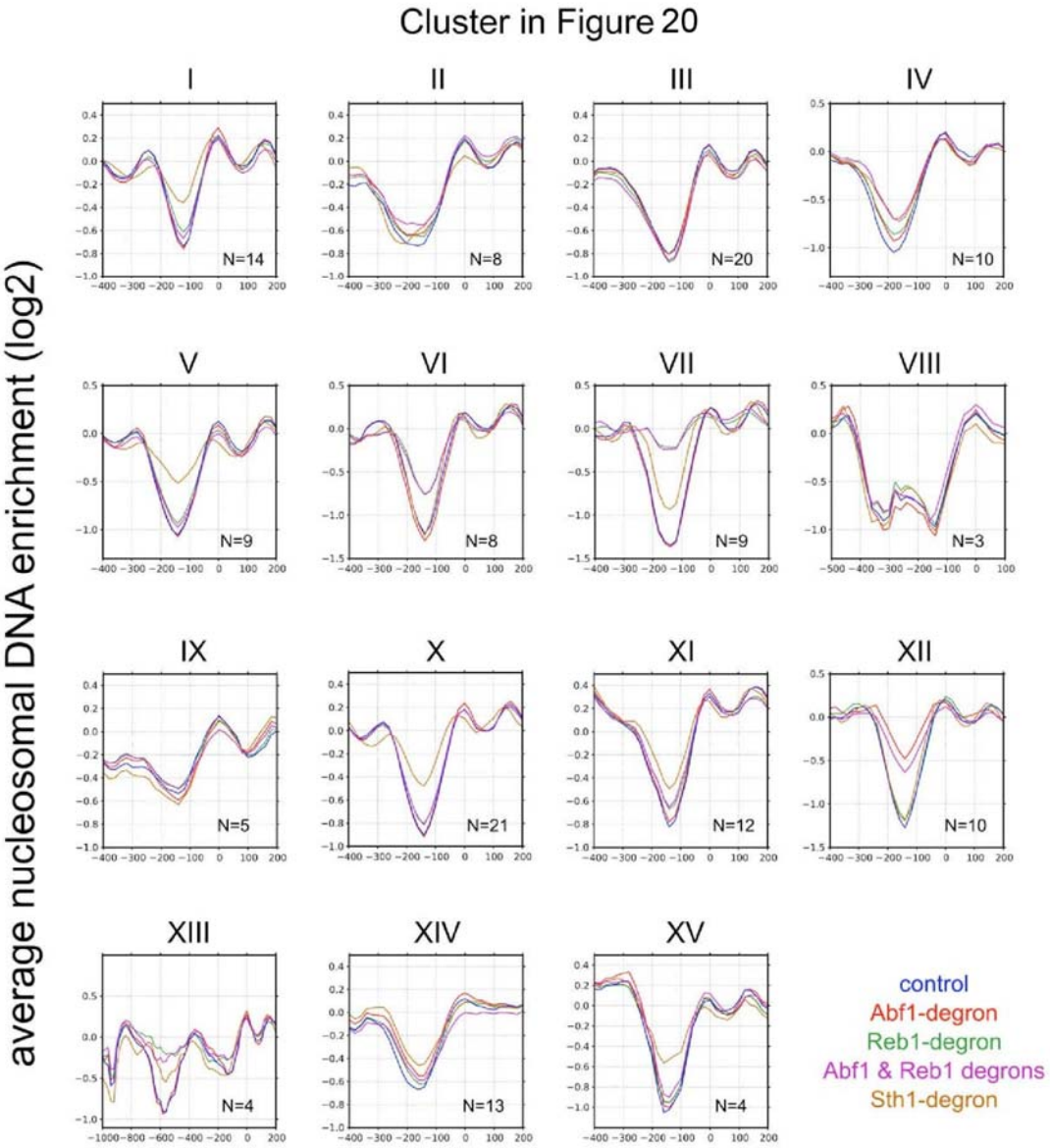
Cluster in Figure 20
average nucleosomal DNA enrichment (log2)
I
N=14
II
N=8
III
N=20
IV
N=10
V
N=9
VI
N=8
VII
N=9
VIII
N=3
IX
N=5
X
N=21
XI
N=12
XII
N=10
XIII
N=4
XIV
N=13
XV
N=4
control
Abf1-degron
Reb1-degron
Abf1 & Reb1 degrons
Sth1-degron

Figure 27. Chromosome-wide tiling array analysis of nucleosome positions in cells defective in H2A.Z nucleosomes

Panels A and B are analogous to Figure 17B and C except that data were derived from cells lacking H2A.Z (*htz1*Δ) or the Swr1 ATPase (*swr1*Δ).

Figure 27

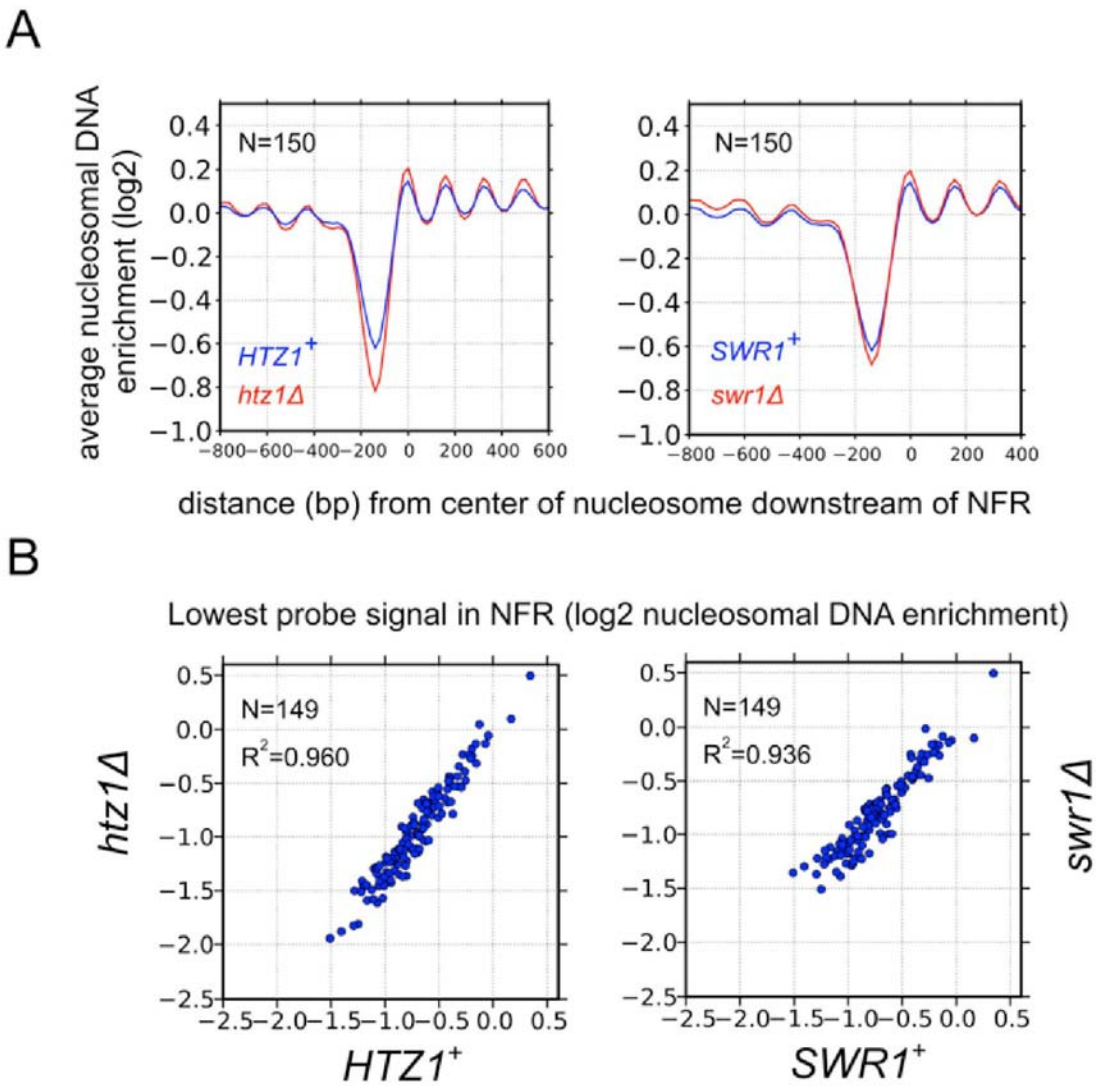
A
average nucleosomal DNA enrichment (log2)
N=150
HTZ1+
htz1Δ
SWR1+
swr1Δ
distance (bp) from center of nucleosome downstream of NFR
B
Lowest probe signal in NFR (log2 nucleosomal DNA enrichment)
N=149
R2=0.960
N=149
R2=0.936
htz1Δ
swr1Δ
HTZ1+
SWR1+

Figure 28.

A. anti-H2A.Z immunoblots of strains used for the experiments described in Figure 21C-F. Shown are 4 timepoints for two strains, one of which has the Sth1-degron, and the other the wild-type Sth1 gene. Timepoints are given as time in degron-inducing media containing galactose (0h, 5h, 8h), and with or without 4-HT (the two 8hr timepoints). As shown, unspliced H2A.Z is produced in both strains upon shift to degron-inducing, galactose-containing media, and this construct is spliced only in the presence of 4-HT.
B. The Sth1-degron strain used for experiments shown in Figure 21C-F was probed with anti-HA antibody to detect the HA epitope tag on the Sth1-degron. Timepoints are as in (A). As shown, Sth1 has been significantly degraded and remains degraded after 5 hours of growth in degron-inducing media.
C. Overexposure of a portion of the Western blot shown in Figure 21B. These two lanes are the same as lanes 3 and 4 in Figure 21B, but the Western was exposed to film 18X longer than the Western shown in Figure 21B. There is a minor amount of splicing of the htz1(A46intein) intein construct in the absence of 4-HT in the context of a 2-micron plasmid.
D. H2A.Z enrichment profiles as determined by ChIP and QPCR at amplicon E in the *BUD3* promoter (see Figure 21C). H2A.Z is normalized to the

input DNA from the ChIP. As shown, H2A.Z deposition into chromatin correlates with the splicing of the H2A.Z intein (A).

Figure 28

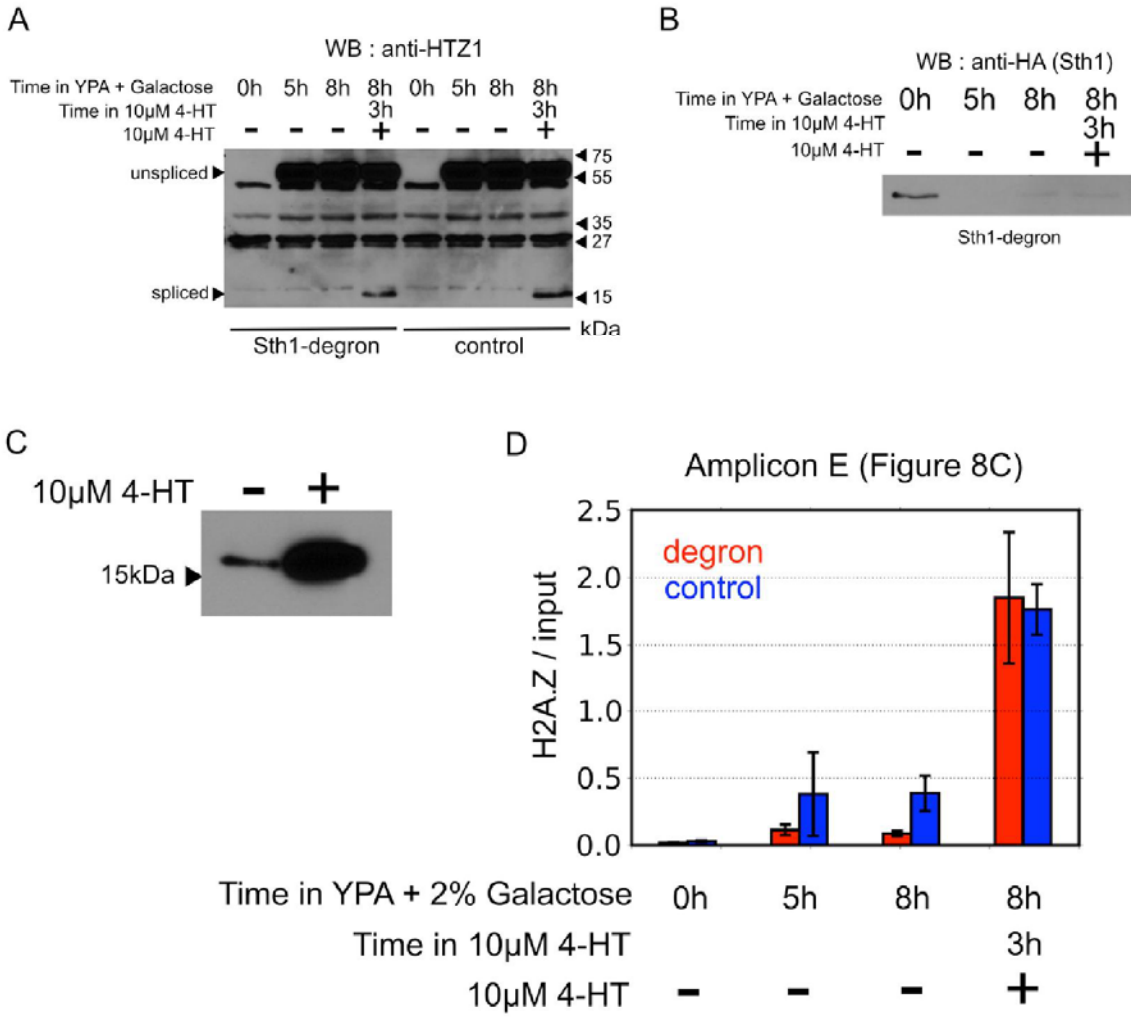
A
WB : anti-HTZ1
Time in YPA + Galactose
Time in 10µM 4-HT
10µM 4-HT
0h 5h 8h 8h 3h 0h 5h 8h 8h 3h
- - - + - - - +
unspliced
spliced
75
55
35
27
15
kDa
Sth1-degron
control
B
WB : anti-HA (Sth1)
Time in YPA + Galactose
Time in 10µM 4-HT
10µM 4-HT
0h 5h 8h 8h 3h
- - - +
Sth1-degron
C
10µM 4-HT - +
15kDa
D
Amplicon E (Figure 8C)
H2A.Z / input
2.5
2.0
1.5
1.0
0.5
0.0
degron
control
Time in YPA + 2% Galactose 0h 5h 8h 8h
Time in 10µM 4-HT 3h
10µM 4-HT - - - +

Figure 29. Histogram plots of peak nucleosome signals as predicted by NPS algorithms

Peak nucleosome signals (*76*) are overlaid on the average nucleosomal DNA enrichment plots for Clusters I and II as given in Figure 19A. Nucleosome positions in a Sth1 degron strain are represented by a red line, while the blue line represents a control strain lacking the degron. The strains were grown under degron-inducing conditions.

Figure 29

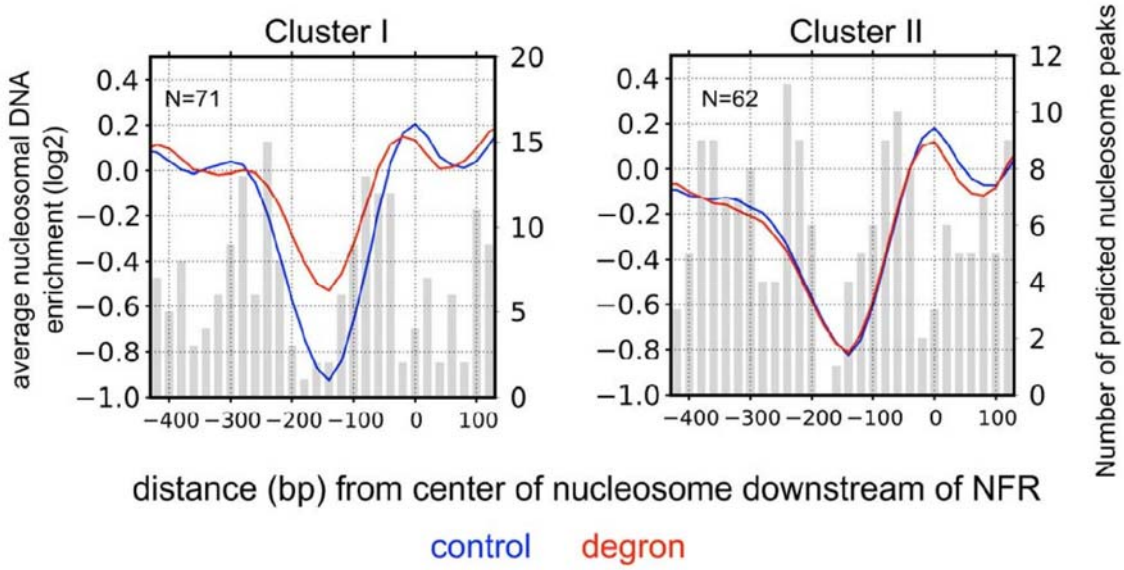
Cluster I
Cluster II
N=71
N=62
average nucleosomal DNA enrichment (log2)
Number of predicted nucleosome peaks
distance (bp) from center of nucleosome downstream of NFR
control
degron

References

1. Luger, K., Mäder, A. W., Richmond, R. K., Sargent, D. F., Richmond, T. J. , *Nature*. **389**, 251-60 (1997).

2. Almer, A., Hörz, W. , *The EMBO journal*. **5**, 2681-7 (1986).

3. Svaren, J., Schmitz, J., Hörz, W. , *The EMBO journal*. **13**, 4856-62 (1994).

4. Venter, U., Svaren, J., Schmitz, J., Schmid, A., Hörz, W. , *The EMBO journal*. **13**, 4848-55 (1994).

5. Lam, F. H., Steger, D. J., O'Shea, E. K. , *Nature*. **453**, 246-50 (2008).

6. Martinez-Campa, C. et al., *Molecular cell*. **15**, 69-81 (2004).

7. Wyrick, J. J. et al., *Nature*. **402**, 418-21 (1999).

8. Yuan, G. et al., *Science (New York, N.Y.)*. **309**, 626-30 (2005).

9. Lee, W. et al., *Nature genetics*. **39**, 1235-44 (2007).

10. Shivaswamy, S. et al., *PLoS biology*. **6**, e65 (2008).

11. Mavrich, T. N. et al., *Genome research*. **18**, 1073-83 (2008).

12. Mavrich, T. N. et al., *Nature*. **453**, 358-62 (2008).

13. Schones, D. E. et al., *Cell*. **132**, 887-98 (2008).

14. Venters, B. J., Pugh, B. F. , *Genome research*. **19**, 360-71 (2009).

15. Segal, E., Widom, J. , *Current opinion in structural biology*. **19**, 65-71 (2009).

16. Iyer, V., Struhl, K. , *The EMBO journal*. **14**, 2570-9 (1995).

17. Widom, J. et al., *Journal of molecular biology*. **288**, 213-29 (1999).

18. Segal, E. et al., *Nature*. **442**, 772-8 (2006).

19. Kaplan, N. et al., *Nature*. **458**, 362-6 (2009).

20. Yuan, G., Liu, J. S. , *PLoS computational biology*. **4**, e13 (2008).

21. Whitehouse, I., Rando, O. J., Delrow, J., Tsukiyama, T. , *Nature*. **450**, 1031-5 (2007).

22. Raisner, R. M. et al., *Cell*. **123**, 233-48 (2005).

23. Albert, I. et al., *Nature*. **446**, 572-6 (2007).

24. Barski, A. et al., *Cell*. **129**, 823-37 (2007).

25. Meneghini, M. D., Madhani, H. D., Wu, M. , *Cell*. **112**, 725-36 (2003).

26. Zhang, H., Roberts, D. N., Cairns, B. R. , *Cell*. **123**, 219-31 (2005).

27. Brickner, D. G. et al., *PLoS biology*. **5**, e81 (2007).

28. Zofall, M. et al., *Nature*. **461**, 419-22 (2009).

29. Krogan, N. J. et al., *Proceedings of the National Academy of Sciences of the United States of America*. **101**, 13513-8 (2004).

30. Kimura, A., Umehara, T., Horikoshi, M. , *Nature genetics*. **32**, 370-7 (2002).

31. Suka, N., Luo, K., Grunstein, M. , *Nature genetics*. **32**, 378-83 (2002).

32. Ng, H. H., Ciccone, D. N., Morshead, K. B., Oettinger, M. A., Struhl, K. , *Proceedings of the National Academy of Sciences of the United States of America*. **100**, 1820-5 (2003).

33. Santos-Rosa, H., Bannister, A. J., Dehe, P. M., Géli, V., Kouzarides, T. , *The Journal of biological chemistry*. **279**, 47506-12 (2004).

34. van Leeuwen, F., Gafken, P. R., Gottschling, D. E. , *Cell*. **109**, 745-56 (2002).

35. Kobor, M. S. et al., *PLoS biology*. **2**, E131 (2004).

36. Krogan, N. J. et al., *Molecular cell*. **12**, 1565-76 (2003).

37. Mizuguchi, G. et al., *Science (New York, N.Y.)*. **303**, 343-8 (2004).

38. Ladurner, A. G., Inouye, C., Jain, R., Tjian, R. , *Molecular cell*. **11**, 365-76 (2003).

39. Matangkasombut, O., Buratowski, S. , *Molecular cell*. **11**, 353-63 (2003).

40. Santisteban, M. S., Kalashnikova, T., Smith, M. M. , *Cell*. **103**, 411-22 (2000).

41. Hwang, W. W. et al., *Molecular cell*. **11**, 261-6 (2003).

42. Donze, D., Adams, C. R., Rine, J., Kamakaka, R. T. , *Genes & development*. **13**, 698-708 (1999).

43. Bolton, E. C., Boeke, J. D. , *Genome research*. **13**, 254-63 (2003).

44. Fraser, H. B., Hirsh, A. E., Giaever, G., Kumm, J., Eisen, M. B. , *PLoS biology*. **2**, e137 (2004).

45. Kim, M. et al., *Nature*. **432**, 517-22 (2004).

46. Chu, S. et al., *Science (New York, N.Y.)*. **282**, 699-705 (1998).

47. Galitski, T., Saldanha, A. J., Styles, C. A., Lander, E. S., Fink, G. R. , *Science (New York, N.Y.)*. **285**, 251-4 (1999).

48. Deckert, J., Struhl, K. , *Molecular and cellular biology*. **21**, 2726-35 (2001).

49. Erdman, S., Lin, L., Malczynski, M., Snyder, M. , *The Journal of cell biology*. **140**, 461-83 (1998).

50. Heiman, M. G., Walter, P. , *The Journal of cell biology*. **151**, 719-30 (2000).

51. Kurdistani, S. K., Tavazoie, S., Grunstein, M. , *Cell*. **117**, 721-33 (2004).

52. Liu, C. L. et al., *PLoS biology*. **3**, e328 (2005).

53. Angermayr, M., Oechsner, U., Bandlow, W. , *The Journal of biological chemistry*. **278**, 17918-26 (2003).

54. Sekinger, E. A., Moqtaderi, Z., Struhl, K. , *Molecular cell*. **18**, 735-48 (2005).

55. Suto, R. K., Clarkson, M. J., Tremethick, D. J., Luger, K. , *Nature structural biology*. **7**, 1121-4 (2000).

56. Bernstein, B. E. et al., *Proceedings of the National Academy of Sciences of the United States of America*. **99**, 8695-700 (2002).

57. Krogan, N. J. et al., *Molecular cell*. **11**, 721-9 (2003).

58. Ng, H. H., Robert, F., Young, R. A., Struhl, K. , *Molecular cell*. **11**, 709-19 (2003).

59. Ling, X., Harkness, T. A., Schultz, M. C., Fisher-Adams, G., Grunstein, M. , *Genes & development*. **10**, 686-99 (1996).

60. Clarke, A. S., Lowell, J. E., Jacobson, S. J., Pillus, L. , *Molecular and cellular biology*. **19**, 2515-26 (1999).

61. Howe, L. et al., *Genes & development*. **15**, 3144-54 (2001).

62. Ju, Q. D., Morrow, B. E., Warner, J. R. , *Molecular and cellular biology*. **10**, 5226-34 (1990).

63. Elemento, O., Tavazoie, S. , *Genome biology*. **6**, R18 (2005).

64. Fourel, G., Miyake, T., Defossez, P., Li, R., Gilson, E. , *The Journal of biological chemistry*. **277**, 41736-43 (2002).

65. Yu, Q. et al., *Nucleic acids research*. **31**, 1224-33 (2003).

66. Bernstein, B. E., Liu, C. L., Humphrey, E. L., Perlstein, E. O., Schreiber, S. L. , *Genome biology*. **5**, R62 (2004).

67. Lee, C., Shibata, Y., Rao, B., Strahl, B. D., Lieb, J. D. , *Nature genetics*. **36**, 900-5 (2004).

68. Pokholok, D. K. et al., *Cell*. **122**, 517-27 (2005).

69. Storici, F., Durham, C. L., Gordenin, D. A., Resnick, M. A. , *Proceedings of the National Academy of Sciences of the United States of America*. **100**, 14994-9 (2003).

70. Liaw, P. C., Brandl, C. J. , *Yeast (Chichester, England)*. **10**, 771-87 (1994).

71. Jakobovits, E. B., Bratosin, S., Aloni, Y. , *Nature*. **285**, 263-5 (1980).

72. Saragosti, S., Moyne, G., Yaniv, M. , *Cell*. **20**, 65-73 (1980).

73. Ozsolak, F., Song, J. S., Liu, X. S., Fisher, D. E. , *Nature biotechnology*. **25**, 244-8 (2007).

74. Zanton, S. J., Pugh, B. F. , *Genes & development*. **20**, 2250-65 (2006).

75. Zilberman, D., Coleman-Derr, D., Ballinger, T., Henikoff, S. , *Nature*. **456**, 125-9 (2008).

76. Ioshikhes, I. P., Albert, I., Zanton, S. J., Pugh, B. F. , *Nature genetics*. **38**, 1210-5 (2006).

77. Peckham, H. E. et al., *Genome research*. **17**, 1170-7 (2007).

78. Segal, M. R. , *Statistical applications in genetics and molecular biology*. **7**, Article14 (2008).

79. Guillemette, B. et al., *PLoS biology*. **3**, e384 (2005).

80. Li, B. et al., *Proceedings of the National Academy of Sciences of the United States of America*. **102**, 18385-90 (2005).

81. Cairns, B. R. et al., *Cell*. **87**, 1249-60 (1996).

82. Cairns, B. R. et al., *Molecular cell*. **4**, 715-23 (1999).

83. Gavin, A. et al., *Nature*. **415**, 141-7 (2002).

84. De Winde, J. H., Van Leeuwen, H. C., Grivell, L. A. , *Yeast (Chichester, England)*. **9**, 847-57 (1993).

85. Dohmen, R. J., Varshavsky, A. , *Methods in Enzymology*. **399**, 799-822 (2005).

86. Parnell, T. J., Huff, J. T., Cairns, B. R. , *The EMBO journal*. **27**, 100-10 (2008).

87. Reed, S. H., Akiyama, M., Stillman, B., Friedberg, E. C. , *Genes & development*. **13**, 3052-8 (1999).

88. Harbison, C. T. et al., *Nature*. **431**, 99-104 (2004).

89. Beinoraviciūte-Kellner, R., Lipps, G., Krauss, G. , *FEBS letters*. **579**, 4535-40 (2005).

90. Nagalakshmi, U. et al., *Science (New York, N.Y.)*. **320**, 1344-9 (2008).

91. Nonet, M., Scafe, C., Sexton, J., Young, R. , *Molecular and cellular biology*. **7**, 1602-11 (1987).

92. Buskirk, A. R., Ong, Y., Gartner, Z. J., Liu, D. R. , *Proceedings of the National Academy of Sciences of the United States of America*. **101**, 10505-10 (2004).

93. Lorch, Y., Zhang, M., Kornberg, R. D. , *Molecular cell*. **7**, 89-95 (2001).

94. Whitehouse, I., Tsukiyama, T. , *Nature structural & molecular biology*. **13**, 633-40 (2006).

95. Ng, H. H., Robert, F., Young, R. A., Struhl, K. , *Genes & development*. **16**, 806-19 (2002).

96. Yang, J. G., Madrid, T. S., Sevastopoulos, E., Narlikar, G. J. , *Nature structural & molecular biology*. **13**, 1078-83 (2006).

97. Yang, Y. H. et al., *Nucleic acids research*. **30**, e15 (2002).

Publishing Agreement

It is the policy of the University to encourage the distribution of all theses, dissertations, and manuscripts. Copies of all UCSF theses, dissertations, and manuscripts will be routed to the library via the Graduate Division. The library will make all theses, dissertations, and manuscripts accessible to the public and will preserve these to the best of their abilities, in perpetuity.

Please sign the following statement:

I hereby grant permission to the Graduate Division of the University of California, San Francisco to release copies of my thesis, dissertation, or manuscript to the Campus Library to provide access and preservation, in whole or in part, in perpetuity.

Author Signature

12/31/09

Date